UNIVERSITY OF TRENTO

Doctoral School in Civil, Environmental and Mechanical Engineering

Curriculum 3. Modelling and Simulation

Andrea Rodella

Analytical and numerical modelling of undulatory locomotion for limbless organisms in granular\viscous media

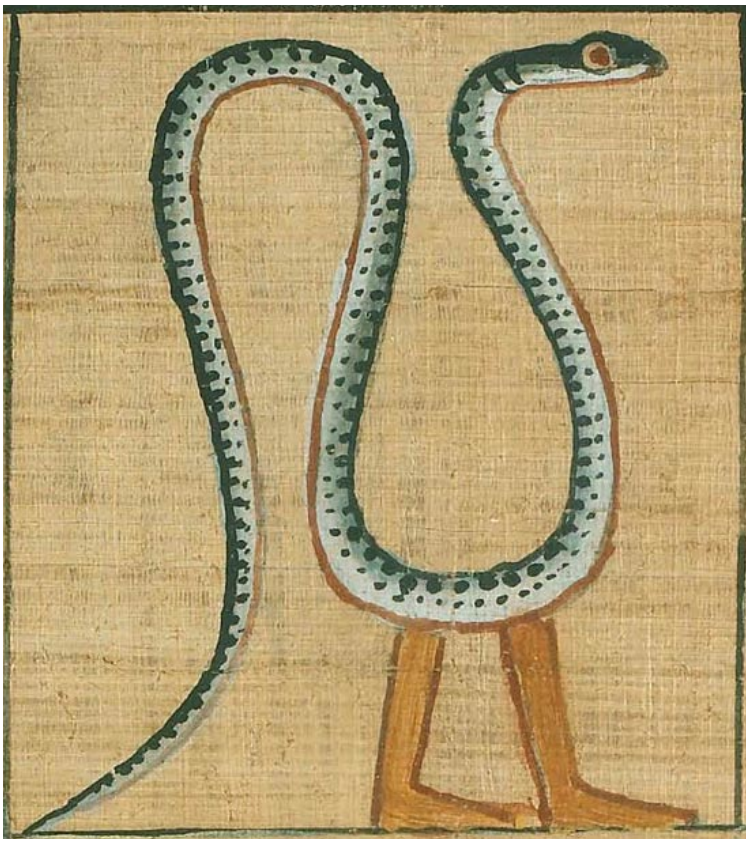

2020 - Doctoral thesis

UNIVERSITY OF TRENTO - Italy
Department of Civil, Environmental and Mechanical Engineering

Doctoral School in Civil, Environmental and Mechanical Engineering
Modelling and Simulation - XXXII Cycle - Scientific Sector ICAR/08

Andrea RODELLA

Analytical and numerical modelling of undulatory locomotion for limbless organisms in granular/viscous media

Supervisors
Nicola Maria PUGNO: University of Trento
Barbara MAZZOLAI: Istituto Italiano di Tecnologia

Credits of the cover image: Book of the Dead of Ani

University of Trento
Doctoral School in Civil, Environmental and Mechanical Engineering
http://web.unitn.it/en/dricam
Via Mesiano 77, I-38123 Trento
Tel. +39 0461 282670 / 2611 - dicamphd@unitn.it

"Acontece isto muitas vezes, não fazemos as perguntas porque ainda não estávamos preparados para ouvir as respostas, ou por termos, simplesmente, medo delas. E, quando encontramos coragem para as lançar, não é raro que não nos respondam . . . "

José Saramago

Abstract

Undulatory locomotion is a common and powerful strategy used in nature at different biological scales by a broad range of living organisms, from flagellated bacteria to prehistoric snakes, which have overcome the complexity of living in "flowable" media. By taking inspiration from this evolution-induced strategy, we aim at modelling the locomotion in a granular and viscous environment with the objective to provide more insights for designing robots for soil-like media exploration. Moreover, in contrast to common types of movement, the granular locomotion is still not well understood and is an open and challenging field.

We approached this phenomenon with several tools: (i.) numerically, via coupling the Finite Element Method (FEM) with the Discrete Element Method (DEM) using ABAQUS; (ii.) analytically, by employing the Lagrangian formalism to derive the equations of motion of a discrete and continuous system subject to non-conservative forces, and (iii.) experimentally, by creating an ad-hoc set up in order to observe the migration of microfibres used for the treatment of spinal cord injuries.

The computational attempts to model the motion in a granular medium involved the simulation of the dynamics of an elastic beam (FEM) surrounded by rigid spherical particles (DEM). A propulsion mechanism was introduced by sinusoidally forcing the beam's tip normally to the longitudinal axis, while the performance of the locomotion was evaluated by means of a parametric study. Depending on the parameters of the external excitation, after a transient phase, the slender body reached a steady-state with a constant translational velocity.

In order to gain physical insights, we studied a simplified version of the previous continuous beam by introducing a discrete multi-bar system. The dynamics of the latter was analytically derived, by taking into account the forces exchanged between the locomotor and the environment, according to the Resistive Force Theory. By numerically solving the equations of motion and evaluating the input energy and dissipations, we were able to define the efficiency and thus provide an effective tool to optimise the locomotion.

It is worth mentioning that the two approaches, despite the different physical hypothesis, show a qualitatively and quantitatively good accordance.

The numerical and analytical models previously analysed have shown promising results for the interpretation of *ad-hoc* experiments that demonstrate the migration of a microfibre embedded in a spinal cord-like matrix. This migration needs to be avoided, once the regenerative microfibre is implanted in the lesioned spinal cord, for the sake of the patients health.

Prof. N. M. Pugno will provide final comments about this thesis in parallel to those of the reviewers.

Contents

List of Figures

List of Tables

To all my families

1

Introduction

1.1 Undulatory locomotion: working principle

The ability of moving from one place to another is one of the most important feature that band together the non-plant life forms. Animals, in fact, in order to survive and dispatch basic needs (e.g. foraging, mating or escaping from predators) had to become real specialists in motion, adapting themselves, their behaviour and even their body in order to overcome the vastness of natural environments and situations. This work takes inspiration from this basic and, at the same time, so advanced skill; in particular the thesis is focused on a specific kind of motion: the undulatory locomotion. This evolutionary-induced strategy consists of the propagation of bending waves from the head of the organism to its tail Gray [41]. The interaction between the body, usually narrow and long (slender), and the environment results in

a directional net force acting on the organism and consequently in the self-propulsion of the body through the hosting medium Kuznetsov, Lugovtsov, and Sher [54]. That the undulatory locomotion is widely present in the animal kingdom, is a well-known fact and is justified by its simplicity and robustness Cohen and Boyle [20]. It is, indeed, a powerful strategy and, in most cases, an energetically optimised solution present in nature Astley et al. [9] at different biological scales and adopted by a broad range of living organisms Cohen and Boyle [20]. At the micro scale, we

Figure 1.1: Undulatory locomotion at different scales. a) A sand snake slithering on the dunes and its sinusoidal trace. b) Scanning Electron Microscope (SEM) image of *Bacillus Bacteria*, $1 - 4$ μm long. c) A colorised electron micrograph image of a nematode of $\approx$ 0.75 mm in length. d) Sandfish lizard, the length of an adult specimen can reach $15 - 20$ cm.

can observe the so called micromotility. Although the subject is quite recent, literature is already very broad. Probably the most studied organisms, to date, are:

- Flagellated bacteria, where *Escherichia coli* is a very famous example of organisms that exhibit undulatory locomotion, as shown by Berg [13] and Vizsnyiczai et al. [87];

- Single eukaryota cells such as the *Sea urchin spermatozoa* described by Gray and Lissmann [39] in one of the main works that shaped the field, while more recent works proposed by Noselli et al. [66] deal with flagellated protists *Euglena gracilis*;

- More complicated organisms, biologically speaking, are nematodes such as the *Caenorhabditis elegans* [14], which is probably one of the most studied organisms not only in the field of undulatory locomotion, but also in the field neuroscience. In a recent study, Cook et al. [21] were able to map the entire nervous system, thereby understanding the neural pattern that generates the locomotion. Another interesting work on the nematode was conducted by Park et al. [69] where the locomotion on different substrates was investigated;

- Exceptions are present everywhere in nature: *Euglenids*, for example, perform a very unconventional strategy consisting of large-amplitude highly concerted deformations of the entire body Arroyo et al. [7]. In this case, the waves propagates on the surface of the organism.

At the macro scale the literature is even more vast and the living organisms studied in the progression of the field contain, but are not limited to:

- Annelid worms such as *polychaetes* are characterised by a backward locomotion due to their high frictional external surface;

- Sandfish lizard [12, 61, 62] and salamander [50] are naturally equipped with limbs: the first exhibits undulatory locomotion in sand and the latter in water to propel themselves without any help from their limbs;

- Lampreys [27] and eels [16] have the ability to swim in water and crawl in mud;
- Common snakes [79] as well as the gigantic prehistoric titanoboa snakes [44] are/were specialists in slithering on complex substrates;
- Even dinosaurs used to take advantage of this specific kind of locomotion. It was recently proven by Ibrahim et al. [48] that the tail of *Spinosaurus aegyptiacus* had an unexpected shape with a large, flexible fin-like extremity capable of extensive lateral excursion.

If there is a common feature or principle to all the organisms listed above it's that *the undulation motion is typically constrained by frictional or drag forces of the environment, rather than by gravitational forces* [46, 20]. In the case where the inertial forces become negligible we are in the so called low Reynolds number regime [71] where the *scallop theorem* [71, 63, 58] becomes essential to explain what is happening at this micro inertia-less scale [4]. The Navier-Stokes equations yield a good approximation of what is happening in this limit condition, even if, solving them analytically is possible only in the simplest cases.

1.2 Reynolds number, Navier-Stoke equations and scallop theorem

The Reynolds number was formally defined for the first time by Stokes [83] based on the precedent work of Reynolds [74]. It is a fundamental quantity in hydrodynamics defined as the ratio between the inertial and viscous forces acting within a fluid, where the fluid is thought of as a pile of infinitesimally thick layers that interact with each other. The Reynolds number Re depends on

the reference velocity v, density ρ, viscosity μ[1], and a characteristic length l, relative to the geometry of the problem (e.g. the main length of the body immersed in the fluid)

$$Re = \frac{\rho v^2 l^2}{\mu v l} = \frac{\rho v l}{\mu} = \frac{\text{inertial forces}}{\text{viscous forces}}$$

This number is, indeed, very important, since it contains important information about the medium as well as the body moving through the medium. The concept can be clarified by writing down the governing equations in fluid dynamics, the Navier-Stokes equations, under the hypothesis of incompressibility ($\nabla \cdot \mathbf{v} = 0$) with,

$$\overbrace{\rho \overbrace{(\nabla \cdot \mathbf{v})}^{=0} \mathbf{v} + \rho \frac{\partial \mathbf{v}}{\partial t}}^{\text{inertial terms}} = \overbrace{-\nabla p + \mu \nabla^2 \mathbf{v}}^{\text{pressure and viscous terms}}$$

which in its nondimensional form reads

$$Re \frac{\partial \tilde{\mathbf{v}}}{\partial \tilde{t}} = -\tilde{\nabla} \tilde{p} + \tilde{\nabla}^2 \tilde{\mathbf{v}}$$

In the latter equation we can appreciate the role of the Reynolds number in the competition between inertial and viscous term. When $Re \ll 1$ the inertial term is, in a good approximation, negligible. Then, we obtain a time independent relation between the gradient of the fluid pressure p and the Laplacian (i.e. the flux density of the gradient) of the velocity $\mathbf{v}$, the so called Stokes flow. The *scallop theorem*, represented in Figure 1.2, emerges directly from the latter observation, by, in fact, imagining a scallop. Scallops consist of two shells connected by a hinge, where, in the

[1]The Reynolds number is defined for a Newtonian fluid, a fluid where the viscosity is a constant property of the fluid. The viscosity in this case represents the ratio between the shear stress and the rate of angular deformation. In non-Newtonian fluids the ratio is not constant anymore and the viscosity may be a function of time and/or deformation, whereas the Reynolds number may not be defined for such a fluid.

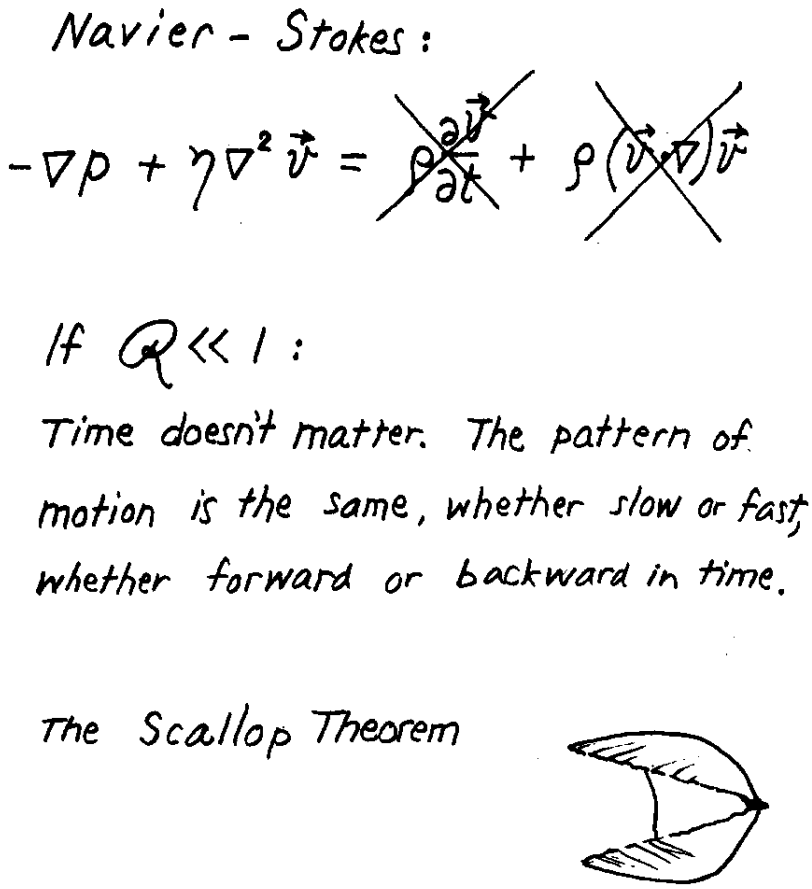

Figure 1.2: Purcell's original illustration of the *scallop theorem* appears in his famous work "Life at low Reynolds number" [71]

absence of inertia, the possible configurations the scallop can assume are limited and reciprocal. This condition leads to a null net displacement for any sequence of motions[2]. In other words, Lauga [58] restated and generalised the theorem in the following way *"If the sequence of shapes displayed by the swimmer is identical to the sequence of shapes displayed when seen in reverse — so-called reciprocal motion — then the average position of the body cannot change over one period"*. To obtain the migration, Stokes equations suggest to violate the time reversibility[1]. Undulatory locomotion is one of the strategies adopted in nature to break the aforementioned symmetry. Taylor's swimming sheet theory [85] and the slender body theory [22, 28] are based on the concepts just exposed, i.e. finding solutions for the Navier-Stokes equation applied to infinite deformed sheets and finite slender shapes, respectively. This task is anything but simple, as demonstrated by Astley et al. [9].

[1] Another way to obtain locomotion in viscous fluid is, actually, to require an anisotropy in the environmental resistance to the motion of the body [20].

Conversely, at a high Reynolds number, $Re \gg 1$, the inertial forces overcome the viscous forces. The theory that describes this opposite limit situation is called elongated-body theory and appeared in [60] in a successful attempt to describe fish locomotion.

Incidentally, in both cases, low and high Re, the dynamics are very close and their study fall under the same general abstract framework, as demonstrated by Chambrion, Giraldi, and Munnier [19] and Cohen and Boyle [20].

1.3 Resistive force theory and granular media

An approximation of slender body theory can be obtained from the so called resistive force theory, that appears for the first time in the work of Gray and Hancock in the middle of the 1950s [40]. Rather than solving the Navier-Stokes equation for a long and slender body, as in the slender-body theory, the resistive-force

[2] *"...it can't swim because it only has one hinge, and if you have only one degree of freedom in configuration space, you are bound to make a reciprocal motion. There is nothing else you can do."* -Purcell [71]

approach assumes: (i) the deforming body can be split into infinitesimal segments, each experiencing drag and thrust due to the presence of the hosting medium, and (ii) the distributed forces acting on the segments are anisotropic, and depend on the velocity and on the spatial orientation of the segments [40, 90]. However, this theory (hypothesis) lacks any correlations between the fluid properties and the spatially extended nature of the swimmer [8, 20]. Despite this, resistive-force theory has proven to be a very simple and effective method that reasonably captures the phenomenon of locomotion in viscous fluids [53, 14, 59, 51]. Moreover, this local-drag framework has proven to work just as well in granular media [61, 90, 9].

Granular materials are composed of numerous discrete particles, which, depending on their loading conditions, can behave as a solid by entering a jamming state or may flow like a fluid [38]. The stress condition of the granular environment is therefore a pivoting parameter for the prediction of granular material behaviour. More precisely, if the stress does not exceed the "yield" value, the medium is able to provide resistance to the stress condition without significant deformations. Conversely, if the local stress exceeds the "yield" value, the material may enter a *frictional fluid* state, a condition similar to low Reynolds fluids [9]. The behaviour of granular materials, their complex transition from solid- to fluid-like media and even more the interaction with a deforming body are still far from complete comprehension. Recently, Askari and Kamrin [8] provided constitutive equations for resistive-force-obeying materials, in order to describe the material transition when an intruding object interacts with a granular material. However, the locomotion in granular materials still remains an open and challenging field [90].

1.4 Applications

Undulatory locomotion is even more fascinating for its multidisciplinary applications. Bio-inspired robotics are one of the new and most prolific fields in which undulatory locomotion can be applied. The goal is to create novel bio-robotic devices capable of traversing a variety of environments by taking inspiration from the evolutionary-improved methodology used in nature, where the salamander-bot conceived by Ijspeert et al. [50] from EPFL's BioRob laboratory is one of the most famous examples. Snake-bots from Carnegie Mellon's Biorobotics laboratory and the commercial HiBot are nowadays employed in underwater, soil and complex media exploration[45], search & rescue operations [64], industrial inspection, archaeology and, even, in surgical medicine [68]. At the micro scale, undulatory locomotion at a low Reynolds number [4], found application in medicine as micro- or nano-robots, as drug delivery systems, diagnostic tools, and therapeutic devices [26, 33, 3].

Literature is also rich in models attempting to mathematically provide a framework for the robotic control [24, 82, 81]. Moreover, the recent advances in neuroscience have provided a new exciting interaction with the bio-inspired robotic field. A deeper comprehension of the locomotor's central pattern generator, i.e. the neural circuits capable of producing coordinated patterns for the locomotion in animals, allows us to understand different mechanisms of travelling waves in body undulation [49]. The immediate consequence is to obtain robots that mimic nature in an even more accurately manner.

Of course, human curiosity is going beyond the "simple" description of mimicking what happens in a natural environment, a totally new concept of experiments recently arose in order to perform more repeatable experiments and avoid to use animals. Robo-physics, in fact, expects to use robots for experimentation as explained by Aydin et al. [10], while undulatory locomotion,

due to its intrinsic complexity, can now be explored in a new way without the natural uncertainty caused by working with living animals.

1.5 Scope and outline of the thesis

This work is focused on the description of the undulatory locomotion, more precisely planar lateral undulation [43], in granular materials. The tools adopted for modelling the phenomenon are both numerical and analytical. The analytical formalism used in the thesis is explained in Chapter 2, dedicated to the theory of the analytical mechanics, which may help the reader to develop analytical models for locomotion, similar to the one proposed in Chapter 3, in a step by step straight forward manner. By means of analytical mechanics, we were able to derive the equations of motion for a discrete multi-bar model presented in Chapter 3. The latter turned out to be a very good approximation for describing a numerical experiment where an elastic beam is forced to locomote through a soil-like medium. In the analytical model, the granular environment is introduced by taking advantage of the hypothesis offered by the resistive-force theory. Moreover, the model represents an easy and versatile tool in order to optimise the locomotion of an eventual robot. Chapter 4 is the natural extension of the discrete model to a continuous beam variant. Again, the mathematical framework is provided via analytical mechanics, and the derivation of the equations of motion for the continuous system is presented. Finally, in Chapter 5 we show an *ad hoc* experiment in order to demonstrate the migration of a micro fibre embedded in a viscous fluid. The work was done in the context of an European project, Neurofibres, aiming to design a device for regenerative medicine targeted at lesioned spinal cords. The conducted experiment highlights the danger of fibre migration, which, for the sake of the patients health, needs to be avoided with highest priority. Chapter 6 summarises the

conclusions drawn from the work done herein and presents some hints for future extension and application.

Structure of the thesis In sum the chapters contain articles and ongoing work. A brief statement of the contents follows below:

- Chapter 2 contains the theory of analytical mechanics which may help the reader to develop analytical models for locomotion.
- Chapter 3 contains the article: [76] *A. Rodella, B. Mazzolai, and N. M. Pugno. "Undulatory locomotion in granular media of an elastic slender body: a comparison between Finite-Discrete element simulations and Resistive Force Theory". Under internal review (2020).* This article contains a comparison between a numerical and an analytical model describing the locomotion of an elastic slender body interacting with a granular medium.
- Chapter 4 is an ongoing work and contains the derivation of the equations of motion for an inextensible elastic rod interacting with a viscous medium.
- Chapter 5 contains the article: [75] *A. Rodella & I. Corridori, D. Misseroni, B. Mazzolai, A. Motta, and N. M. Pugno. "An experimental and numerical study of the migration of a carbon microfibre used for intraspinal microsimulation". Under internal review (2020).* This article contains an experimental demonstration of the migration of a microfibre embedded in a spinal cord-like environment.
- Chapter 6 closes the thesis with conclusions and future developments.

2

Analytical mechanics

In this chapter, we provide some basic notions on the subjects of analytical mechanics [56, 42, 37, 32], useful to the comprehension of the next chapters. In analytical mechanics, two scalar quantities are at the base of the variational approach to mechanics: kinetic energy and potential energy. These two quantities are connected by the *energy theorem* which states that the sum of kinetic and potential energy remain unchanged during the motion. The most extraordinary fact is that these two fundamental scalars contain the complete dynamics of even the most complex system we can take into consideration. In particular, the true power of this method culminates in the *least action* principle, where a certain quantity is assumed stationary, i.e. the *action*, thereby implicitly including the entire set of equations necessary to describe the motion.

2.1 Basic concepts

2.1.1 Generalised coordinates

The concept of coordinates in analytical mechanics is a crucial point, through them we can translate the physical world into a mathematical one. The coordinates are the one-to-one correspondence between the points of the physical space and the algebraic quantities. The abstraction of this theory permits us to forget about the physical meaning of these quantities and proceed with our calculation. Only at the very end, we translate them back to their physical meaning.

Let us consider a system composed of N particles, not restricted by any kinematic condition. The position of the mechanical system is therefore described by the following relations,

$$\mathbf{r_i}(t) = \{x_i(t), y_i(t), z_i(t)\}; \quad i \in [1, N] \tag{2.1}$$

in a rectangular frame. One could also solve the same problem by expressing the rectangular coordinates in terms of other quantities,

$$\hat{\mathbf{q}}(t) = \{q_1(t), q_2(t), \ldots, q_{3N}(t)\} \tag{2.2}$$

The relations between the two sets of coordinates are described by the arbitrary functions,

$$\begin{aligned} x_1(t) &= f_1(q_1(t), q_2(t), \ldots, q_{3N}(t)) \\ &\vdots \\ z_N(t) &= f_{3N}(q_1(t), q_2(t), \ldots, q_{3N}(t)) \end{aligned} \tag{2.3}$$

Here, a coordinate transformation was performed that substitutes the determination of $\mathbf{r_i}(t)$ with $\mathbf{q}(t)$. The possibility to chose the *right* set of generalised coordinates may facilitate the solution of the problem.

Now, if our mechanical system consists of N particles and we impose m independent kinematic conditions, a specific configuration of our system can be characterised uniquely by,

$$n = 3N - m \tag{2.4}$$

independent coordinates

$$\mathbf{q}(t) = \{q_1(t), q_2(t), \ldots, q_n(t)\} \tag{2.5}$$

Consequently Equation (2.3) can be rewritten as follows,

$$\begin{aligned} x_1(t) &= f_1(q_1(t), q_2(t), \ldots, q_n(t)) \\ &\vdots \\ z_N(t) &= f_{3N}(q_1(t), q_2(t), \ldots, q_n(t)) \end{aligned} \tag{2.6}$$

where $q_i(t)$ denotes the so-called *generalised coordinates* of the system. These n parameters are necessary and sufficient to uniquely characterise the configuration of a mechanical system, and therefore represent the n degrees of freedom (DoFs) relevant for a mathematical representation.

The generalised coordinates may or may not have a geometrical significance with respect to the physical system. None the less, the functions in Equation (2.6) are required to satisfy the following properties: i) shall be finite; ii) shall be single valued; iii) shall be continuous and differentiable; and iv) the Jacobian shall be different from zero (for at least one combination of the n functions).

In addition, we may have a situation where the generalised coordinates are restricted to obey the following m conditions,

$$\phi_i(q_1(t), q_2(t), \ldots, q_n(t)) = 0; \quad i \in [1, m] \tag{2.7}$$

the number of DoF of this new system amount to,

$$n' = n - m \tag{2.8}$$

2.1.2 The configuration space

The configuration space is, perhaps, the most abstract concept in analytical mechanics. The dimension of the space is equal to the degree of freedom of the system we are analysing. In this n-dimensional space, a specific configuration of the system is nothing but a point P, a *C-point*. Consequently, the solution of a dynamical problem can be thought of as a *C-curve*, a curve in n-dimensions. Therefore, any material system can be pictured as a single point in *C-space*, no matter how complicated the system is. Again, this space is not related at all with the physical reality (e.g. the position of a rigid body in the euclidean space is represented with a single point in the 6-dimensional space of the 6 DoF of the body).

Point transformation Due to the fact that no prescription is imposed on the choice of the set of n coordinates describing the system, we can always choose an equivalent but different one,

$$\bar{\mathbf{q}}(t) = \{\bar{q}_1(t), \dots, \bar{q}_n(t)\} \tag{2.9}$$

the relations with the set reported in Equation (2.5) must be expressed as

$$\begin{aligned} \bar{q}_1(t) &= f_1(q_1(t), \dots, q_n(t)) \\ &\vdots \\ \bar{q}_n(t) &= f_n(q_1(t), \dots, q_n(t)) \end{aligned} \tag{2.10}$$

By taking the differentials, we obtain a relation, between the sets, showing their linear dependence[2]

$$d\bar{q}_i = \frac{\partial f_i}{\partial q_1} dq_1 + \cdots + \frac{\partial f_i}{\partial q_n} dq_n; \quad \forall i \in [1, n] \tag{2.11}$$

[2] From now on, for the sake of simplicity, we drop the dependence of the time t unless it is strictly necessary for the overall comprehension.

Therefore, we have obtained a mapping from one set to the other where the continuity, in the two spaces, is preserved. Meaning that: a point P in q-space remains a point in $\bar{q}$-space. Lines, however, become curves, since angles and distances are not preserved.

2.1.3 Constraints

Holonomic constraints If the system is subjected to kinematic conditions as finite relations between the coordinates of the form,

$$\phi_i(q_1, \ldots, q_n, t) = 0; \quad i \in [1, m] \tag{2.12}$$

the constraint is classified as holonomic, and so is the system.

An important sub-classification of mechanical systems is the explicit presence of time, t, in the constraint equations. In Equation (2.12) time appears explicitly and the system is, therefore, classified as rheonomic. A necessary and sufficient condition that belongs to this class is that time should explicitly appear in, at least, one of the m equations. Instead, if time does not appear in any of the relations (2.12) the system is called scleronomic and all the constraints can be represented in the following form,

$$\phi_i(q_1, \ldots, q_n) = 0; \quad i \in [1, m] \tag{2.13}$$

Therefore, we can describe our system with $n' = n - m$ coordinates, an independent sub-set of the DoFs. The method is called *elimination of variables*. Alternatively, we can take into account the complete set of equations for all DoF and use the Lagrangian

multipliers method, where the constraint forces are applied to the relevant DoF via Lagrange multipliers λ_m. The method will be extensively discussed in Section 2.2.2.

Non-holonomic constraints Conversely, if the relationship between the coordinates cannot be expressed directly, but needs to be defined based on the differentials of the coordinates, we are facing a non-holonomic system. The particularity of this type of system is that we cannot neglect any of the generalised coordinates, in contrast to the holonomic case.

2.1.4 Kinetic energy

The kinetic energy is one of the two fundamental quantities in the theory of analytical mechanics. This scalar plays the same role as the rate of change of momentum $\dot{\mathbf{p}}$ in the *equations of motion*,

$$\mathbf{F} = m\mathbf{a} = m\frac{d\mathbf{v}}{dt} = \frac{dm\mathbf{v}}{dt} = \frac{d\mathbf{p}}{dt} = \dot{\mathbf{p}}$$

If $\dot{\mathbf{p}}$ takes care of the inertial side in Newton's equation in the vectorial description of the mechanics of motion, we can state that the kinetic energy is its analytical counterpart.

Let us consider a mechanical system composed of N particles located in an inertial reference frame described through the Cartesian components of the vector $\mathbf{r}_k$, Equation (2.1). The total kinetic energy of the system is nothing but the sum of the individual contributions of kinetic energy of each material point with mass m_k,

$$T = \frac{1}{2}\sum_{k=1}^{N} m_k \dot{\mathbf{r}}_k^2 \tag{2.14}$$

where $\dot{\mathbf{r}}_k^2 = \dot{\mathbf{r}}_k \cdot \dot{\mathbf{r}}_k$ or in index notation $\dot{\mathbf{r}}_k^2 = \dot{x}_k^2 + \dot{y}_k^2 + \dot{z}_k^2$ while the dot represents the derivative over time.

We can, firstly, perform the time derivative of Equation (2.6),

$$\begin{aligned} \dot{x}_1(t) &= \sum_{i=1}^{n} \frac{\partial f_1}{\partial q_i}\dot{q}_i \\ &\vdots \\ \dot{z}_N(t) &= \sum_{i=1}^{n} \frac{\partial f_{3N}}{\partial q_i}\dot{q}_i \end{aligned} \tag{2.15}$$

By rewriting the kinetic energy of Equation (2.14) in terms of generalised coordinates, through Equation (2.15), we obtain,

$$\begin{aligned} T(\mathbf{q},\dot{\mathbf{q}}) &= \frac{1}{2}\sum_{k=1}^{3N} m_k \left(\sum_{i=1}^{n} \frac{\partial f_k}{\partial q_i}\dot{q}_i\right)^2 \\ &= \frac{1}{2}\sum_{k=1}^{3N} m_k \sum_{i=1}^{n} \frac{\partial f_k}{\partial q_i}\dot{q}_i \sum_{j=1}^{n} \frac{\partial f_k}{\partial q_j}\dot{q}_j \\ &= \frac{1}{2}\sum_{i=1}^{n}\sum_{j=1}^{n} \left(\sum_{k=1}^{3N} m_k \frac{\partial f_k}{\partial q_i}\frac{\partial f_k}{\partial q_j}\right)\dot{q}_i\dot{q}_j \\ &= \frac{1}{2}\sum_{i=1}^{n}\sum_{j=1}^{n} m_{ij}\dot{q}_i\dot{q}_j \end{aligned} \tag{2.16}$$

a homogeneous positive definite quadratic function of the $\dot{q}$'s. The positiveness definition subsist if and only if the prescription $m_k > 0; \quad \forall k \in [0, 3N]$ is respected[3].

[3] In this notation we implicitly assumed that $m_1 = m_2 = m_3$ are the mass for the particle one, particle two has mass equal to $m_4 = m_5 = m_6$ and so on.

Note that Equation (2.16) has been obtained by starting from Equation (2.6), de-facto a scleronomic system, that does not take into account the possibility that the functions f_i also depend on t. Conversely, if we consider a rheonomic system Equation (2.6) must be rewritten as,

$$\begin{aligned} x_1(t) &= f_1(q_1(t), q_2(t), \ldots, q_n(t), t) \\ &\vdots \\ z_N(t) &= f_{3N}(q_1(t), q_2(t), \ldots, q_n(t), t) \end{aligned} \tag{2.17}$$

and we must obtain new terms in Equation (2.15),

$$\begin{aligned} \dot{x}_1(t) &= \sum_{i=1}^{n} \frac{\partial f_1}{\partial q_i}\dot{q}_i + \frac{\partial f_1}{\partial t} \\ &\vdots \\ \dot{z}_N(t) &= \sum_{i=1}^{n} \frac{\partial f_{3N}}{\partial q_i}\dot{q}_i + \frac{\partial f_{3N}}{\partial t} \end{aligned} \tag{2.18}$$

Therefore, the kinetic energy in it's most general form reads,

$$\begin{aligned} T(\mathbf{q},\dot{\mathbf{q}}) &= \frac{1}{2}\sum_{k=1}^{3N} m_k \left(\sum_{i=1}^{n} \frac{\partial f_k}{\partial q_i}\dot{q}_i + \frac{\partial f_k}{\partial t}\right)^2 \\ &= \frac{1}{2}\left[\sum_{i=1}^{n}\sum_{j=1}^{n} m_{ij}\dot{q}_i\dot{q}_j + 2\sum_{i=1}^{n} a_i\dot{q}_i + \sum_{k=1}^{3N} m_k\left(\frac{\partial f_k}{\partial t}\right)^2\right] \\ &= \underbrace{\frac{1}{2}\sum_{i=1}^{n}\sum_{j=1}^{n} m_{ij}\dot{q}_i\dot{q}_j}_{\text{quadratic}} + \underbrace{\sum_{i=1}^{n} a_i\dot{q}_i}_{\text{linear}} + \frac{1}{2}\sum_{k=1}^{3N} m_k\left(\frac{\partial f_k}{\partial t}\right)^2 \end{aligned} \tag{2.19}$$

where,

$$m_{ij} = m_{ji} = \sum_{k=1}^{3N} m_k \frac{\partial f_k}{\partial q_i}\frac{\partial f_k}{\partial q_j} \tag{2.20}$$

and,

$$a_i = \sum_{k=1}^{3N} m_k \frac{\partial f_k}{\partial q_i}\frac{\partial f_k}{\partial t} \tag{2.21}$$

The kinetic energy written in the form of Equation (2.19) is a sum of three contributions: i) an homogeneous quadratic function of $\dot{q}_i$; ii) an homogeneous linear function of $\dot{q}_i$; and iii) the remaining terms of q_i and t.

2.1.5 Work function and generalised force

The other fundamental quantity in the field of analytical mechanics is the work function. We can think of this scalar quantity as the counterpart to the forcing term **F** in the Newtonian description of the mechanics of motion. Analytical mechanics does not consider the force as something primitive, but as a quantity that could be derived from another essential quantity: the work.

Let us consider a mechanical system composed of N particles with their positions described by the vector $\mathbf{r}_k$, Equation (2.1). Let us further assume that each particle has mass m_k and experiences a force $\mathbf{F}_k = \{F_{x_k}, F_{y_k}, F_{z_k}\}$. The total infinitesimal work of all imposed forces is,

$$\begin{aligned} \overline{dw} &= \sum_{k=1}^{N} \mathbf{F}_k \cdot d\mathbf{r}_k \\ &= \sum_{k=1}^{N} F_{x_k} dx_k + F_{y_k} dy_k + F_{z_k} dz_k \end{aligned} \tag{2.22}$$

where the differentials $d\mathbf{r}_k = \{dx_k, dy_k, dz_k\}$ can be expressed through the generalised coordinates from Equation (2.6) with,

$$d\mathbf{r}_k = \left\{ \sum_{i=1}^{n} \frac{\partial f_{3k-2}}{\partial q_i} dq_i, \sum_{i=1}^{n} \frac{\partial f_{3k-1}}{\partial q_i} dq_i, \sum_{i=1}^{n} \frac{\partial f_{3k}}{\partial q_i} dq_i \right\} \tag{2.23}$$

The infinitesimal work can, therefore, be rewritten in the following form,

$$\begin{aligned}
\overline{dw} &= \sum_{k=1}^{N} F_{x_k} \sum_{i=1}^{n} \frac{\partial f_{3k-2}}{\partial q_i} dq_i + F_{y_k} \sum_{i=1}^{n} \frac{\partial f_{3k-1}}{\partial q_i} dq_i + F_{z_k} \sum_{i=1}^{n} \frac{\partial f_{3k}}{\partial q_i} dq_i \\
&= \sum_{i=1}^{n} \left(\sum_{k=1}^{N} F_{x_k} \frac{\partial f_{3k-2}}{\partial q_i} + F_{y_k} \frac{\partial f_{3k-1}}{\partial q_i} + F_{z_k} \frac{\partial f_{3k}}{\partial q_i} \right) dq_i \\
&= \sum_{i=1}^{n} \left(\sum_{k=1}^{N} \mathbf{F}_k \cdot \frac{\partial \mathbf{r}_k}{\partial q_i} \right) dq_i \\
&= \sum_{i=1}^{n} Q_i dq_i
\end{aligned} \tag{2.24}$$

where Q_i are the components of the generalised force $\mathbf{Q}$. The latter is a vector of n dimensions belonging to the configuration space. Moreover, the last line of Equation (2.24) points out the relationship between work and generalised coordinate, that is, a linear differential form of q_i.

Now, if the infinitesimal work $\overline{dw}$ is the true differential of a certain function, this function is called the *work function* and is denoted with U.

$$\overline{dw} = dU \tag{2.25}$$

where the work function is a function of the generalised coordinates $U = U(\mathbf{q})$ and its differential is,

$$dU = \sum_{i=1}^{n} \frac{\partial U}{\partial q_i} dq_i \tag{2.26}$$

By comparing Equation (2.24) with Equation (2.26) we obtain,

$$\underbrace{\sum_{i=1}^{n} Q_i dq_i}_{\overline{dw}} = \underbrace{\sum_{i=1}^{n} \frac{\partial U}{\partial q_i} dq_i}_{dU} \qquad \Rightarrow \qquad Q_i = \frac{\partial U}{\partial q_i} \tag{2.27}$$

The potential energy V is defined as the the negative work function $V = -U$ and therefore, Equation (2.27) can be rewritten as,

$$Q_i = -\frac{\partial V}{\partial q_i} \tag{2.28}$$

where $V = V(\mathbf{q})$. This type of force is also called conservative force[1].

In nature, forces may be derivable from a time-dependent work function $U = U(\mathbf{q}; t)$, which entails that the generalised force loses the property of being conservative.

Another possibility is that a force may be conservative, but not derivable from a work function. Forces derivable from a scalar function are called *monogenic*, while forces non derivable from a work function are called polygenic.

In the most general case a monogenic generalised force can be derived from a work function of the following type,

$$U = U(\mathbf{q}; \dot{\mathbf{q}}; t) \tag{2.29}$$

Where U becomes a function of the generalised coordinates and velocities, as well as time. A typical example in which we recognise the above dependencies may be related to the dissipative

[1]Conservative forces are derivable from a scalar U, which is a function of the coordinates q_i only. If this condition is satisfied, we can consider the work done by the force $\mathbf{Q}$ while the system moves from a point A to a point B,

$$\int_A^B \mathbf{Q} \cdot d\mathbf{q} = U_B - U_A = V_A - V_B$$

the integral is path-independent and only depends on the initial and final positions. Consequently, the work done along a closed path results to be null,

$$\oint \mathbf{Q} \cdot d\mathbf{q} = 0\,.$$

forces. In this specific case the forces assume the form,

$$Q_i = \sum_{j=1}^{n} c_{ij}(\mathbf{q}, t)\dot{q}_i \tag{2.30}$$

where c_{ij} represent the damping coefficients, and form a symmetric matrix. The associated work function takes up the following form,

$$U(\mathbf{q}, \dot{\mathbf{q}}, t) = \frac{1}{2}\sum_{j=1}^{n} c_{ij}(\mathbf{q}, t)\dot{q}_i \cdot \dot{q}_j \tag{2.31}$$

which shows a quadratic form in the velocties $\dot{q}_i$ and is also known as *Rayleigh's dissipative function*.

2.2 The calculus of variation

2.2.1 Stationary value of a function

Let us consider a sufficiently smooth function F of the n variables u_k,

$$F = F(u_1, \ldots, u_n) \tag{2.32}$$

The goal of this section is to provide a methodology for finding the stationary value of the function F. To accomplish this, we need to introduce the concept of variation. More precisely, we produce an infinitesimal change in the neighbourhood of a specific point, in order to explore the behaviour of the function F. However, this infinitesimal change δ is profoundly different from the process of the infinitesimal change d, pertaining to differential calculus. The latter involves an actual change of an independent variable, while variational calculus makes use of virtual change. Note that virtual change entails the variation of multiple variables, while actual change treats only one independent variable.

For example, a virtual displacement of a given point of the system, is a displacement that explores all the kinematically admissible displacements in the infinitesimal region around that point.

The infinitesimal change of the coordinates is denoted with $\delta\mathbf{u}$, while the first variation of the function F is defined as,

$$\begin{aligned}\delta F &= \frac{\partial F}{\partial u_1}\delta u_1 + \cdots + \frac{\partial F}{\partial u_n}\delta u_n \\ &= \sum_{k=1}^{n}\frac{\partial F}{\partial u_k}\delta u_k\end{aligned} \tag{2.33}$$

Due to the fact that it's more convenient to work with finite instead of infinitesimal quantities, we can rewrite $\delta\mathbf{u}$ as

$$\begin{bmatrix}\delta u_1 \\ \vdots \\ \delta u_n\end{bmatrix} = \epsilon \begin{bmatrix}a_1 \\ \vdots \\ a_n\end{bmatrix} \tag{2.34}$$

where a_k are the direction cosines of the chosen direction we want to test our function in (or perform the variation), while ϵ is a parameter approaching zero ($\epsilon \to 0$). In any specified direction the function F changes it's value with,

$$\frac{\delta F}{\epsilon} = \sum_{k=1}^{n}\frac{\partial F}{\partial u_k}a_k = 0 \tag{2.35}$$

This expression needs to vanish, in order to be stationary. Furthermore, since the directions a_k are arbitrary, due to the virtuality of the displacement, Equation (2.35) holds true if and only if,

$$\frac{\partial F}{\partial u_k} = 0 \qquad \forall k \in [1, n] \tag{2.36}$$

Conversely, if the latter condition is satisfied, also the rate of change of function F, evaluated in all kinemtically admissible directions,

must vanish. The two conditions are summarised in the following statement,

$$F \text{ is stationary} \quad \Leftrightarrow \quad \frac{\partial F}{\partial u_k} = 0 \tag{2.37}$$

Extremum value For the sake of completeness we briefly discuss the concept of extremum value (true minimum or maximum), even though problems of motion are generally not influenced by conditions of extremum values. However, this concept is intimately connected to the sign of the second variation $\delta^2 F$, and therefore useful when looking for an extremum in the configuration space. Note that the criterion to state if a point in the configuration space is an extremum, is close to the concept of functional analysis. To find the expression of the second variation, we start with the following quantity,

$$\Delta F = F(\mathbf{u} + \epsilon \mathbf{a}) - F(\mathbf{u}) \tag{2.38}$$

subsequently we perform a Taylor series expansion around the point $\mathbf{u}$,

$$\begin{aligned} \Delta F &= \epsilon \sum_{k=1}^{n} \frac{\partial F}{\partial u_k} a_k + \frac{1}{2}\epsilon^2 \sum_{j,k=1}^{n} \frac{\partial^2 F}{\partial u_j \partial u_k} a_j a_k + o(\epsilon^2) \\ &= \delta F + \frac{1}{2}\delta^2 F + o(\epsilon^2) \end{aligned} \tag{2.39}$$

Due to the conditions established in (Equation (2.37)), the first variation vanishes $\delta F = 0 \; \forall a_k$. Concerning the second variation, we can state that a point is located at an extremum value for the function F, if $\delta^2 F = 0$ is not satisfied for real values of a_k, which entails that $\delta^2 F$ cannot change its sign. As well known from differential calculus, a curve shows an extremum value where the curve's first derivative is 0, with local minima being characterised by a positive second derivative, whereas a negative second derivative marks a local maxima. The sign shall remain the same for

any kinematically admissible or virtual displacement in the infinitesimal region around the point.

At the boundary of the configuration space, where the generalised displacement is not reversible, an extremum is possible without a stationary value for function F.

2.2.2 The Lagrangian λ-method

The problem treated thus far, takes into account a variation of a function F with n non restricted variables. Therefore, the problem is defined as a free variation problem, in the sense that we can always operate variation in any infinitesimal direction. Conversely, the configuration space may be restricted in a way that some relations exist between the generalised coordinates. Also known as *auxiliary* conditions, these kinematic constraints have the effect of reducing the degrees of freedom and consequently the dimensions of the configuration space. In Section 2.1.3 we have shown the elimination of variables method, which makes use of these restrictions.

The objective of this section is to show another method that takes into account the auxiliary conditions, while maintaining the variation problem as unconstraint (i.e. free). The method is called λ-method or *method of the undetermined multipliers* and was reported for the first time in [55].

Let us consider the function (2.32) restricted by the auxiliary condition,

$$f(u_1, \dots, u_n) = 0 \tag{2.40}$$

and let us take the variation of the latter,

$$\delta f = \frac{\partial f}{\partial u_1}\delta u_1 + \cdots + \frac{\partial f}{\partial u_n}\delta u_n = \sum_{k=1}^{n} \frac{\partial f}{\partial u_k}\delta u_k = 0 \tag{2.41}$$

This condition states that the variation δu_k is linearly dependent on all other $n-1$ variations. Therefore, δu_k is not free to be "varied" anymore. For the sake of clarity we assume δu_n to be one dependent variable among the entire set. Now, we are looking for the stationary value of F restricted to Equation (2.40). The first step is to let the first variation of F vanish,

$$\delta F = \frac{\partial F}{\partial u_1}\delta u_1 + \cdots + \frac{\partial F}{\partial u_n}\delta u_n = \sum_{k=1}^{n} \frac{\partial F}{\partial u_k}\delta u_k = 0 \tag{2.42}$$

If all variations δu_k are free, we can use, straight away, statement (2.37), in order to find the stationarity conditions. However, this is not the case, since we have assumed that δu_n is linearly dependent on the rest. Therefore, we slightly modify Equation (2.42) by adding condition 2.41, which by definition is a null quantity and multiply by the unknown parameter $\lambda = \lambda(\mathbf{u})$ as reported below,

$$\begin{aligned} \frac{\partial F}{\partial u_1}\delta u_1 + \cdots + \frac{\partial F}{\partial u_n}\delta u_n + \lambda \overbrace{\left(\frac{\partial f}{\partial u_1}\delta u_1 + \cdots + \frac{\partial f}{\partial u_n}\delta u_n\right)}^{\text{equal to } 0} = 0 \\ \sum_{k=1}^{n} \frac{\partial F}{\partial u_k}\delta u_k + \lambda \left(\sum_{k=1}^{n} \frac{\partial f}{\partial u_k}\delta u_k\right) = 0 \\ \sum_{k=1}^{n} \left(\frac{\partial F}{\partial u_k} + \lambda \frac{\partial f}{\partial u_k}\right)\delta u_k = 0 \end{aligned} \tag{2.43}$$

Since we have assumed linear dependency, δu_n results to be constrained, we would like to find a condition that eliminates it from Equation (2.42). This is possible by choosing a λ that makes the coefficient of δu_n vanish with,

$$\frac{\partial F}{\partial u_n} + \lambda \frac{\partial f}{\partial u_n} = 0 \tag{2.44}$$

Thus, Equation (2.43) becomes,

$$\sum_{k=1}^{n-1}\left(\frac{\partial F}{\partial u_k}+\lambda\frac{\partial f}{\partial u_k}\right)\delta u_k = 0 \tag{2.45}$$

where all the δu_K are unconstrained variations. Finally, the conditions of a free variation problem can be applied with,

$$\frac{\partial F}{\partial u_k}+\lambda\frac{\partial f}{\partial u_k} = 0 \qquad \forall k \in [1, n-1] \tag{2.46}$$

this equation combined with condition (2.44) demonstrates that we can apply the condition of a free variation problem directly to Equation (2.43). In fact, under the aid of this method we can consider all the δu_k as free variation despite our initial assumption of δu_n being linearly dependent. Moreover, we can show that a variation of,

$$\tilde{F} = F + \lambda f \tag{2.47}$$

leads to the same result, when following the process described previously,

$$\delta\tilde{F} = \delta(F+\lambda f) = \delta F + \underbrace{f\delta\lambda}_{=0} + \lambda\delta f = \delta F + \lambda\delta f \tag{2.48}$$

The method can be generalised to multiple constraints. In sum, if we have m auxiliary equations of type (2.40) that constrain function F, which has to be made stationary, we can rewrite the problem as a free variation problem by introducing a number of m parameters. Of course, the unknowns become $n+m$ to solve in n equations, due to the free variation of u_k, plus m additional auxiliary conditions obtained a posteriori. The new function $\tilde{F}$ shall take the following form,

$$\tilde{F} = F + \sum_{i=1}^{m}\lambda_i f_i \tag{2.49}$$

2.2.3 The fundamental processes of the calculus of variation

The stationary value of a definite integral: problem statement Solving problems that involve motion basically require us to find the stationarity of a definite integral, and not, as we have seen so far, the stationarity of a simple function. It is important to note that the unknowns, so far, were the variables u_k, while what we are looking for now are unknown functions (and their derivatives) that make the integral stationary. The branch of mathematics that provides the tools to solve this problem is known as the calculus of variation.

In this section the problem of the stationarity of a definite integral and some of the properties of the process of variation are introduced. We will use all these concepts later in the next section. Hence, let's consider a sufficiently smooth function F,

$$F = F(y, y', x) \tag{2.50}$$

Given the definite integral of the function F between two points a and b of the domain,

$$I = \int_a^b F(y, y', x)dx \tag{2.51}$$

with the following boundary conditions,

$$f(a) = \alpha; \quad f(b) = \beta \tag{2.52}$$

the statement of the problem could be formulated as: find the function,

$$y = f(x) \tag{2.53}$$

that respects the boundary conditions 2.52, in order to make the integral I (Equation (2.51)) stationary.

Now let's consider a different function $y = \overline{f(x)}$ defined in the following way,

$$\overline{f(x)} = f(x) + \epsilon\phi(x) \tag{2.54}$$

where $\phi(x)$ is some arbitrary function sufficiently smooth that must satisfy the boundary conditions 2.52, while ϵ denotes an arbitrarily small parameter. Now, by taking a specific point $\tilde{x}$, as

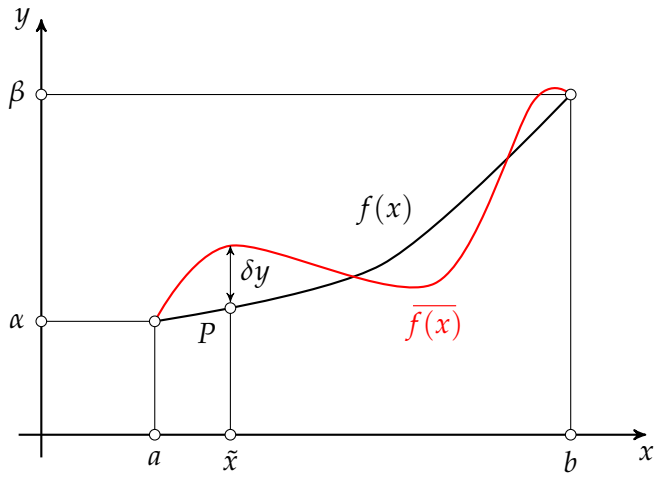

Figure 2.1: The variation of $f(x)$ indicated in the graph as δy, is an infinitesimal and virtual change that produce a new function $\overline{f(x)}$. Note that the variation does not involve the independent variable x.

represented in Figure 2.1, we perform the difference between the two functions,

$$\delta y = \overline{f(x)} - f(x) = \epsilon\phi(x) \tag{2.55}$$

We have obtained the variation[2], an infinitesimal and virtual change, of the function y. Moreover, as we can appreciate from Figure 2.1,

[2]There is a fundamental difference between δy and dy. While both are infinitesimal, the former has the peculiarity to be virtual and therefore produces a new function. The latter on the other hand is caused by the change in the independent variable x.

if the boundary conditions are prescribed, Equation (2.52), the variation of the function calculated in those points, must vanish,

$$\begin{aligned} \delta f(x)\Big|_{x=a} &= 0 \\ \delta f(x)\Big|_{x=b} &= 0 \end{aligned} \tag{2.56}$$

Properties of the δ-process The operation of making a variation has the property to be commutative with respect to the differentiation and to the integration.

Therefore, in the case of differentiation[3] subsists the following equivalence,

$$\frac{d}{dx}\delta y = \delta\frac{d}{dx}y \tag{2.57}$$

Similarly for the integration[4] process, the commutative property can be write as,

$$\int_a^b \delta y\, dx = \delta \int_a^b y\, dx$$

2.2.4 Stationary value of a definite integral

The idea is similar to the one exposed in Section 2.2.1. In order to find the condition of the stationary value of a definite integral we proceed by making the variation of the quantity I as defined

[3] Differentiation:

$$\frac{d}{dx}\delta y = \frac{d}{dx}\left(\overline{f(x)} - f(x)\right) = \frac{d}{dx}\left(\epsilon\phi(x)\right) = \epsilon\phi'(x)$$
$$\delta\frac{d}{dx}y = \overline{f'(x)} - f'(x) = \left(y' + \epsilon\phi'\right) - y' = \epsilon\phi'(x)$$

[4] Integration:

$$\int_a^b \delta y\, dx = \int_a^b \left(\overline{f(x)} - f(x)\right)\, dx = \int_a^b \overline{f(x)}\, dx - \int_a^b f(x)\, dx = \delta\int_a^b y\, dx$$

in Equation (2.51),

$$\begin{aligned}
\delta I &= \delta \int_a^b F(y', y, x)\, dx \\
&= \int_a^b \delta F(y', y, x)\, dx \\
&= \int_a^b \left(\frac{\partial F}{\partial y}\delta y + \frac{\partial F}{\partial y'}\delta y' \right) dx \\
&= \int_a^b \left(\frac{\partial F}{\partial y}\epsilon\phi + \frac{\partial F}{\partial y'}\epsilon\phi' \right) dx \\
&= \epsilon \int_a^b \left(\frac{\partial F}{\partial y}\phi + \frac{\partial F}{\partial y'}\phi' \right) dx
\end{aligned} \tag{2.58}$$

The first step applies the commutative property for the integration, which leads, in the third line, to the first variation of F as shown earlier in Equation (2.42). By recalling Equation (2.55) we can replace the variations δy and $\delta y'$. Furthermore, we can collect ϵ and recognise a similar form with respect to Equation (2.35). In order to obtain the rate of change of I, we divide both sides by the arbitrarily small parameter ϵ,

$$\frac{\delta I}{\epsilon} = \int_a^b \left(\frac{\partial F}{\partial y}\phi + \frac{\partial F}{\partial y'}\phi' \right) dx \tag{2.59}$$

Subsequently, we need to manipulate the equation and apply the rule of integration by parts,

$$\int_a^b \frac{\partial F}{\partial y'}\phi'\, dx = \frac{\partial F}{\partial y'}\phi \Big|_a^b - \int_a^b \frac{d}{dx}\left(\frac{\partial F}{\partial y'} \right) \phi\, dx \tag{2.60}$$

Finally, we rewrite Equation (2.59) and collect the function ϕ, also known as *test function*.

$$\frac{\delta I}{\epsilon} = \int_a^b \left(\frac{\partial F}{\partial y} - \frac{d}{dx}\frac{\partial F}{\partial y'} \right) \phi\, dx \tag{2.61}$$

As discussed in Section 2.2.1, we can now find the conditions necessary to let δI vanish and, therefore, accomplish the goal of finding the conditions of stationarity for function F. Due to the arbitrary nature of the function $\phi = \phi(x)$, as reported in Equation (2.55), Equation (2.61) vanishes if and only if the first integrand assumes a null value in any point of the domain,

$$\frac{\partial F}{\partial y} - \frac{d}{dx}\frac{\partial F}{\partial y'} = 0 \qquad \forall x \in [a, b] \tag{2.62}$$

In sum, the ordinary differential equation (2.62) is the necessary and sufficient condition that makes the definite integral I stationary under the boundary conditions Equation (2.52).

2.2.5 The Euler-Lagrange equations for a discrete system

In mechanics, the aforementioned problem of variation is translated to the following statement: find the stationary value of the definite integral,

$$\begin{aligned} I &= \int_{t_1}^{t_2} L\left(q_1, \ldots, q_n; \dot{q}_1, \ldots, \dot{q}_n; t\right)\ dt \\ &= \int_{t_1}^{t_2} L\left(\mathbf{q}, \dot{\mathbf{q}}, t\right) \end{aligned} \tag{2.63}$$

where the generalised coordinates q_k, function of time t, are subjected to some boundary conditions at the begging and the end of the process. Therefore, as shown in Figure 2.1, their variations must be null,

$$\delta\mathbf{q}\big|_{t=t_1} = 0 \qquad \delta\mathbf{q}\big|_{t=t_2} = 0 \tag{2.64}$$

at the time points t_1 and t_2. The goal is, again, to find the functions, in this case the generalised coordinates, that make the integral I stationary. In other words, δI must be zero.

By following the procedure shown in Section 2.2.4 we take the variation of I with,

$$\begin{aligned}\delta I &= \delta \int_{t_1}^{t_2} L\left(q_1, \ldots, q_n; \dot{q}_1, \ldots, \dot{q}_n; t\right) dt \\ &= \int_{t_1}^{t_2} \delta L\left(q_1, \ldots, q_n; \dot{q}_1, \ldots, \dot{q}_n; t\right) dt \\ &= \int_{t_1}^{t_2} \sum_{i=1}^{n} \left(\frac{\partial L}{\partial q_i} \delta q_i + \frac{\partial L}{\partial \dot{q}_i} \delta \dot{q}_i \right) dt \\ &= \sum_{i=1}^{n} \int_{t_1}^{t_2} \left(\frac{\partial L}{\partial q_i} \delta q_i + \frac{\partial L}{\partial \dot{q}_i} \delta \dot{q}_i \right) dt\end{aligned} \tag{2.65}$$

We can recognise the same structure as in Equation (2.58). By taking advantage of the integration by parts formula, which permits the release of the time derivative from $\delta \dot{q}_i$ to $\frac{\partial L}{\partial \dot{q}_i}$, we obtain,

$$\int_{t_1}^{t_2} \left(\frac{\partial L}{\partial \dot{q}_i} \delta \dot{q}_i \right) dt = \frac{\partial L}{\partial \dot{q}_i} \delta q_i \Big|_{t_1}^{t_2} - \int_{t_1}^{t_2} \frac{d}{dt} \left(\frac{\partial L}{\partial \dot{q}_i} \right) \delta q_i \, dt \tag{2.66}$$

Therefore, Equation (2.65) becomes,

$$\delta I = \sum_{i=1}^{n} \int_{t_1}^{t_2} \left(\frac{\partial L}{\partial q_i} - \frac{d}{dt} \frac{\partial L}{\partial \dot{q}_i} \right) \delta q_i \, dt \tag{2.67}$$

Now, we let δI vanish, in order to find the stationarity conditions. This coincide with the vanishing of the term inside the parenthesis in Equation (2.67) at any point t within the time interval $[t_1, t_2]$ for all n generalised coordinates simultaneously,

$$\frac{\partial L}{\partial q_i} - \frac{d}{dt} \frac{\partial L}{\partial \dot{q}_i} = 0 \qquad \forall t \in [t_1, t_2] \tag{2.68}$$

This is, actually, a system of n second order ordinary differential equations, also known as the Lagrangian equations of motion or the *Euler-Lagrange equations*. In order to solve the system, $2n$ boundary conditions need to be established for the n generalised coordinates q_i at the border of the domain of integration t_1 and t_2.

Auxiliary conditions and the λ-method Let us assume that our mechanical system is constrained by m kinematic conditions,

$$f_k(q_1, \ldots, q_n) = 0, \text{ with } k = 1, \ldots, m \tag{2.69}$$

whose variations are define as below,

$$\delta f_k = \sum_{i=1}^{n} \frac{\partial f_k}{\partial q_i} \delta q_i, \text{ with } k = 1, \ldots, m \tag{2.70}$$

As in Section 2.2.2, we can consider the alternative equivalent variational problem by modifying the function L as follows,

$$\tilde{L} = L + \sum_{k=1}^{m} \lambda_k f_k \tag{2.71}$$

where $\lambda = \lambda(t)$ are the m unknown parameters to take into account the auxiliary conditions. The free variation problem reads,

$$\begin{aligned}
\delta I &= \int_{t_1}^{t_2} \delta \tilde{L} \left(q_1, \ldots, q_n; \dot{q}_1, \ldots, \dot{q}_n; \lambda_1, \ldots, \lambda_m; t\right) dt \\
&= \int_{t_1}^{t_2} \delta \left(L + \sum_{k=1}^{m} \lambda_k f_k \right) dt \\
&= \int_{t_1}^{t_2} \left(\delta L + \delta \sum_{k=1}^{m} \lambda_k f_k \right) dt \\
&= \int_{t_1}^{t_2} \left(\delta L + \underbrace{\sum_{k=1}^{m} \delta \lambda_k f_k}_{=0} + \sum_{k=1}^{m} \lambda_k \delta f_k \right) dt
\end{aligned} \tag{2.72}$$

Now, by combining Equation (2.70) and Equation (2.67) in Equation (2.72) we obtain,

$$\begin{aligned}\delta I &= \int_{t_1}^{t_2} \left[\sum_{i=1}^{n} \left(\frac{\partial L}{\partial q_i} - \frac{d}{dt}\frac{\partial L}{\partial \dot{q}_i} \right) \delta q_i + \sum_{k=1}^{m} \lambda_k \sum_{i=1}^{n} \frac{\partial f_k}{\partial q_i} \delta q_i \right] dt \\ &= \sum_{i=1}^{n} \int_{t_1}^{t_2} \left(\frac{\partial L}{\partial q_i} - \frac{d}{dt}\frac{\partial L}{\partial \dot{q}_i} + \sum_{k=1}^{m} \lambda_k \frac{\partial f_k}{\partial q_i} \right) \delta q_i \, dt\end{aligned} \tag{2.73}$$

Hence, the Euler-Lagrange equations, under the consideration of the m constraints, become a system of $n + m$ unknowns and read,

$$\frac{\partial L}{\partial q_i} - \frac{d}{dt}\frac{\partial L}{\partial \dot{q}_i} + \sum_{k=1}^{m} \lambda_k \frac{\partial f_k}{\partial q_i} = 0 \quad \forall i \in [1, n] \tag{2.74}$$

2.3 Principles in analytical mechanics

2.3.1 The principle of virtual work

In mechanics the principle of virtual work is a fundamental variational principle regarding the equilibrium of the systems. It permits finding conditions on the static behaviour, in a system characterised by reversible displacements. In Newtonian mechanics, a system of particles is in equilibrium if the sum of the forces (impressed and reacting forces) acting on it is equal to zero. Obviously, if the system in object is, for example, a rigid continuous body, the particles involved are infinite, which also entails infinite kinematic forces among the particles that need to be taken into account. The treatment is, therefore, impossible. Analytical mechanics, as we have already discussed, takes into account only the degrees of freedom, or generalised coordinates, of the system, that for a rigid continuous body in the euclidean space are only 6.

The principle states the following: *a given mechanical system will be in equilibrium if, and only if, the total virtual work of all the*

imposed forces vanishes for any infinitesimal and reversible variation of the configuration of the system in harmony with the given kinematic constraints. By recalling the concepts in Section 2.1, the statement can be formulated in its variational form as,

$$\overline{\delta w} = \sum_{i=1}^{n} F_i \delta q_i = \mathbf{F} \cdot \delta \mathbf{q} = 0 \tag{2.75}$$

Where F_i are the components of the generalised force, while δq_i represents the variations of the generalised coordinates. The vectorial form of Equation (2.75) suggests an immediate geometrical interpretation of the principle: in order to achieve the vanishing of the total virtual work, the generalised force must be null or perpendicular to any virtual change in coordinates. Null when the system is free and perpendicular when the system is subjected to kinematic constraints.

Monogenic force If the generalised force $\mathbf{F}$ is derivable from a single scalar function, the virtual work coincides with the negative of the potential energy $\overline{\delta w} = \delta U = -\delta V$ and the equilibrium of the system is reduced to satisfy the condition: $\delta V = 0$.

2.3.2 D'Alembert's principle

The most important contribution that D'Alembert's [23] principle gave to the comprehension of the mechanics of motion, is its interpretation of the forces of inertia. This new point of view in the history of theoretical mechanics leads to the extension of the applicability of the principle of virtual work also to dynamics. In fact, D'Alembert introduced the force of inertia[4] as a force created by the motion, which is define as,

$$\mathbf{I} = -m\ddot{\mathbf{r}} = -\dot{\mathbf{p}} \tag{2.76}$$

[4] Note that the virtual work of the forces of inertia is not reducible to a variation of a scalar function. This is because of the intrinsic nature of the force. Inertial forces are polygenic.

Therefore the Newton's law can be expressed as,

$$\mathbf{F} + \mathbf{I} = 0 \tag{2.77}$$

The sum of impressed force and force of inertia is known as *effective force*. The principle states that: *any system of forces is in equilibrium if we add to the impressed forces the forces of inertia*. Or alternately: *the total virtual work of the effective forces (impressed forces plus inertial forces) vanishes for reversible displacements*:

$$\overline{\delta w} = \sum_{i=1}^{N} (\mathbf{F}_i - m_i \ddot{\mathbf{r}}_i) \cdot \delta \mathbf{r}_i = \sum_{i=1}^{N} \left(\mathbf{F}_i + m_i \frac{d}{dt} \mathbf{v}_i \right) \cdot \delta \mathbf{r}_i = 0 \tag{2.78}$$

In summary, with d'Alembert's principle, we have a tool to treat a problem, where dynamics is involved, as an equivalent static problem, by introducing the inertial forces to the force equilibrium or the virtual work of the system.

2.3.3 The Lagrangian equation of motion: a variational principle

Hamilton's principle Hamilton's principle is one of the different ways to write down the *principle of least action*. This principle is the first natural transformation of d'Alembert's into a stationary principle (or a minimum). We can, then, specialise the principle in order to obtain a more detailed form of the Euler-Lagrange equations by operating a coordinate transformation. Let's start by considering a definite integral of the virtual work of a system composed of N particles and written in rectangular coordinates, Equation (2.78),

$$\int_{t_1}^{t_2} \overline{\delta w} dt = \int_{t_1}^{t_2} \sum_{i=1}^{N} (\mathbf{F}_i - m_i \ddot{\mathbf{r}}_i) \cdot \delta \mathbf{r}_i dt \tag{2.79}$$

By assuming that the impressed forces are derivable from a work function $U(\mathbf{r}) = -V(\mathbf{r})$ and by taking advantage of the definition

(2.33), we can rewrite the first part of the integral as,

$$\begin{aligned}\int_{t_1}^{t_2} \sum_{i=1}^{N} \mathbf{F}_i \cdot \delta\mathbf{r}_i dt &= -\int_{t_1}^{t_2} \sum_{i=1}^{N} \frac{\partial V}{\partial \mathbf{r}_i} \cdot \delta\mathbf{r}_i dt \\ &= -\int_{t_1}^{t_2} \delta V dt \\ &= -\delta \int_{t_1}^{t_2} V dt\end{aligned} \tag{2.80}$$

The inertial part of the integral can be transformed by using the integration by parts rule:

$$\begin{aligned}\int_{t_1}^{t_2} \sum_{i=1}^{N} m_i \ddot{\mathbf{r}}_i \cdot \delta\mathbf{r}_i dt &= \left(\sum_{i=1}^{N} m_i \dot{\mathbf{r}}_i \cdot \delta\mathbf{r}_i \right) \Bigg|_{t_1}^{t_2} - \int_{t_1}^{t_2} \sum_{i=1}^{N} m_i \dot{\mathbf{r}}_i \cdot \delta\dot{\mathbf{r}}_i \, dt \\ &= \left(\sum_{i=1}^{N} m_i \dot{\mathbf{r}}_i \cdot \delta\mathbf{r}_i \right) \Bigg|_{t_1}^{t_2} - \frac{1}{2} \int_{t_1}^{t_2} \sum_{i=1}^{N} m_i \delta \left(\dot{\mathbf{r}}_i \cdot \dot{\mathbf{r}}_i \right) dt \\ &= \left(\sum_{i=1}^{N} m_i \dot{\mathbf{r}}_i \cdot \delta\mathbf{r}_i \right) \Bigg|_{t_1}^{t_2} - \delta \frac{1}{2} \int_{t_1}^{t_2} \sum_{i=1}^{N} m_i \dot{\mathbf{r}}_i^2 \, dt\end{aligned} \tag{2.81}$$

Note that $\delta(\mathbf{a} \cdot \mathbf{a}) = \delta\mathbf{a} \cdot \mathbf{a} + \mathbf{a} \cdot \delta\mathbf{a} = 2\mathbf{a} \cdot \delta\mathbf{a}$. We can also assume the variations $\delta\mathbf{r}_i$ at the boundary time limits, t_1 and t_2, as prescribed, which entails that they must vanish. Hence, the definite integral of the virtual work, Equation (2.79), can be rewritten as,

$$\begin{aligned}\int_{t_1}^{t_2} \overline{\delta w} \, dt &= \delta \int_{t_1}^{t_2} \frac{1}{2} m_i \dot{\mathbf{r}}_i^2 \, dt - \delta \int_{t_1}^{t_2} V \, dt \\ &= \delta \int_{t_1}^{t_2} T \, dt - \delta \int_{t_1}^{t_2} V \, dt \\ &= \delta \int_{t_1}^{t_2} (T - V) dt\end{aligned} \tag{2.82}$$

Where T is the kinetic energy as defined in Equation (2.14). The difference between the two fundamental scalars of analytical mechanics: kinetic energy and potential energy is defined as *Lagrangian function*.

$$L = T - V \tag{2.83}$$

Finally, by applying d'Alembert's principle, which demands that the virtual work vanishes at every time instant and by introducing the quantity, A, namely the *action*; we can finally enunciate Hamilton's principle

$$\delta A = \int_{t_1}^{t_2} \overline{\delta w}\, dt = \delta \int_{t_1}^{t_2} L\, dt = 0 \tag{2.84}$$

Provided the initial and final configuration of an arbitrary mechanical system, its motion occurs in such a way that the action becomes stationary for any arbitrary variation of the configuration of the system.

Note that we developed the principle for systems subjected to monogenic forces and holonomic auxiliary conditions, however, in principle, they could be time-dependent (rheonomic systems).

Point transformation and invariance of the Euler-Lagrange equations Let us express in another way the coordinates of our system, by passing from the rectangular coordinates to the generalised ones, as in Equation (2.5). Consequently, also the kinetic and potential energy will become functions of the coordinates q_i and the velocities $\dot{q}_i$, as well as the Lagrangian function: $L = L(\mathbf{q}, \dot{\mathbf{q}}, t)$. Hence, we are in the same situation as in Section 2.2.5. In particular, we can affirm the legitimacy of the conditions (2.68) on the stationarity of the definite integral I. In this new context the quantity I is nothing but the action integral (Equation (2.84)), with its stationarity conditions being,

$$\frac{\partial L}{\partial q_i} - \frac{d}{dt}\frac{\partial L}{\partial \dot{q}_i} = 0 \qquad \forall i \in \mathbb{N} \,|\, i = \{1, \ldots, n\} \tag{2.85}$$

A system of n second order partial differential equations with n unknowns (the generalised coordinates). In order to obtain the motion of the system, the conditions of Equation (2.85) must be satisfied simultaneously. Note that the scalar quantity defined as Lagrangian function has the peculiarity of determining the entire dynamics of the system.

Due to the fact that we will be treating dynamic systems, let us extend the configuration space, by introducing time t as a new dimension. The extended configuration space, at this point, is composed by $n+1$ dimensions, and the motion of our system is pictured as a curve in this space, constrained at the initial and final time. A variation of the system's configuration at any point in the time domain, is therefore a variation of this curve. Nobody can prevent us from choosing a new set of generalised coordinates $\bar{\mathbf{q}}$ as elaborated in Equation (2.10). In this case the extended configuration space $(\mathbf{q}, t)$-space is mapping itself to the new $(\bar{\mathbf{q}}, t)$-space, the limits of the definite integral A are mapped to new limits, and the curve of motion to a new curve. Moreover, the action integral must vanish also in the new configuration space. The Euler-Lagrange equations are still valid in the new reference system. This does not mean that the equations remain the same, the equations change. What doesn't changing is the action integral, from which the Euler-Lagrange equations derive. This principle is called *invariance* with respect to arbitrary point-transformations.

Energy theorem as a consequence of the Hamilton principle It is always possible to choose among all the virtual variations of the generalised coordinates $q_i(t)$ the actual variation in the infinitesimal time interval $dt = \tau$,

$$\delta q_i = \underbrace{\frac{dq_i}{dt}\delta t}_{\text{virtual}} = \underbrace{\frac{dq_i}{dt}dt}_{\text{actual}} = \dot{q}_i dt = \dot{q}_i \tau \tag{2.86}$$

A direct repercussion is that we can no longer eliminate the border term as we did in Equation (2.82),

$$\delta \int_{t_1}^{t_2} L \, dt = \underbrace{\left(\sum_{i=1}^{N} \frac{\partial L}{\partial \dot{q}_i} \delta q_i \right) \Bigg|_{t_1}^{t_2}}_{\neq 0} \tag{2.87}$$

According to Equation (2.86), if we assume $L = L(\mathbf{q}, \dot{\mathbf{q}})$ to be a scleronomic system, the actual change of the Lagrange function results to be,

$$\begin{aligned} \delta L &= \sum_{i=1}^{n} \left(\frac{\partial L}{\partial q_i} \delta q_i + \frac{\partial L}{\partial \dot{q}_i} \delta \dot{q}_i \right) \\ &= \sum_{i=1}^{n} \left(\frac{\partial L}{\partial q_i} \delta q_i + \frac{\partial L}{\partial \dot{q}_i} \delta \dot{q}_i \right) \\ &= \sum_{i=1}^{n} \left(\frac{\partial L}{\partial q_i} \frac{dq_i}{dt} dt + \frac{\partial L}{\partial \dot{q}_i} \frac{\dot{q}_i}{dt} dt \right) \\ &= \sum_{i=1}^{n} \left(\frac{\partial L}{\partial q_i} \frac{dq_i}{dt} + \frac{\partial L}{\partial \dot{q}_i} \frac{\dot{q}_i}{dt} \right) dt \\ &= \frac{dL}{dt} dt \\ &= \dot{L} \tau \end{aligned} \tag{2.88}$$

Let us introduce the generalised momenta p_i as partial derivative of the Lagrangian function with respect to the generalised velocities,

$$p_i = \frac{\partial L}{\partial \dot{q}_i} \tag{2.89}$$

By rewriting the right-hand-side of Equation (2.87) and by combining it with the definition of the generalised momenta and Equation (2.86) we obtain,

$$\begin{aligned}\left(\sum_{i=1}^{N}\frac{\partial L}{\partial \dot{q}_i}\delta q_i\right)\Bigg|_{t_1}^{t_2} &= \left(\sum_{i=1}^{N} p_i \delta q_i\right)\Bigg|_{t_1}^{t_2} \\ &= \tau\left(\sum_{i=1}^{N} p_i \dot{q}_i\right)\Bigg|_{t_1}^{t_2}\end{aligned} \tag{2.90}$$

Finally we are ready to write Equation (2.87) in its final form,

$$\begin{aligned}\int_{t_1}^{t_2} \dot{L}\tau \, dt &= \tau\left(\sum_{i=1}^{N} p_i \dot{q}_i\right)\Bigg|_{t_1}^{t_2} \\ L\Big|_{t_1}^{t_2} &= \left(\sum_{i=1}^{N} p_i \dot{q}_i\right)\Bigg|_{t_1}^{t_2} \\ \left(\sum_{i=1}^{N} p_i \dot{q}_i - L\right)\Bigg|_{t_1}^{t_2} &= 0\end{aligned} \tag{2.91}$$

Due to the fact that the two time limits are arbitrary, the quantity to be evaluated must be constant at any time. Therefore, we may define it as *total energy* E,

$$\sum_{i=1}^{N} p_i \dot{q}_i - L = E \tag{2.92}$$

In order to manipulate the first term of this equation, two conditions need to be fulfilled, namely: i) the kinetic energy can be written as a quadratic form of $\dot{q}_i$ as in Equation (2.16); and ii) the work function can be completely identified as the potential energy $V = V(\mathbf{q})$. Under the aid of these conditions and by taking advantage of the identity $L = T - V$, we can manipulate the first

term of the previous equation to read,

$$\begin{aligned}\sum_{i=1}^{N} p_i \dot{q}_i &= \sum_{i=1}^{N} \frac{\partial L}{\partial \dot{q}} \dot{q}_i = \sum_{i=1}^{N} \frac{\partial T}{\partial \dot{q}} \dot{q}_i = 2 \overbrace{\frac{1}{2} \sum_{i=1}^{N} \sum_{j=1}^{N} m_{ij} \dot{q}_j \dot{q}_i}^{T} \\ &= 2T\end{aligned} \tag{2.93}$$

Eventually, Equation (2.92) takes the following form,

$$2T - L = 2T - (T - V) = T + V = E \tag{2.94}$$

also known as, the law of the conservation of energy.

Let's now consider a rheonomic system. In this case, the Lagrangian function explicitly depends on time t: $L = L(\mathbf{q}, \dot{\mathbf{q}}, t)$. The latter assumption makes Equation (2.88) take up a different form,

$$\begin{aligned}\delta L &= \sum_{i=1}^{n} \left(\frac{\partial L}{\partial q_i} \delta q_i + \frac{\partial L}{\partial \dot{q}_i} \delta \dot{q}_i \right) + \frac{\partial L}{\partial t} dt \\ &= \left(\dot{L} + \frac{\partial L}{\partial t} \right) \tau\end{aligned} \tag{2.95}$$

Hence, Equation (2.91) wont be equal to zero anymore, but exactly equal to,

$$\underbrace{\left(\sum_{i=1}^{N} p_i \dot{q}_i - L \right) \Big|_{t_1}^{t_2}}_{\Delta E} = \int_{t_1}^{t_2} \frac{\partial L}{\partial t} \, dt \tag{2.96}$$

Therefore we cannot refer to the conservation of the total energy E anymore, but need to regard this quantity as varying according to Equation (2.96).

Physical interpretation of Lagrangian multipliers As discussed in Section 2.2.2 the *lambda*-method is useful every time we want to treat a constrained problem as a free variation problem.

In order to do so, we must change our Lagrange function to read,

$$\tilde{L} = L - \sum_{i=1}^{m} \lambda_m f_m \tag{2.97}$$

Moreover we can take advantage of the definition of the Lagrangian function $L = T - V$ and give a meaning to the second term of the previous equation,

$$\tilde{L} = T - \left(V + \sum_{k=1}^{m} \lambda_k f_k \right) \quad = T - (V + \tilde{V}) \tag{2.98}$$

Once again we can state that T is the kinetic energy, which takes the inertial forces into account. The potential energy V, as we saw previously, contains in itself the impressed forces acting on the system. Then, $\tilde{V}$ can be identified as the potential energy of the forces which maintain the given kinematic constraints. These reaction forces can be derived from the potential energy $\tilde{V}$,

$$\begin{aligned} K_i &= -\frac{\partial}{\partial q_i} \left(\sum_{k=1}^{m} \lambda_k f_k \right) \\ &= -\left(\sum_{k=1}^{m} \lambda_k \frac{\partial f_k}{\partial q_i} + \sum_{k=1}^{m} f_k \frac{\partial \lambda_k}{\partial q_i} \right) \quad \text{(the second sum} \to 0\text{)} \\ &= -\left(\sum_{k=1}^{m} \lambda_k \frac{\partial f_k}{\partial q_i} \right) \end{aligned} \tag{2.99}$$

2.4 Lagrangian formalism for continuous systems

This section is dedicated to the extension of the theory described so far. The branch that studies continua and fields is called field theory, and is basically used to study the dynamics of systems with infinite degrees of freedom, i.e. continua.

Space-time field theory In this case the independent variables are the Cartesian coordinates $\mathbf{x} = \{x_1, x_2, x_3\}$ and time t. The generalised coordinates are then substituted by the scalar fields, function of the variables. For the sake of simplicity, let us assume that the scalar field ϕ is enough to describe the system,

$$\phi = \phi(\mathbf{x}, t) \tag{2.100}$$

The Lagrangian function, in this case, is defined as an integral over a volume Ω with a density, the Lagrangian density $\mathcal{L}$,

$$L = \int_{\Omega} \mathcal{L}\left(\phi, \nabla\phi, \dot{\phi}; \mathbf{x}, t\right) d\omega \tag{2.101}$$

where the gradient of the field ϕ is defined as,

$$\nabla\phi = \left\{ \frac{\partial\phi}{\partial x_1}, \frac{\partial\phi}{\partial x_2}, \frac{\partial\phi}{\partial x_3} \right\} \tag{2.102}$$

and $\dot{\phi}_i$ is nothing but the time derivative,

$$\dot{\phi}_i = \frac{\partial\phi}{\partial t} \tag{2.103}$$

Equation (2.84) gives the general definition of the action $\mathcal{A}$, a definite integral of the Lagrangian function over time,

$$\mathcal{A} = \int_{t_1}^{t_2} \int_{\Omega} \mathcal{L}\left(\phi, \nabla\phi, \dot{\phi}; \mathbf{x}, t\right) d\omega dt \tag{2.104}$$

In order to obtain the stationarity of functional $\mathcal{A}$, we should calculate its variation and find the complete set of Euler-Lagrange equations of motion.

One dimensional space-time Before continuing, let us simplify the problem, since, in Chapter 4, we are going to apply the equations exposed in this section extensively.

In the frame of 1D space-time, the spatial variable is the curvilinear abscissa s. Hence, Equation (2.102) simply becomes,

$$\phi' = \frac{\partial \phi}{\partial s} \tag{2.105}$$

The action $\mathcal{A}$ can be rewritten as,

$$\mathcal{A} = \int_{t_1}^{t_2} \int_{\Gamma} \mathcal{L}\left(\phi, \phi', \dot{\phi}; s, t\right) d\gamma dt \tag{2.106}$$

where Γ is the one dimensional spatial domain. By definition the variation of the action $\mathcal{A}$ that leads to the equations of motion is,

$$\begin{aligned} \delta\mathcal{A} &= \delta \int_{t_1}^{t_2} \int_{\Gamma} \mathcal{L}\left(\phi, \phi', \dot{\phi}; s, t\right) d\gamma dt \\ &= \int_{t_1}^{t_2} \int_{\Gamma} \delta\mathcal{L}\left(\phi, \phi', \dot{\phi}; s, t\right) d\gamma dt \\ &= \int_{t_1}^{t_2} \int_{\Gamma} \left(\mathcal{L}_{\phi}\delta\phi + \mathcal{L}_{\phi'}\delta\phi' + \mathcal{L}_{\dot{\phi}}\delta\dot{\phi}\right) d\gamma dt \end{aligned} \tag{2.107}$$

where we have introduced the new notation $\mathcal{L}_{\#} = \frac{\partial \mathcal{L}}{\partial \#}$, that symbolises the partial derivation of the Lagrangian density with respect to #. Furthermore, by applying the rule of integration by parts, the derivatives of $\delta\phi'$ and $\delta\dot{\phi}$ can be released,

$$\int_{\Gamma} \frac{\partial \mathcal{L}}{\partial \phi'} \delta\phi' d\gamma = \mathcal{L}_{\phi'}\delta\phi\Big|_{\Gamma} - \int_{\Gamma} \frac{d}{ds}\left(\frac{\partial \mathcal{L}}{\partial \phi'}\right) \delta\phi d\gamma \tag{2.108}$$

$$\int_{t_1}^{t_2} \frac{\partial \mathcal{L}}{\partial \dot{\phi}} \delta\dot{\phi} dt = \cancelto{0}{\mathcal{L}_{\dot{\phi}}\delta\phi\Big|_{t_1}^{t_2}} - \int_{t_1}^{t_2} \frac{d}{dt}\left(\frac{\partial \mathcal{L}}{\partial \dot{\phi}}\right) \delta\phi dt \tag{2.109}$$

The terms evaluated at the borders of the time domain must vanish due to the nature of the variations, see Section 2.2.3. By combining the latter two Equations (2.108, 2.109) with Equation (2.107)

we obtain,

$$\delta\mathcal{A} = \int_{t_1}^{t_2} \left\{ \frac{\partial \mathcal{L}}{\partial \phi'} \delta\phi \Big|_\Gamma + \int_\Gamma \left[\frac{\partial \mathcal{L}}{\partial \phi} \delta\phi - \frac{d}{ds}\left(\frac{\partial \mathcal{L}}{\partial \phi'} \right) \delta\phi + \right. \right. \\ \left. \left. - \frac{d}{dt}\left(\frac{\partial \mathcal{L}}{\partial \dot{\phi}} \right) \delta\phi \right] d\gamma \right\} dt \quad (2.110)$$

and by collecting the variation of ϕ we can write,

$$\delta\mathcal{A} = \int_{t_1}^{t_2} \left\{ \frac{\partial \mathcal{L}}{\partial \phi'} \delta\phi \Big|_\Gamma + \int_\Gamma \left[\frac{\partial \mathcal{L}}{\partial \phi} - \frac{d}{ds}\left(\frac{\partial \mathcal{L}}{\partial \phi'} \right) + \right. \right. \\ \left. \left. - \frac{d}{dt}\left(\frac{\partial \mathcal{L}}{\partial \dot{\phi}} \right) \right] \delta\phi d\gamma \right\} dt \quad (2.111)$$

For Hamilton's principle the $\delta\mathcal{A}$ must vanish for all $\delta\phi, \delta\phi\big|_\Gamma$. Finally, the Euler-Lagrange equations read,

$$\frac{\partial \mathcal{L}}{\partial \phi} - \frac{d}{ds}\left(\frac{\partial \mathcal{L}}{\partial \phi'} \right) - \frac{d}{dt}\left(\frac{\partial \mathcal{L}}{\partial \dot{\phi}} \right) = 0 \qquad \forall \delta\phi \quad (2.112)$$

with the conditions on the border of Γ being $s = \{0, l\}$,

$$\frac{\partial \mathcal{L}}{\partial \phi'}\Big|_{s=0} = \frac{\partial \mathcal{L}}{\partial \phi'}\Big|_{s=l} = 0$$

Auxiliary conditions So far the continuous system was considered free. Let us constrain our system with the auxiliary condition,

$$g(\phi, \phi', \dot{\phi}; s, t) = 0 \quad (2.113)$$

By following what we have done in Section 2.2.2, we can always apply the λ-method, in order to move the problem from a constrained to an equivalent unconstrained one. This is achieved by

modifying the Lagrangian density $\mathcal{L}$ to read,

$$\tilde{L} = \int_\Gamma (\mathcal{L} + \lambda g)\, d\gamma = \int_\Gamma \tilde{\mathcal{L}}\left(\phi, \phi', \dot{\phi}; s, t; \lambda, g\right) d\gamma \tag{2.114}$$

The variation of the definite integral is now a function of the constraint g and the field $\lambda = \lambda\left(\phi, \phi', \dot{\phi}; s, t\right)$. Therefore, the variation of action $\mathcal{A}$ becomes,

$$\begin{aligned}\delta\mathcal{A} &= \delta \int_{t_1}^{t_2} \int_\Gamma \tilde{\mathcal{L}}\left(\phi, \phi', \dot{\phi}; s, t; \lambda, g\right) d\gamma dt \\ &= \int_{t_1}^{t_2} \int_\Gamma \left(\tilde{\mathcal{L}}_\phi \delta\phi + \tilde{\mathcal{L}}_{\phi'} \delta\phi' + \tilde{\mathcal{L}}_{\dot{\phi}} \delta\dot{\phi} + \tilde{\mathcal{L}}_\lambda \delta\lambda + \tilde{\mathcal{L}}_g \delta g\right) d\gamma dt\end{aligned} \tag{2.115}$$

It's useful to apply integration by parts in order to obtain,

$$\int_\Gamma \frac{\partial\tilde{\mathcal{L}}}{\partial\phi'}\delta\phi' d\gamma = \frac{\partial\tilde{\mathcal{L}}}{\partial\phi'}\delta\phi\Big|_\Gamma - \int_\Gamma \frac{d}{ds}\left(\frac{\partial\tilde{\mathcal{L}}}{\partial\phi'}\right)\delta\phi d\gamma \tag{2.116}$$

$$\int_{t_1}^{t_2} \frac{\partial\tilde{\mathcal{L}}}{\partial\dot{\phi}}\delta\dot{\phi} dt = \cancelto{0}{\tilde{\mathcal{L}}_{\dot{\phi}}\delta\phi\Big|_{t_1}^{t_2}} - \int_{t_1}^{t_2} \frac{d}{dt}\left(\frac{\partial\tilde{\mathcal{L}}}{\partial\dot{\phi}}\right)\delta\phi dt \tag{2.117}$$

where the modified Lagragian density $\tilde{\mathcal{L}}$ is $\mathcal{L} + \lambda g$. When taking the partial derivatives of $\tilde{\mathcal{L}}$, the λ parameter and the constraint $g = 0$ must be taken into account, which yields,

$$\frac{\partial\tilde{\mathcal{L}}}{\partial\phi}\delta\phi = \left(\frac{\partial\mathcal{L}}{\partial\phi} + \lambda\frac{\partial g}{\partial\phi} + \cancelto{0}{g\frac{\partial\lambda}{\partial\phi}}\right)\delta\phi \tag{2.118}$$

$$\frac{\partial\tilde{\mathcal{L}}}{\partial\phi'}\delta\phi' = \left(\frac{\partial\mathcal{L}}{\partial\phi'} + \lambda\frac{\partial g}{\partial\phi'} + \cancelto{0}{g\frac{\partial\lambda}{\partial\phi'}}\right)\delta\phi' \tag{2.119}$$

$$\frac{\partial\tilde{\mathcal{L}}}{\partial\dot{\phi}}\delta\dot{\phi} = \left(\frac{\partial\mathcal{L}}{\partial\dot{\phi}} + \lambda\frac{\partial g}{\partial\dot{\phi}} + \cancelto{0}{g\frac{\partial\lambda}{\partial\dot{\phi}}}\right)\delta\dot{\phi} \tag{2.120}$$

The final form of the variation of the action is therefore,

$$\begin{aligned}\delta\mathcal{A} = \int_{t_1}^{t_2} \Bigg\{ & \left(\frac{\partial\mathcal{L}}{\partial\phi'} + \lambda\frac{\partial g}{\partial\phi'}\right)\delta\phi\Big|_\Gamma + \\ & + \int_\Gamma \Bigg\{ \frac{\partial\mathcal{L}}{\partial\phi} - \frac{d}{ds}\left(\frac{\partial\mathcal{L}}{\partial\phi'}\right) - \frac{d}{dt}\left(\frac{\partial\mathcal{L}}{\partial\dot{\phi}}\right) + \\ & \quad + \lambda\left[\frac{\partial g}{\partial\phi} - \frac{d}{ds}\left(\frac{\partial g}{\partial\phi'}\right) - \frac{d}{dt}\left(\frac{\partial g}{\partial\dot{\phi}}\right)\right]\Bigg\}\delta\phi d\gamma\Bigg\} dt \quad (2.121)\end{aligned}$$

which needs to be null, in order to find a new set of equations of motion that make the action, for all variations of ϕ, stationary,

$$\frac{\partial\mathcal{L}}{\partial\phi} + \lambda\frac{\partial g}{\partial\phi} - \frac{d}{ds}\left(\frac{\partial\mathcal{L}}{\partial\phi'} + \lambda\frac{\partial g}{\partial\phi'}\right) - \frac{d}{dt}\left(\frac{\partial\mathcal{L}}{\partial\dot{\phi}} + \lambda\frac{\partial g}{\partial\dot{\phi}}\right) = 0 \quad (2.122)$$

3

Modelling and simulation of the undulatory locomotion

Undulatory locomotion is a common and powerful strategy used in nature at different biological scales [20] by a broad range of living organisms, from flagellated bacteria to prehistoric snakes, which faced and face the complexity of moving in a "*flowable*" material. By taking inspiration from this strategy developed during their evolution, we aim to model locomotion in a granular environment with the objective to give more insights for designing robots for soil exploration. Moreover, granular locomotion is still not well understood, compared to other kinds of motion, and is, therefore, an open and challenging field.

Firstly, we approached this phenomenon by performing Finite Element and Discrete Element analysis of a slender body immersed in a layer of mono-disperse spherical particles in the absence of friction. We present a parametric study where the

propulsion of the body, in an undulatory way, is numerically observed. Indeed, after a transitory period, the slender body reaches a steady state behaviour, in terms of velocity, depending on the applied parameters of solicitation.

Secondly, we analytically derived the Lagrangian equations of motion [42] for a discrete multi-bar system subjected to following and viscous forces that emulate the granular environment. The forces exchanged between the locomotor and the environment, according to the resistive force theory [40], play a crucial role for a better comprehension of granular motion. Another essential feature of the model is the strategy adopted for generating a propulsive wave [82] and, thus, controlling the motion of the system.

The two approaches, despite the different physical hypothesis, show a qualitatively and quantitatively good accordance.

3.1 Introduction

The ubiquity of the undulatory locomotion in animals characterised by a slender and limbless body is a well-known fact. It is justified by the simplicity and the robustness of this strategy [20] that consists of the propagation of bending waves from the head of the organism to its tail. Thus, the interaction with the environment results in a directional net force acting on the organism and consequently in the locomotion of the body through the hosting medium [54]. The mechanical behaviour of slender bodies immersed in soil-like materials is an open and challenging field, since, to date, the locomotion through granular media is not well understood. In fact, soil-like materials have the peculiarity to behave as fluids as well as solids depending on the situation [90]. Even though several experimental research works have been carried out, comprehensive numerical simulations are computationally extremely expensive and therefore still missing. In this work we propose a parametric study where an elastic beam,

discretised with the Finite Element Method (FEM), dynamically interacts with rigid spheres, modelled with the Discrete Element Method (DEM), representing the soil-like environment. The aim is to better understand the role of the parameters involved in the phenomenon (e.g. amplitude and frequency of solicitations, diameters of the grains, ...) for an accurate prediction of the velocity of locomotion. Furthermore, inspired by the snake-bot [45], we present also a theoretical derivation of the Lagrangian equations of a mechanical system subjected to the resistive force theory (RFT). RFT appeared for the fist time in the work of Gray and Hancock [40] in the 1950s along with other theories like slender body theory [28] with the aim to describe the undulatory locomotion in low Reynolds number environment of micro-organisms. These pioneering works permitted us to understand the physics behind the undulatory locomotion and are still largely used. Recently [90] has proposed a modification of the theory to describe the locomotion of a sandfish lizard. In particular, RFT assumes: i) the deforming body can be split into segments, each experiencing drag/thrust due to the presence of the hosting medium, and ii) the distributed forces acting on the small elements are positional and viscous [40, 90]. This conceptual model developed herein gives a physical explanation to the numerical observations and can be used as a tool to energetically optimise the phenomenon.

3.2 Model and numerical methods

The simulations carried out in this work were made by using the commercial software ABAQUS/Explicit. In order to describe the motion of an elastic body inside a granular material, it was necessary to couple a model based on FEM with the spherical rigid bodies modelled via DEM.

Scope In Section 3.2.1 we present the details of the model, focusing on the geometry, the model assembly of the set-up and

the mechanical properties of the parts involved in the simulation.

Section 3.2.2 is dedicated to the description of the set-up, the applied boundary conditions and the parameters used.

Finally, Section 3.2.3 has the purpose of presenting and discussing the principal results of the parametric study.

3.2.1 Numerical model details

The model is composed of three different parts as shown in Figure 3.1, where a slender body is surrounded by particles, which in turn are confined by rigid shells.

The slender body has a constant square section, with a length ($l = 1$m) that amounts to 100 times the base (side length $b = 10^{-2}$m) of the section. The beam is discretised with fully integrated linear brick elements (C3D8) involving 6400 nodes. Particles are modelled as rigid spheres with discrete elements (PD3D) and disposed with a 2D volume fraction, $\phi \approx 0.86$, a value comparable to the density of natural soils. The boundary of the domain is modelled with shells that physically confine the sphere and the rod. Particles and rigid shells are undeformable, thus necessitating only the material properties of the elastic body to be defined. The geometrical and mechanical properties used in the simulations are listed in Table 3.1.

The properties of the contact between the parts are modelled as friction-less, only normal forces, without any dissipation, are involved in the contact. Furthermore, tangential forces have been neglected and the interpenetration between any two components is prohibited.

3.2.2 Locomotion by actuation

In this section we simulate locomotion of the rod via the propagation of a wave along the body, the so called undulatory locomotion. The latter, in fact, is a typical strategy used in nature

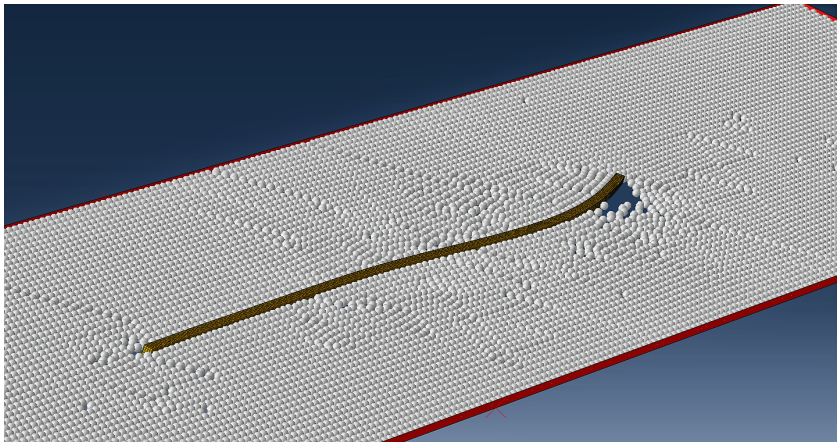

Figure 3.1: Model assembly, where the beam, coloured yellow, is immersed in the particles confined by the red rigid shells.

	Symbol	Unit	Value
Slender body	E	[GPa]	10^2
	ρ	[Kg m^{-3}]	2230
	ν	[-]	0.3
	l	[m]	1
	b	[m]	10^{-2}
Granular material	ϕ	[-]	0.86
	r_{GM}	[m]	5.0 10^{-3}

Table 3.1: Mechanical and geometrical properties of the slender body. The parameter ϕ is the volume fraction of the granular material and r_{GM} is the radius of the grain.

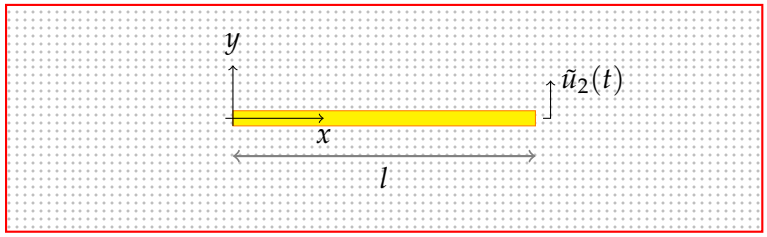

Figure 3.2: Set-up of the simulations. The rectangular shape, in yellow, represented the slender body, placed in the centre of the box, in red. The gray dots show the presence of the spheres. The figure represent the situation at $t = 0$ where the beam is set at rest. Afterwards a vertical displacement is applied on the right tip.

by legless organisms such as snakes [54], sandfish lizards [61] as well as bacteria and cells [40].

The simulations are carried with the following setup: at the beginning of the simulation the beam and the spheres are at rest, i.e all parts involved in the simulation are in contact without exchanging any force. Subsequently, a sinusoidal displacement is imposed as a periodic function of time to the right tip of the beam, as shown in Figure 3.2, with,

$$\tilde{u_2}(t) = A \sin(\omega t) \tag{3.1}$$

acting normally with respect to the beam's middle axis.

By varying the amplitude, A, and the frequency, ω, a parametric study is performed. As shown in the first two columns of Table 3.2, fifteen different pairs of amplitudes and angular frequencies are tested. The amplitudes vary between $b/2 < A < 10b$, where b denotes the breadth of the beam, while the values of the frequencies are chosen to be 1, 10 and 100 Hz, that are 2π, 20π, 200π rad s^{-1} in angular frequencies, ω. 1 Hz and 10 Hz are values common at the macroscale undulatory locomotion [61]. 100 Hz is a value close to the first natural eigenfrequency of an unconstrained 2D beam.

In order to simulate the locomotion of the beam through its surrounding, an explicit dynamic analysis is created with ABAQUS/Explicit. Explicit dynamics is a mathematical technique for integrating the equations of motion through time. The time integration strategy implemented in the software is based on the forward Euler formula where the time increment must be sufficiently small in order to obtain the convergence of the method. The parameters required are: (i) the total simulation time, set equal to 0.6 s, (ii) the time step size is chosen automatically so that it always satisfies the stability limit, (iii) the geometry nonlinearities are taken into account in the simulation. The explicit solver introduces by default a small amount of bulk viscosity damping

where the linear coefficient b_1 and the quadratic coefficient b_2 are equal to 0.06 and 1.2, respectively.

Test	A [m]	ω [rad s^{-1}]	$\bar{u}_1$ [m]	$\hat{v}_1$ [m s^{-1}]	t [s]
c1	0.010	20π	0.345	0.0	0.600
c2	0.005	20π	0.325	0.0	0.600
c3	0.050	20π	0.996	2.3	0.420
c4	0.010	2π	-0.096	0.0	0.600
c5	0.005	2π	0.000	0.0	0.600
c6	0.050	2π	0.179	0.0	0.600
c7	0.010	200π	0.035	0.0	0.600
c8	0.005	200π	0.295	0.0	0.600
c9	0.050	200π	0.993	13.0	0.076
c10	0.025	20π	0.189	0.0	0.600
c11	0.025	2π	0.196	0.0	0.600
c12	0.025	200π	0.995	3.0	0.328
c13	0.100	20π	0.996	5.2	0.192
c14	0.100	2π	0.606	(n.d.)	0.600
c15	0.100	200π	0.942	16.8	0.056

Table 3.2: A and ω are the parameters used for the sinusoidal displacement $\tilde{u}_2(t)$ in Equation (3.1). From third to sixth column are shown the main results of the simulation, where $\bar{u}_1$ is the horizontal net displacement reached from the centre of the mass of the body and $\hat{v}_1$ is the average velocity computed in the steady state trunk of the simulation.

3.2.3 Numerical results

In Figure 3.3 we report the horizontal displacement of the beam's centre of mass (CoM) with respect to time for all simulations listed in Table 3.2. We can observe that five cases experience a proper locomotion (c15, c9, c13, c12 and c3) and reach the geometrical limit of the domain (set at one body length far away from the tip, see Figure 3.2). When observing the aforementioned simulations with proper locomotion, we can note that they tend to a steady state, where the slope of the curves shows a linear trend, i.e. a constant velocity. The values of the velocities averaged in

those steady state trunks, $\hat{v}_1$, are reported in the fifth column of Table 3.2.

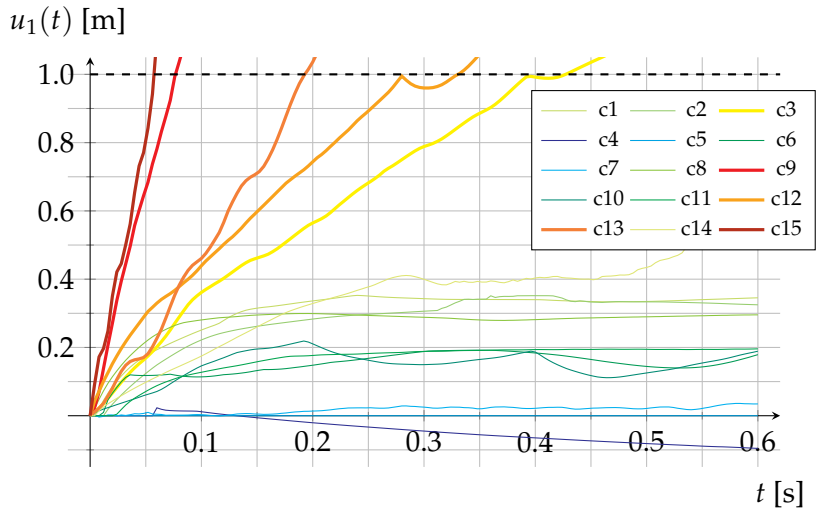

Figure 3.3: Horizontal displacement of the locomotor's centre of mass in function of time for 15 different parameter pairs of A and ω. Thick lines represent the simulations that reach a steady state condition. The dashed black line highlight the domain limit.

From Figure 3.4 to 3.5 the vertical dashed lines represent the value of the applied amplitude, A, while moving along the coloured solid lines means to remain at constant frequency ω. The dots are labelled with their identification name, following the nomenclature presented in 3.2. In particular Figure 3.4 shows the trend of the displacement reached at the last step of the simulation. Figure 3.5 depicts the averaged velocities, where both figures relate the results to the imposed amplitude at a specific angular frequency.

In Figure 3.6 and Figure 3.7 on the other hand, the amplitude, A, is set and we can observe the variation of $\bar{u}_1$ and $\hat{v}_1$, respectively, when frequency ω increases. Vertical dashed lines represent, in this case, the magnitude of the applied angular frequency, ω. Following the solid lines means to remain at constant applied amplitude A.

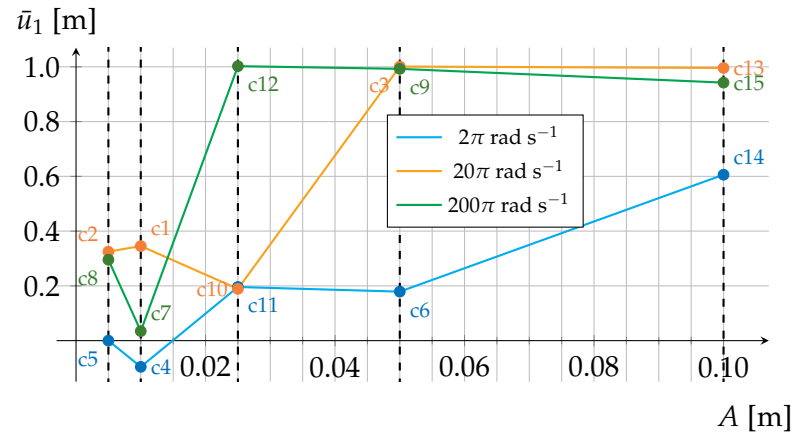

Figure 3.4: Final net horizontal displacement $\bar{u}_1$ in function of the amplitude, where the applied amplitudes are marked with vertical dashed black lines. The dots represent the final displacement and they are labelled with the identification name of the simulation, as in Table 3.2. The solid lines link the results obtained at constant frequency.

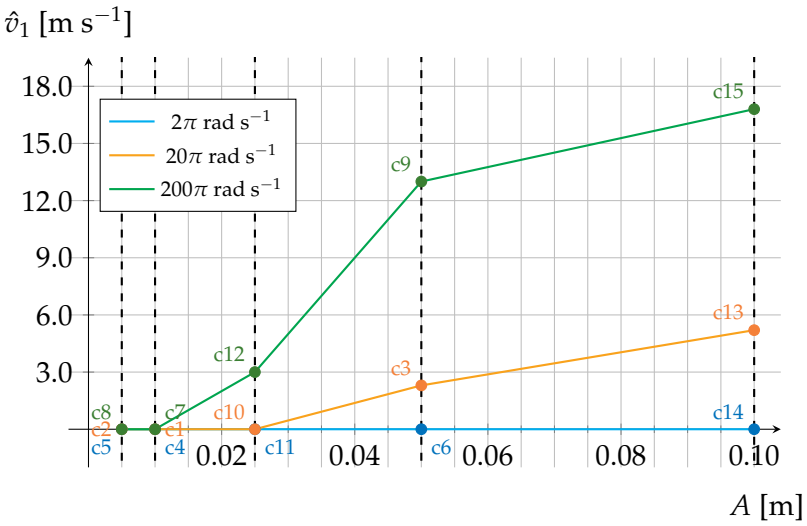

Figure 3.5: Average horizontal velocity $\hat{v}_1$ in function of the amplitude, where the applied amplitudes are marked with vertical dashed black lines. The dots are labelled with the identification name of the simulation, as in Table 3.2. The solid lines link the results obtained at constant frequency.

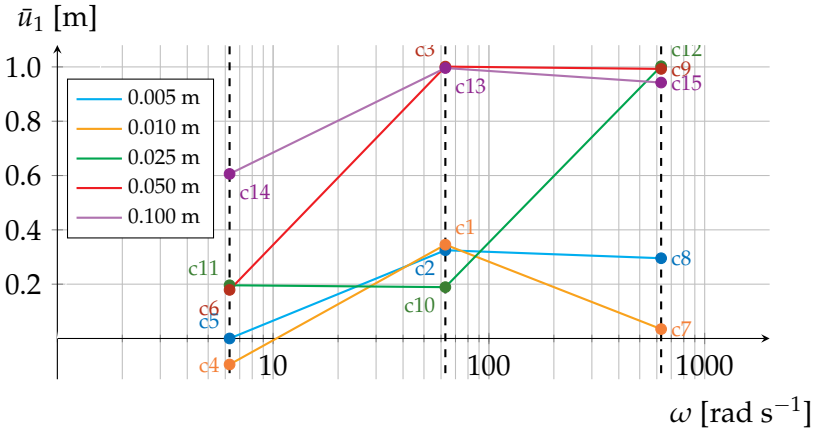

Figure 3.6: Final net horizontal displacement $\bar{u}_1$ in function of the frequency, where the used frequencies are marked with vertical dashed black lines. The dots represent the final displacement and they are labelled with the simulation name, as in Table 3.2. The solid lines link the results obtained at constant amplitude.

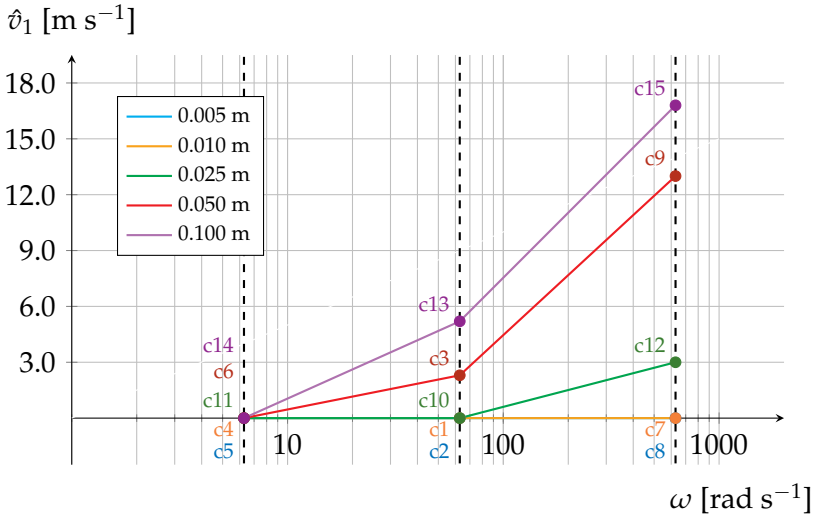

Figure 3.7: Average horizontal velocity $\hat{v}_1$ in function of the frequency, where the used frequencies are marked with vertical dashed black lines. The dots are labelled with the identification name of the simulation, as in Table 3.2. The solid lines link the results obtained at constant amplitude.

Figure 3.8 summarises the results contained in the figures just mentioned, 3.5 and 3.7. The locomotion is, therefore, triggered only when the right combination of amplitude and frequency is chosen. We can observe that the phenomenon takes place when the amplitude is sufficiently large, more than 0.010 m (i.e. larger than the diameters of the grains). In fact, when $A \leq 0.010$ m, the velocity equals 0, even for the maximum frequency of solicitation, as can clearly be seen in Figure 3.5 (green line, dots c7 and c8). Moreover, a very large solicitation amplitude, let us say $1/10$ of the body length ($A = 0.10$ m), does not guarantee the occurrence of the phenomenon, since low-frequency excitations may not trigger undulatory locomotion, as made evident by the blue line in Figure 3.5.

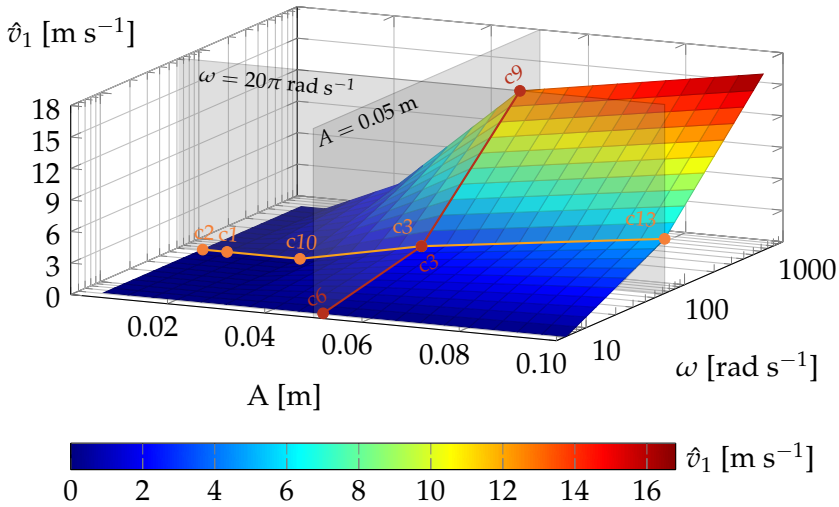

Figure 3.8: Average velocity $\hat{v}_1$ of the system plotted against solicitation amplitude and solicitation frequency. The colour gradient represents the magnitude of the velocity. The graph combines the results presented in Figure 3.5 and Figure 3.7, as highlited by the intersection between the surface and the planes: $A = 0.5$ m and $\omega = 20\pi$ rad s^{-1}.

Figure 3.9 is related to simulation c9 and shows the deformation of the beam's middle-axis over time. We can observe that the beam is moving in the positive direction of the x-axis, while the

propagation of the propulsive wave is travelling in the opposite direction. Moreover, the progression, i.e. the distance between two following peaks, is mostly constant and the amplitude of the tail is reduced approximately by 1/10 with a delay of half a period with respect to the imposed excitation on the right tip. For clarity's sake, Figure 3.9 (below) focuses on one cycle of Figure 3.9 (above) and depicts clearly the behaviour of the system when moving through one cycle of excitation.

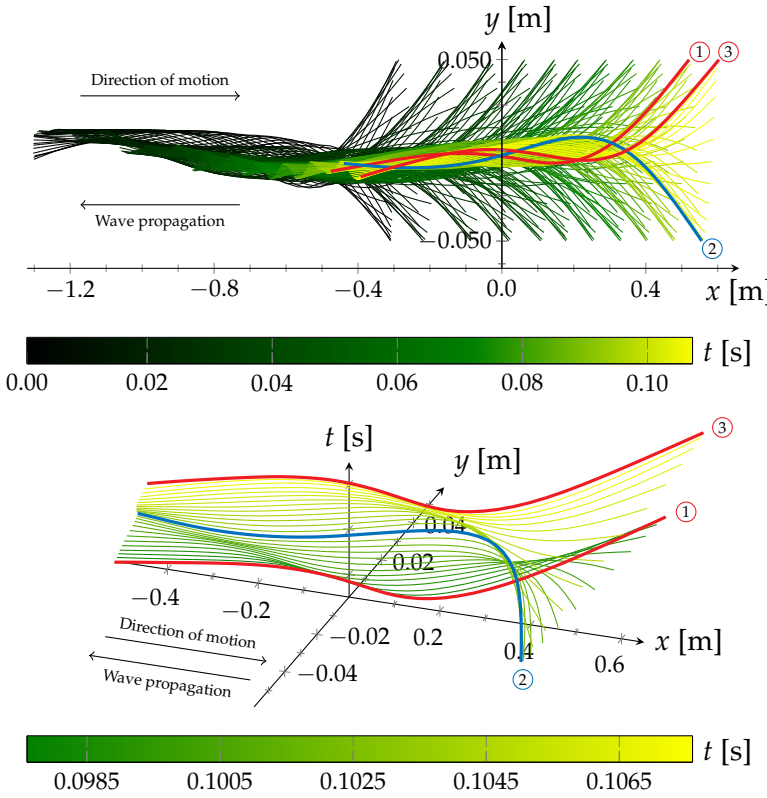

Figure 3.9: (above) Deformed mid-line axis of the beam for simulation c9 over time. The figure shows the locomotion of the beam in the direction of the positive horizontal axis. The wave is generated, by applying Equation (3.1), from the right tip and propagated through the left one. The colour gradient identifies the time progression. The symbols (1), (2) and (3) identify the extremes over one cycle of solicitation. (below) The sequence over the aforementioned cycle is displayed in more detail.

In Figure 3.10 a comparison between three different radii is shown. The parameters we chose are the same of simulation c9 and the radii of the spheres are set as follows $r \in \{5.0, 2.5, 1.25\} \cdot 10^{-3}$ m. According to [62] the role of the radius marginally influences the locomotion, in fact the slope of the curves is approximately the same, $\hat{v}_1 \approx 13$ m/s.

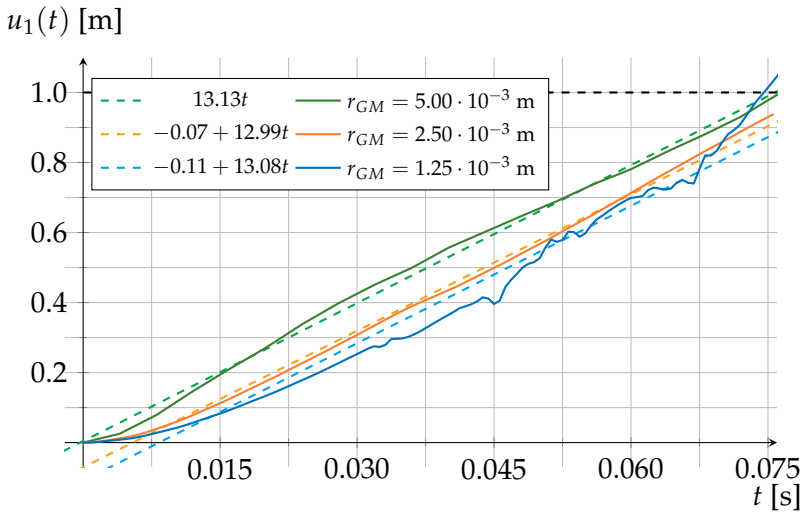

Figure 3.10: Comparison of three simulations with different grain's radius, at fixed amplitude, $A = 0.050$ m, and frequency, $\omega = 200\pi$ Hz. The slope of the curves is approximately the same, $\hat{v}_1 \approx 13$ m/s.

3.3 Modelling undulatory locomotion

To describe mechanically the phenomenon of the undulatory locomotion, it is necessary to couple at least three different concepts: the mechanics of the body, its interaction with the environment and the strategy to control it.

Scope In Section 3.3.1 we provide an analytic derivation of the equations of motion of the body. Section 3.3.2 on the other hand, is dedicated to the description of the environment we think our

body is immersed in and Section 3.3.3 shows a method for controlling the system.

3.3.1 Mechanical model of the body

We consider the holonomic system represented in Figure 3.11, composed of n bars connected by visco-elastic rotational springs. The motion of the system is described in 2D, which allows us to write the Lagrangian coordinates $\mathbf{q}(t)$, needed to describe its motion, with,

$$\mathbf{q}(t) = \begin{bmatrix} u_x(t) \\ u_y(t) \\ \theta_1(t) \\ \vdots \\ \theta_n(t) \end{bmatrix} \tag{3.2}$$

where $u_x(t)$ and $u_y(t)$ are, respectively, the horizontal and vertical displacement of the starting point of the bar chain, while $\theta_i(t),\ i \in [1, n]$ is the rotational angle of the i-th bar with respect the horizontal axis (positive in the clockwise direction). Furthermore, vector $\mathbf{q}(t)$ contains the degrees of freedom (DOF) necessary and sufficient to describe the dynamics of the system.

The position of each point belonging to the i-th bar is described by the vector $\mathbf{r}_i$,

$$\mathbf{r}_i = \begin{bmatrix} u_x(t) + \sum_{j=1}^{i-1} l_j \cos[\theta_j(t)] + s_i \cos[\theta_i(t)] \\ u_y(t) + \sum_{j=1}^{i-1} l_j \sin[\theta_j(t)] + s_i \sin[\theta_i(t)] \end{bmatrix} \tag{3.3}$$

where l_j represents the length of the j-th bar (note that $l_0 = 0$), while $s_i \in [0, l_i]$ is the curvilinear abscissa of the i-th bar. By performing the time derivative of the aforementioned vector, Equation (3.3), we obtain the velocity of the points belonging to the

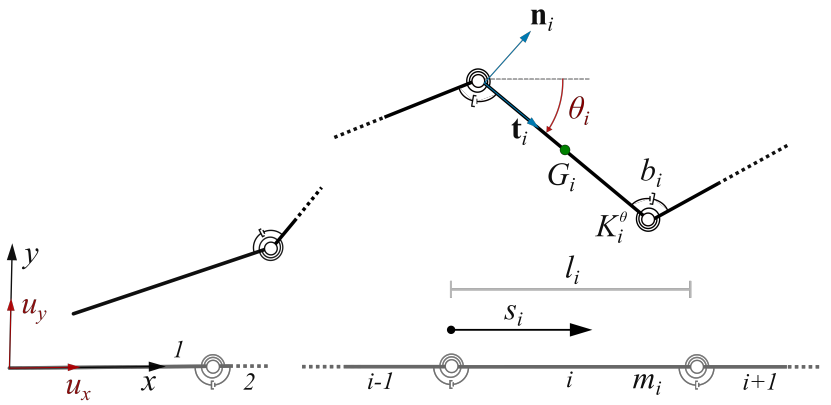

Figure 3.11: Schematics of a system, with an arbitrary number of segments, in its deformed state. In red are evidenced the degrees of freedom of the structure. The light-blue arrows indicate the local system. K_i^θ and b_i are the elastic and dissipative constants of the i-th spring.

i-th bar,

$$\dot{\mathbf{r}}_i = \frac{\partial \mathbf{r}_i}{\partial t} = \begin{bmatrix} \dot{u}_x(t) - \sum_{j=1}^{i-1} l_j \sin[\theta_j(t)]\dot{\theta}_j(t) - s_i \sin[\theta_i(t)]\dot{\theta}_i(t) \\ \dot{u}_y(t) + \sum_{j=1}^{i-1} l_j \cos[\theta_j(t)]\dot{\theta}_j(t) + s_i \cos[\theta_i(t)]\dot{\theta}_i(t) \end{bmatrix} \tag{3.4}$$

Hence, the kinetic energy of the system can be calculated as follows,

$$T(\dot{\mathbf{q}}, \mathbf{q}, t) = \frac{1}{2} \sum_{i=1}^{n} m_i \left(\dot{\mathbf{r}}_i^G\right)^2 + \frac{1}{2} \sum_{i=1}^{n} I_i^G \left(\dot{\theta}_i\right)^2 \tag{3.5}$$

where m_i is the mass of the i-th bar, and I_i^G is the rotational inertia with respect to the centre of mass. For the sake of simplicity, we consider the mass homogeneously distributed along the bars, thus $\dot{\mathbf{r}}_i^G$ represents the velocity of the centre of mass located at $s_i = l_i/2$.

Another essential ingredient, in order to obtain the *Lagrangian* function, is the potential energy. For the system in object the potential energy consists only in the elastic energy stored in

the elastic part of the $n-1$ rotational springs that link the bars together and reads,

$$V(\mathbf{q},t) = \frac{1}{2}\sum_{i=1}^{n-1} K_i^{\theta}(\theta_{i+1}-\theta_i)^2 \tag{3.6}$$

where K_i^{θ} represents the rotational stiffness. The *Lagrangian* function can, therefore, be evaluated using the following relation that holds in systems without non-conservative forces,

$$L(\dot{\mathbf{q}},\mathbf{q},t) = T(\dot{\mathbf{q}},\mathbf{q},t) - V(\mathbf{q},t) \tag{3.7}$$

Finally, according to [56, 37], we obtain the classic formulation of the equations of motion in the following form,

$$\frac{d}{dt}\left(\frac{\partial L}{\partial \dot{\mathbf{q}}_h}\right) - \frac{\partial L}{\partial \mathbf{q}_h} = 0 \tag{3.8}$$

also known as *Euler-Lagrange equations*[5]. The homogeneous system (3.8) is composed of $n+2$ nonlinear second order differential equations where the unknowns are the Lagrangian coordinates listed in Equation (3.2).

[5] In Equation (3.8) $\mathbf{q}_h$ and $\dot{\mathbf{q}}_h$ stand for the h-th component of the vector $\mathbf{q}$ and $\dot{\mathbf{q}}$, respectively.

In order to introduce the forces due to the presence of the dissipative environment, it is necessary to add a non-conservative term to the right-hand-side of Equation (3.8), which will be elaborated in Section 3.3.2.

3.3.2 Interaction with the environment - Resistive Force Theory

With the purpose to describe the environment we apply the RFT to the analytical model introduced in the previous subsection. Basically, RFT consists of splitting the body in several segments and subjecting each of them to drag (and thrust), modelled as decoupled tangential and normal forces. These forces are functions of

the local properties: velocity, orientation and length of the segment. We can therefore write for any generic point belonging to the i-th segment of the bar chain the viscous forces, $\mathbf{L}_i$ and $\mathbf{N}_i$, representing the longitudinally and normally acting forces, respectively, with,

$$\mathbf{L}_i = -C_L \left(\dot{\mathbf{r}}_i \cdot \mathbf{t}_i\right) \mathbf{t}_i \tag{3.9}$$

$$\mathbf{N}_i = -C_N \left(\dot{\mathbf{r}}_i \cdot \mathbf{n}_i\right) \mathbf{n}_i \tag{3.10}$$

where C_L and C_N represent the coefficients of resistance of the environment in the two directions. Note that the minus indicates that these forces are pointing in the opposite direction with respect to velocity $\dot{\mathbf{r}}_i$, as shown in Figure 3.12. The unit vectors $\mathbf{n}_i$ and $\mathbf{t_i}$ are represented below in the system coordinates,

$$\mathbf{t}_i(\mathbf{q}, t) = \begin{bmatrix} \cos[\theta_i(t)] \\ -\sin[\theta_i(t)] \end{bmatrix} \tag{3.11a}$$

$$\mathbf{n}_i(\mathbf{q}, t) = \begin{bmatrix} \sin[\theta_i(t)] \\ \cos[\theta_i(t)] \end{bmatrix} \tag{3.11b}$$

The total resistive force per unit length, that the generic point of the segment experiences, is therefore,

$$\mathbf{F}_i = \mathbf{L}_i + \mathbf{N}_i \tag{3.12}$$

The total generalised non-conservative force is the sum of the resistive forces per unit length integrated along the individual bars and reads,

$$Q_h = \sum_{i=1}^{n} \int_0^{l_i} \left[\mathbf{F}_i(\dot{\mathbf{q}}, \mathbf{q}, t, s_i) \cdot \frac{\partial \mathbf{r}_i}{\partial \mathbf{q}_h} \right] ds \tag{3.13}$$

Finally we can rewrite Equation (3.8) under the consideration of the forces acting on the system with,

$$\frac{d}{dt}\left(\frac{\partial L}{\partial \dot{\mathbf{q}}_h}\right) - \frac{\partial L}{\partial \mathbf{q}_h} = Q_h \tag{3.14}$$

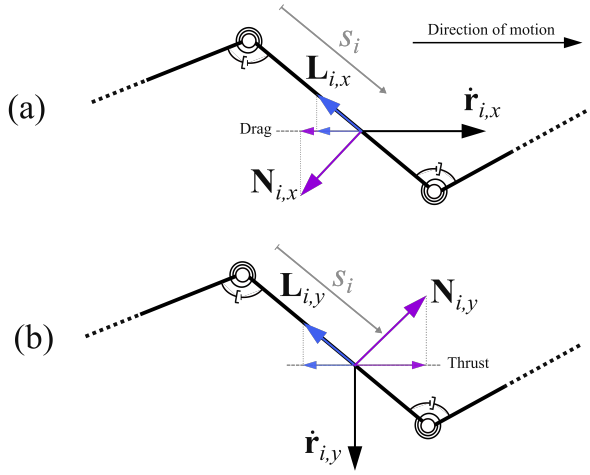

Figure 3.12: Resistive and propulsive forces acting on the system because of the environment. In (a) the diagram represents the components of the drag forces acting at the abscissa s_i of the i-th bar due to the horizontal component of the velocity, $\dot{\mathbf{r}}_{i,x}$. In (b) we can note that the horizontal component of $\mathbf{N}_{i,y}$ generates the thrust for the forward locomotion of the system.

Another source of dissipation in the model is due to the presence of the rotational dash-pots. The dissipation function is taken as a quadratic form of the differences of the rotational velocities of two contiguous bars, as follows,

$$R(\dot{\mathbf{q}}, t) = \frac{1}{2}\sum_{i=1}^{n-1} b_i \left(\dot{\theta}_{i+1} - \dot{\theta}_i\right)^2 \tag{3.15}$$

where b_i is the viscous constant of the i-th spring. Therefore, the final form of the h-th Lagrangian equation of the system can

be rewritten as,

$$\frac{d}{dt}\left(\frac{\partial L}{\partial \dot{\mathbf{q}}_h}\right) - \frac{\partial L}{\partial \mathbf{q}_h} = Q_h - \frac{\partial R}{\partial \dot{\mathbf{q}}_h} \tag{3.16}$$

For the complete derivation of these equations, please, refer to Appendix 3.A.

3.3.3 The control strategy

As previously mentioned, in the very beginning of this section, the control strategy is another fundamental part of the system's dynamics. In this work we focus our attention on the forward locomotion. In nature, this kind of locomotion is reached by a propagation of a sinusoidal-like wave along the organism's body, from the head to the tail. The wave, interacting with the environment, produces a propulsion of the body in a net direction. This strategy has the advantage of being relatively simple and, at the same time, robust, which permitted its diffusion and ubiquity throughout organisms characterised by a slender bodies and others.

With the purpose to generate the propulsive wave that allows the locomotion, we apply the following rheonomic constraint to our system,

$$\theta_1(t) = \alpha \sin(\omega t) \tag{3.17}$$

We are therefore controlling the rotation of the first bar of the system. Practically, $\theta_1(t)$ is not an unknown in the description of the dynamics anymore, while instead, it is now a known function of time. By imposing the aforementioned constraint, a wave is propagated from the head, first bar, to the tail, n-th bar, through the springs.

Another approach, known in the literature as explicit joint angle control, consists of controlling directly all the rotations of the bars $\theta_j(t)$. In this case the sprigs are not relevant anymore, since

a lag angle ϕ_l is imposed as follows,

$$\theta_j(t) = \alpha \sin(\omega t + j\phi_l) \tag{3.18}$$

This methodology, however, forces the system to assume a prescribed deformation and, consequently, ignores a change in shape due to the presence of the environment. Note that, in this case, the degrees of freedom of the system are limited to the horizontal and vertical displacement, see Equation (3.2).

Conversely, the first strategy, as shown in Equation (3.17), allows the system to adjust itself to the environment, thereby providing a more *natural* body's waveform during the locomotion [20].

Results The solutions are obtained by solving numerically the following system implemented in the commercial software Mathematica,

$$\begin{cases} \dfrac{d}{dt}\left(\dfrac{\partial L}{\partial \dot{\mathbf{q}}_h}\right) - \dfrac{\partial L}{\partial \mathbf{q}_h} = Q_h - \dfrac{\partial R}{\partial \dot{\mathbf{q}}_h} \\ \mathbf{q}(0) = \mathbf{0} \\ \dot{\mathbf{q}}(0) = \mathbf{0} \\ \theta_1(t) = \alpha \sin(\omega t) \end{cases} \tag{3.19}$$

where the subscript h satisfies the following conditions $h \in [1, n+2] \ \wedge \ h \neq 3$, since $q_3 = \theta_1(t)$ is a known function of time. In fact, for $h = 3$, and by imposing the rheonomic constraint Equation (3.17), we obtain an unbalanced equation. Furthermore, λ_{θ_1} has the physical meaning of the reaction force due to the constraint and reads,

$$\lambda_{\theta_1} = \frac{d}{dt}\left(\frac{\partial L}{\partial \dot{\theta}_1}\right) - \frac{\partial L}{\partial \theta_1} - Q_h + \frac{\partial R}{\partial \dot{\theta}_1} \neq 0 \tag{3.20}$$

It is thus possible to obtain the same result following the procedure of Lagrangian multipliers shown in Appendix 3.A, where

the constraints are taken into account from the very beginning of the calculations.

The total energy, E_{tot}, in a cycle of solicitation is computed as the sum of the work done by the constraint, E_{in}, plus the work dissipated by the viscous forces E_{out},

$$\begin{aligned} E_{tot} &= E_{in} + E_{out} \\ (T+V)\big|_{t_0}^{t_1} &= \int_{t_0}^{t_1} (W_{out})\, dt + \int_{t_0}^{t_1} (W_{in})\, dt \\ \left(\frac{\partial L}{\partial \dot{\mathbf{q}}_h}\dot{\mathbf{q}}_h - L\right)\Bigg|_{t_0}^{t_1} &= \int_{t_0}^{t_1} \left[\left(Q_h - \frac{\partial R}{\partial \dot{\mathbf{q}}_h}\right)\dot{\mathbf{q}}_h\right] dt + \int_{t_0}^{t_1} \left(\lambda_{\theta_1}\dot{\theta}_1\right) dt \end{aligned} \tag{3.21}$$

The two integrals on the right-hand-side of Equation (3.21) must assume opposing values when the system reaches its steady state (see Appendix 3.B).

Example In this paragraph we provide the results obtained for the system characterised by the parameters listed in Table 3.3.

	Value	Unit	Description
n_b	4	[-]	number of the bars
n_s	3	[-]	number of the springs
m_i	$5.58 \cdot 10^{-2}$	[Kg]	mass of the i-th bar
l_i	$2.5 \cdot 10^{-1}$	[m]	length of the i-th bar
K_i^θ	27	[N m]	rotational stiffness of the i-th spring
C_L^N	$4.50 \cdot 10^2$	[-]	ratio between the coefficients of resistance of the environment
b_i	8.00	[N m s]	viscosity coefficient of the i-th spring
α	20	[°]	amplitude of oscillation
ω	200π	[rad s^{-1}]	angular frequency

Table 3.3: Parameters used in the example.

The propagation of the body inside the medium is well represented by the horizontal displacement, in function of time, of

the CoM as in Figure 3.13. We note that the system reaches almost immediately its steady state. By focusing on the time interval $t \in [0.30, 0.31]$s we can evaluate the energies, introduced and dissipated, in the system as shown in Figure 3.14.

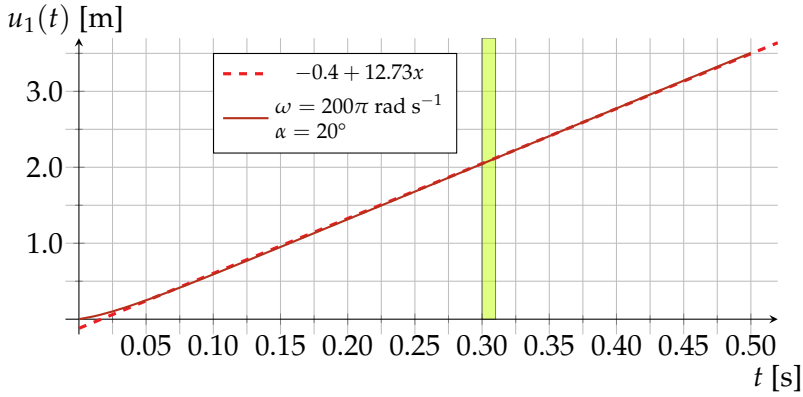

Figure 3.13: Horizontal displacement of the system's CoM and its linear fit. The velocity of locomotion is thus constant, meaning the system reached the steady state. The green area highlights the cycle where we make energetic considerations.

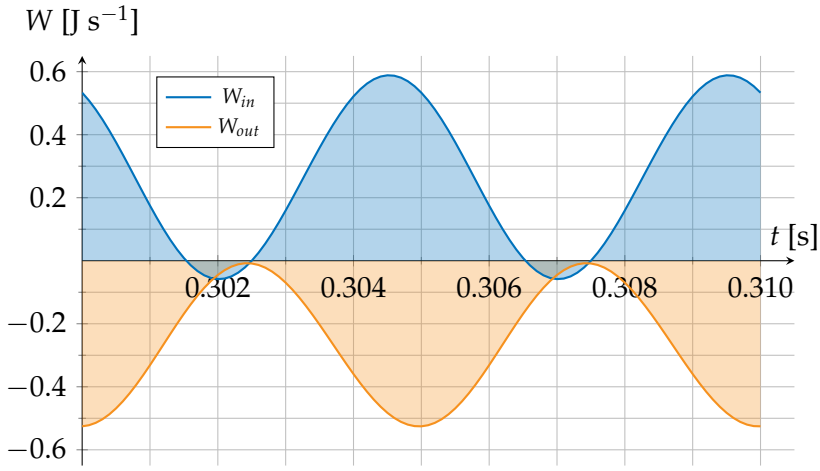

Figure 3.14: When the system reaches the steady state, the energy introduced to the system, here represented by the the blue area, must be equal to the dissipated energy, orange area, within one load cycle.

It is therefore possible to calculate the optimum angle α of solicitation by defining an efficiency,

$$\eta_\alpha = \frac{T_G}{\int_{t_0}^{t_1} \lambda_{\theta_1}(t)\dot{\theta}_1(t)dt} \tag{3.22}$$

where $T_G = \frac{m_{tot}}{2}{v_G}^2$ represents the kinetic energy of the system's CoM, which is travelling at v_G, while the denominator of Equation (3.22) describes the energy induced by the constraint, Equation (3.17). Figure 3.15 shows the efficiency of locomotion normalised to its maximum efficiency $\eta(\alpha) = \frac{\eta_\alpha}{\max_\alpha[\eta_\alpha]}$, where the optimal value for α can be found at 12.5°. In other words, the mechanism described by the parameters found in Table 3.3 achieves the most energy efficient motion when the head tilt amounts to 12.5°.

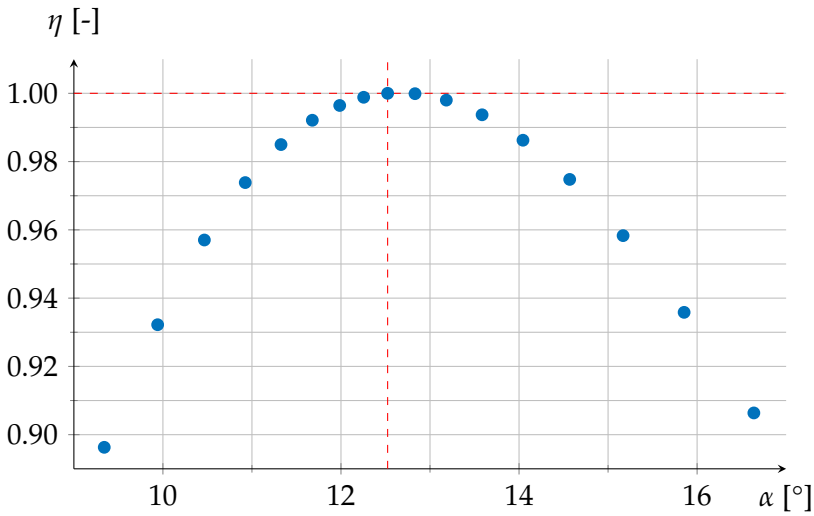

Figure 3.15: Normalised energy efficiency $\eta(\alpha) = \frac{\eta_\alpha}{\max_\alpha[\eta_\alpha]}$ dependent on the maximum rotation of the first bar, α.

3.4 Comparison between the models

In this section we provide a mutual validation of the methods treated up to now. The parameters used for the mechanical model, discussed in Section 3.3.1, are listed in Table 3.4. In this table we relate the parameters of the analytical model to the mechanical and geometrical properties used in the simulations.

	Formula	Value	Unit	Description
n_b	-	9	[-]	number of bars[6]
n_s	$n_b - 1$	8	[-]	number of springs
m_i	$\frac{\rho b^2 l}{n_b}$	$2.48 \cdot 10^{-2}$	[Kg]	mass of i-th bar
l_i	$\frac{l}{n_b}$	$1.\bar{1} \cdot 10^{-1}$	[m]	length of i-th bar
K_i^θ	$\frac{EI}{l} n_s$	10.42	[N m]	rotational stiffness of i-th spring
C_N^L	$\frac{C_L}{C_N} \propto \frac{lb}{b^2}$	$4.50 \cdot 10^2$	[-]	ratio between the coefficients of resistance of the environment
b_i	-	8.00	[N m s]	viscosity coefficient of i-th spring

Table 3.4: Parameters used in the analytic model and their relations with the properties of the numerical simulation listed in Table 3.1.

[6] The choice of 9 bars is a compromise between: (i) maximising the system's velocity, (ii) reducing the computational time cost and (iii) obtaining a solution that can reasonably describe the numerical results in terms of deformed shape.

The main results obtained are shown in Figure 3.16, where we solved the system, Equation (3.19), for a rotation of the last bar of $0 < \alpha < 7/10$ rad (or $0° < \alpha < 40°$), which resulted in vertical displacement amplitudes of the tip between 0.00 m and 0.10 m (i.e. $0 < A < 0.10$ m). Figure 3.16 shows a very good agreement between the two methods, but also the limit of the analytical model in describing the phenomenon when the radius of the grain is comparable to the cross section of the rod.

Furthermore we propose a comparison between simulation c9 and the analytic results obtained by imposing the same parameters. Figure 3.17 shows the horizontal displacement of the

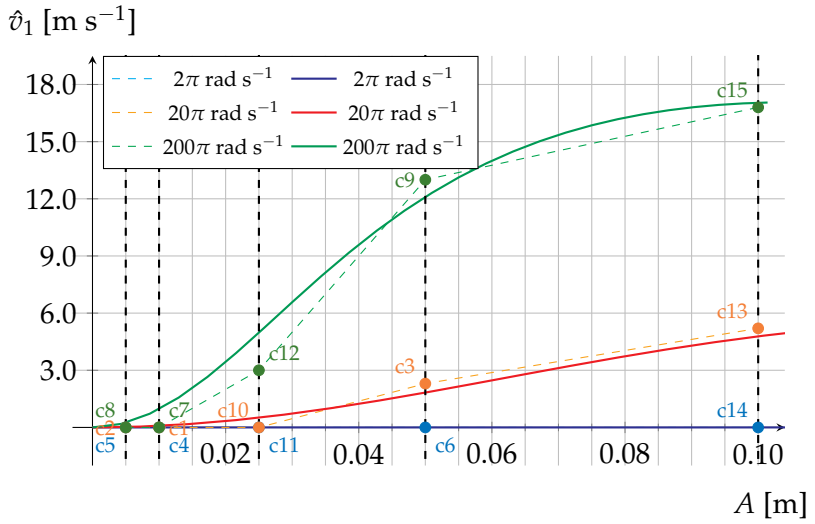

Figure 3.16: Velocity of locomotion $\hat{v}_1$ m/s (or body length per second) as a function of the amplitude A. Comparison between the two methods: numerical (piecewise lines) and theoretical (smooth lines) at three different frequencies of solicitation ω (green 200π rad s^{-1}, orange 20π rad s^{-1}, blue 2π rad s^{-1}).

analytical model in function of time, which grows mostly in a linear way, except for the region in proximity of $t = 0$, where the system hasn't reached the steady state configuration yet. The velocity is therefore the slope of the curve and the value is in good agreement with the results shown in Figure 3.10

The last observation is about the comparison between the deformed mid-line obtained with both methods. In Figure 3.18 we focus our attention on two precise instants of the simulations, where the system reached its steady state (red (1) and blue (2) lines in Figure 3.9) namely:

(a). when the amplitude applied on the right tip is at the maximum oscillation value $A = 0.05$ m

(b). when the amplitude applied on the right tip is at the minimum oscillation value $A = -0.05$ m

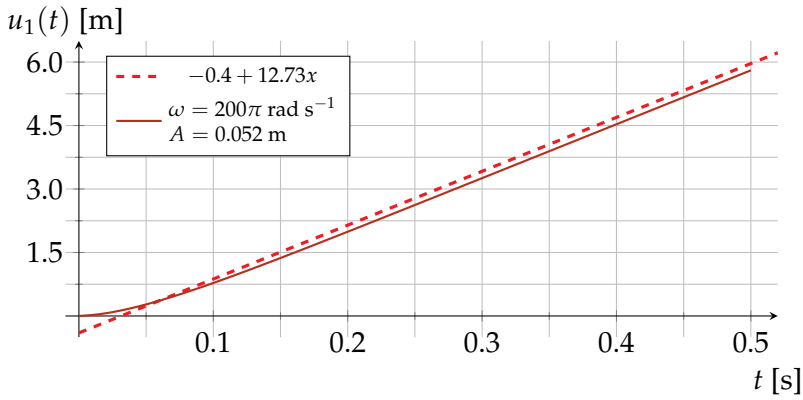

Figure 3.17: Horizontal displacement of the system's CoM in function of time, continuous red line, and its linear interpolation, dashed red line. The velocity is comparable with the simulation reported in Figure 3.10.

Clearly, the analytical model yields very close results to the numerical simulations and can therefore be considered a good approximation of the system.

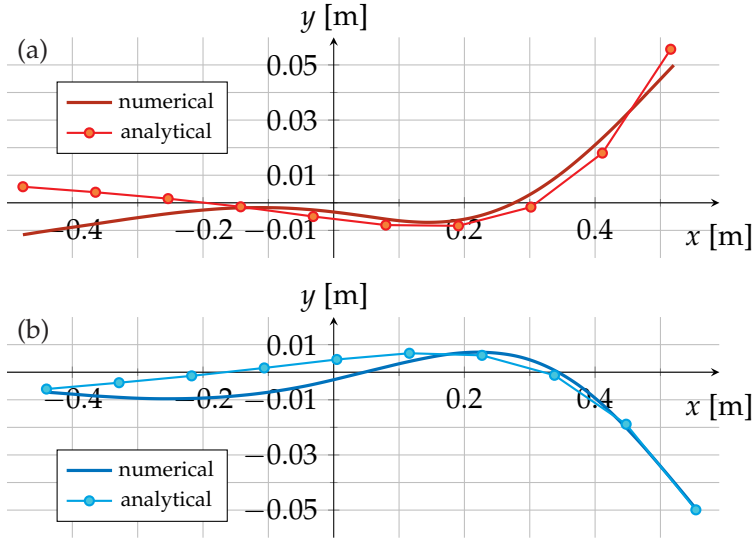

Figure 3.18: Comparison between the deformed mid-line axis during simulation c9 and the analytical model presented. Figure (a) refers to the instant of maximum positive amplitude and (b) to the maximum negative amplitude.

3.5 Conclusion and future work

In order to study the mechanical behaviour of an elastic slender body interacting with granular matter, we have presented a FEM-DEM approach along with an analytic formulation. In the first section we presented the numerical model: the set-up, the properties and the parameters involved in the simulations. In particular, the fundamental assumption, on which the simulations are based, consists of the absence of tangential friction. Furthermore, we performed a parametric study to understand which are the parameters that trigger the phenomenon of undulatory locomotion. In all of the investigated cases where the locomotion occurred, the forward progression of the beam was close to linear. Inspired by the snake-bots, we then introduced and studied a mechanical system composed of rigid bars connected via visco-elastic springs and subjected to resistive forces that is effectively able to approximate the behaviour of the numerical simulations. The equations of motion of the system were derived analytically under the aid of the Lagrangian description and can be used to optimise the motion of the system based on the introduced and dissipated energy. Furthermore, a comparison of the results obtained from the two different methodologies showed a very good agreement qualitatively as well as quantitatively, where particularly the velocities and deformed shapes of the two approaches yielded very similar results. While the motion studied herein represents a simple locomotive mechanism, the analytical model used for the approximation could easily be expanded to more complicated movements such as sinusoidal force transmissions along the slender body. In fact, since the analytical system was able to represent undulatory locomotion in a granular medium, future studies will attempt to model the motion of slender body organisms with the proposed equations. Besides this, the established equations may also help optimising the motion

of bio-inspired robots for increased energy efficiency and movement control in the future.

Appendix

3.A Complete derivation of the equations of motion

Another way to obtain the Lagrange equations is to take into account the constraints of the system from the very beginning, by re-defining the *Lagrangian* function in the following way,

$$\tilde{L}(\dot{\mathbf{q}}, \mathbf{q}, t, \lambda_{\theta_1}) = L(\dot{\mathbf{q}}, \mathbf{q}, t) + \lambda_{\theta_1}[q_3 - \theta_1(t)] \tag{3.23}$$

where $L(\dot{\mathbf{q}}, \mathbf{q}, t)$ is the *Lagrangian* function as defined in Equation (3.7). Instead, the RHS's second term of Equation (3.23) represents the constraint acting on the DOF times the lagrangian multiplier, λ_{θ_1}.

According to [37], in order to obtain the lagrangian equations of motion, we have to apply the principle of *Hamilton's least action*, which is a variational principle that makes the action applied to a mechanical system, $A(t)$, stationary. The variation of the action is defined as follows,

$$\delta A(t) = \int_{t_0}^{t_1} \delta\tilde{L}(\dot{\mathbf{q}}, \mathbf{q}, t, \lambda_{\theta_1}) dt + \underbrace{\int_{t_0}^{t_1} (\mathbf{Q} \cdot \delta\mathbf{q})\, dt}_{\text{due to a dissipative virtual work}} = 0 \tag{3.24}$$

where the first term in the RHS of the previous equation is

$$\int_{t_0}^{t_1} \delta\tilde{L}(\dot{\mathbf{q}}, \mathbf{q}, t, \lambda_{\theta_1}) dt = \int_{t_0}^{t_1} \left(\frac{\partial \tilde{L}}{\partial \mathbf{q}} \cdot \delta\mathbf{q} + \frac{\partial \tilde{L}}{\partial \dot{\mathbf{q}}} \cdot \delta\dot{\mathbf{q}} + \frac{\partial \tilde{L}}{\partial \lambda_{\theta_1}} \delta\lambda_{\theta_1} \right) dt \tag{3.25}$$

Therefore, by evaluating term by term of Equation (3.25),

$$\int_{t_0}^{t_1} \left(\frac{\partial \tilde{L}}{\partial \mathbf{q}} \cdot \delta\mathbf{q} \right) dt = \int_{t_0}^{t_1} \left(\frac{\partial L}{\partial \mathbf{q}} \cdot \delta\mathbf{q} + \lambda_{\theta_1} \delta q_3 \right) dt \tag{3.26}$$

that result,

$$\begin{aligned} \int_{t_0}^{t_1} \left(\frac{\partial \tilde{L}}{\partial \dot{\mathbf{q}}} \cdot \delta\dot{\mathbf{q}} \right) dt &= \cancel{\left(\frac{\partial \tilde{L}}{\partial \dot{\mathbf{q}}} \cdot \delta\mathbf{q} \right) \Big|_{t_0}^{t_1 \to 0}} - \int_{t_0}^{t_1} \left(\frac{d}{dt} \frac{\partial \tilde{L}}{\partial \dot{\mathbf{q}}} \cdot \delta\mathbf{q} \right) dt \\ &= - \int_{t_0}^{t_1} \left(\frac{d}{dt} \frac{\partial L}{\partial \dot{\mathbf{q}}} \cdot \delta\mathbf{q} \right) dt \end{aligned} \tag{3.27}$$

$$\int_{t_0}^{t_1} \left(\frac{\partial \tilde{L}}{\partial \lambda_{\theta_1}} \delta\lambda_{\theta_1} \right) dt = \int_{t_0}^{t_1} \left\{ \left[q_3 - \theta_1(t) \right] \delta\lambda_{\theta_1} \right\} dt \tag{3.28}$$

Eventually, by combining the previous results, Equations (3.26-3.28), in Equation (3.24), we obtain,

$$\int_{t_0}^{t_1} \left\{ \left(\frac{\partial L}{\partial \mathbf{q}} - \frac{d}{dt} \frac{\partial L}{\partial \dot{\mathbf{q}}} + \mathbf{Q} \right) \cdot \delta\mathbf{q} + \lambda_{\theta_1} \delta q_3 + \left[q_3 - \theta_1(t) \right] \delta\lambda_{\theta_1} \right\} dt = 0 \tag{3.29}$$

Equation (3.29) holds for any interval of time $t_0 < t < t_1$ and it is satisfied for any variation of q_h, as follows,

$$\begin{aligned} \frac{\partial L}{\partial q_3} - \frac{d}{dt} \frac{\partial L}{\partial \dot{q}_3} + Q_3 + \lambda_{\theta_1} = 0, \qquad & \forall \delta q_3 \\ \frac{\partial L}{\partial q_h} - \frac{d}{dt} \frac{\partial L}{\partial \dot{q}_h} + Q_h = 0, \qquad & \forall \delta q_h \text{ with } h \neq 3 \end{aligned} \tag{3.30}$$

3.B Total energy of the system

In accordance with [37] the total energy of the system can be evaluated by starting from the time derivative of the Lagrangian function,

$$\begin{aligned}\frac{d}{dt}\tilde{L}(\dot{\mathbf{q}},\mathbf{q},t,\lambda_{\theta_1}) &= \frac{\partial\tilde{L}}{\partial\mathbf{q}}\cdot\frac{\partial\mathbf{q}}{\partial t}+\frac{\partial\tilde{L}}{\partial\dot{\mathbf{q}}}\cdot\frac{\partial\dot{\mathbf{q}}}{\partial t}+\cancel{\frac{\partial\tilde{L}}{\partial t}\frac{\partial t}{\partial t}}+\frac{\partial\tilde{L}}{\partial\lambda_{\theta_1}}\frac{\partial\lambda_{\theta_1}}{\partial t}\\ &= \frac{\partial\tilde{L}}{\partial\mathbf{q}}\cdot\dot{\mathbf{q}}+\frac{\partial\tilde{L}}{\partial\dot{\mathbf{q}}}\cdot\ddot{\mathbf{q}}+\frac{\partial\tilde{L}}{\partial t}+\frac{\partial\tilde{L}}{\partial\lambda_{\theta_1}}\dot{\lambda}_{\theta_1}\end{aligned} \tag{3.31}$$

and, therefore, evaluated in an interval of time $t_0 < t < t_1$,

$$\begin{aligned}\int_{t_0}^{t_1}\left[\frac{d}{dt}\tilde{L}(\dot{\mathbf{q}},\mathbf{q},t,\lambda_{\theta_1})\right]dt = \int_{t_0}^{t_1}\Bigg[&\frac{\partial\tilde{L}}{\partial\mathbf{q}}\cdot\dot{\mathbf{q}}+\frac{\partial\tilde{L}}{\partial\dot{\mathbf{q}}}\cdot\ddot{\mathbf{q}}+\\ &+\frac{\partial\tilde{L}}{\partial t}+\frac{\partial\tilde{L}}{\partial\lambda_{\theta_1}}\dot{\lambda}_{\theta_1}\Bigg]dt\end{aligned} \tag{3.32}$$

where the single terms of the previous Equation (3.32) reads,

$$\begin{aligned}&\int_{t_0}^{t_1}\left[\frac{d}{dt}\tilde{L}(\dot{\mathbf{q}},\mathbf{q},t,\lambda_{\theta_1})\right]dt = \tilde{L}\Big|_{t_0}^{t_1} = \{L+\lambda_{\theta_1}[q_3-\theta_1(t)]\}\Big|_{t_0}^{t_1}\\ &\int_{t_0}^{t_1}\left(\frac{\partial\tilde{L}}{\partial\mathbf{q}}\cdot\dot{\mathbf{q}}\right)dt = \int_{t_0}^{t_1}\left(\frac{\partial L}{\partial\mathbf{q}}\cdot\dot{\mathbf{q}}+\lambda_{\theta_1}\dot{q}_3\right)dt\\ &\int_{t_0}^{t_1}\left(\frac{\partial\tilde{L}}{\partial\dot{\mathbf{q}}}\cdot\ddot{\mathbf{q}}\right)dt = \left(\frac{\partial\tilde{L}}{\partial\dot{\mathbf{q}}}\cdot\dot{\mathbf{q}}\right)\Bigg|_{t_0}^{t_1}-\int_{t_0}^{t_1}\left(\frac{d}{dt}\frac{\partial\tilde{L}}{\partial\dot{\mathbf{q}}}\cdot\dot{\mathbf{q}}\right)dt\\ &\qquad\qquad = \left(\frac{\partial L}{\partial\dot{\mathbf{q}}}\cdot\dot{\mathbf{q}}\right)\Bigg|_{t_0}^{t_1}-\int_{t_0}^{t_1}\left(\frac{d}{dt}\frac{\partial L}{\partial\dot{\mathbf{q}}}\cdot\dot{\mathbf{q}}\right)dt\end{aligned}$$

$$\int_{t_0}^{t_1}\left(\frac{\partial \tilde{L}}{\partial t}\right)dt = \int_{t_0}^{t_1}\left(\cancelto{0}{\frac{\partial L}{\partial t}} + \frac{\partial \lambda_{\theta_1}[q_3-\theta_1(t)]}{\partial t}\right)dt$$
$$= -\int_{t_0}^{t_1}\lambda_{\theta_1}\dot{\theta}_1(t)dt$$
$$\int_{t_0}^{t_1}\left(\frac{\partial \tilde{L}}{\partial \lambda_{\theta_1}}\dot{\lambda}_{\theta_1}\right)dt = \int_{t_0}^{t_1}\left\{[q_3-\theta_1(t)]\,\dot{\lambda}_{\theta_1}\right\}dt$$

By using the system reported in Equation (3.30) and by taking advantage of the fact that in solution $q_3 = \theta_1(t)$ and its time derivative $\dot{q}_3 = \dot{\theta}_1(t)$ we can,

$$\left(L - \frac{\partial L}{\partial \dot{\mathbf{q}}}\cdot\dot{\mathbf{q}} + \lambda_{\theta_1}\cancel{[q_3-\theta_1(t)]}\right)\Bigg|_{t_0}^{t_1} = \int_{t_0}^{t_1}\Bigg\{\left(\frac{\partial L}{\partial \mathbf{q}} - \frac{d}{dt}\frac{\partial L}{\partial \dot{\mathbf{q}}}\right)\cdot\dot{\mathbf{q}} +$$
$$+\cancel{[\dot{q}_3-\dot{\theta}_1(t)]}\,\lambda_{\theta_1} + \cancel{[q_3-\theta_1(t)]}\,\dot{\lambda}_{\theta_1}\Bigg\}dt$$
$$\left(L - \frac{\partial L}{\partial \dot{\mathbf{q}}}\cdot\dot{\mathbf{q}}\right)\Bigg|_{t_0}^{t_1} = -\int_{t_0}^{t_1}\left(\mathbf{Q}\cdot\dot{\mathbf{q}} + \lambda_{\theta_1}\dot{q}_3\right)dt \tag{3.33}$$

Furthermore, in solution, we can rewrite Equation (3.33) in a more compact way,

$$\left(\frac{\partial \tilde{L}}{\partial \dot{\mathbf{q}}}\cdot\dot{\mathbf{q}} - \tilde{L}\right)\Bigg|_{t_0}^{t_1} = \int_{t_0}^{t_1}\left(\mathbf{Q}\cdot\dot{\mathbf{q}} - \frac{\partial \tilde{L}}{\partial t}\right)dt \tag{3.34}$$

As reported in Equation (3.7) L is nothing but the difference between the kinetic energy and the elastic energy,

$$\begin{aligned}\frac{\partial \tilde{L}(\mathbf{q},\dot{\mathbf{q}},t)}{\partial \dot{\mathbf{q}}} &= \frac{\partial}{\partial \dot{\mathbf{q}}}\left[L(\mathbf{q},\dot{\mathbf{q}}) + f(\mathbf{q},t)]\right) = \\ &= \frac{\partial L(\mathbf{q},\dot{\mathbf{q}})}{\partial \dot{\mathbf{q}}} = \\ &= \frac{\partial}{\partial \dot{\mathbf{q}}}\left[T(\mathbf{q},\dot{\mathbf{q}}) - E(\mathbf{q})\right] = \\ &= \frac{\partial T(\mathbf{q},\dot{\mathbf{q}})}{\partial \dot{\mathbf{q}}}\end{aligned} \tag{3.35}$$

Now if T is defined as a quadratic form (as a matter of fact, it holds in the present work),

$$T(\mathbf{q},\dot{\mathbf{q}}) = \frac{1}{2}A(\mathbf{q})\dot{\mathbf{q}}\cdot\dot{\mathbf{q}} \qquad \Rightarrow \qquad \frac{\partial T(\mathbf{q},\dot{\mathbf{q}})}{\partial \dot{\mathbf{q}}} = A(\mathbf{q})\dot{\mathbf{q}} \tag{3.36}$$

where $A(\mathbf{q}) \in Sym$. Now, by combining Equation (3.36) in Equation (3.35) we obtain,

$$\frac{\partial \tilde{L}(\mathbf{q},\dot{\mathbf{q}},t)}{\partial \dot{\mathbf{q}}}\cdot\dot{\mathbf{q}} = \frac{\partial T(\mathbf{q},\dot{\mathbf{q}})}{\partial \dot{\mathbf{q}}}\cdot\dot{\mathbf{q}} = A(\mathbf{q})\dot{\mathbf{q}}\cdot\dot{\mathbf{q}} = 2T(\mathbf{q},\dot{\mathbf{q}}) \tag{3.37}$$

That is the double of the kinetic energy of the system. Therefore the first term of Equation (3.34) is nothing but the total energy of the system evaluated in a time interval between t_0 and t_1,

$$\left(\frac{\partial \tilde{L}}{\partial \dot{\mathbf{q}}}\cdot\dot{\mathbf{q}} - \tilde{L}\right)\Bigg|_{t_0}^{t_1} = (2T - T + V)\Big|_{t_0}^{t_1} = (T+V)\Big|_{t_0}^{t_1} = E_{tot}\Big|_{t_0}^{t_1} \tag{3.38}$$

4

Euler-Lagrange equations for a continuous inextensible elastic rod

This chapter presents an extension to the analytical part treated in the previous chapter. The Lagrangian formalism of field theory is applied, in order to analytically derive the equations of motion for a continuous inextensible elastic rod. The proposed extension, once integrated, has the purpose to provide a more accurate and computationally fast tool with respect the Abaqus model (see Chapter 3) for describing the locomotion in soil-like medium.

The first section, Section 4.1, is dedicated to the most intuitive way to develop the extension. Three fields are considered: horizontal and vertical positions, as well as the rotation of the rod. The fields are functions of the curvilinear abscissa s and time t. The elastica is, therefore, subjected to a monogenic force, due to

the presence of the viscous environment, while a rotation is imposed on one of the two ends. This rotation is taken into account as a concentrated rheonomic constraint. The formulation leads to a system of integro-partial differential equations presented in a non-dimensional form.

Section 4.2 reformulates the problem, in order to provide a set of equations of motion easier to manipulate and integrate.

In Section 4.3, we present another formulation, by taking advantage of d'Alambert principle (virtual work principle in dynamics) in order to provide a formulation that could be, in future, implemented in FEniCS [2], a python-based open-source package for finite element analysis.

4.1 A first approach: three fields

4.1.1 A variational approach to the derivation of the equations of motion

We start by defining the kinematics of an inextensible rod, which is rectilinear in its undeformed configuration. The variable s is introduced, in order to span the total length l of the rod, $s \in [0, l]$. We describe our rod by introducing three fields: two positionals collected in the position vector $\mathbf{r} = \{x, y\}$ and one that describes the rotation θ along the curvilinear abscissa s at each instant of time,

$$\phi_1 = x(s,t); \quad \phi_2 = y(s,t); \quad \phi_3 = \theta(s,t) \tag{4.1}$$

The inextensibility is introduced in the model through the following conditions on the spatial derivatives,

$$x'(s,t) = \cos\theta(s,t) \tag{4.2a}$$
$$y'(s,t) = \sin\theta(s,t) \tag{4.2b}$$

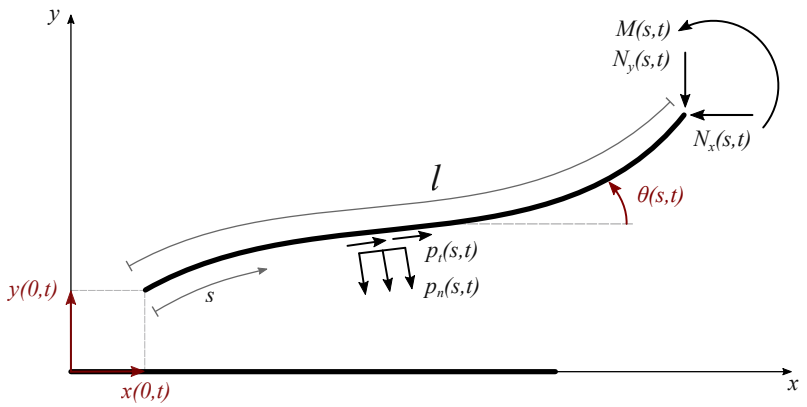

Figure 4.1.1: Schematics of the rod. Positional fields and rotation are represented in red, while the Cartesian reference frame is depicted in grey. Distributed tangential and normal viscous loads are applied to the rod by the environment (p_t, p_n). At the right end of the rod the generalised internal forces, which are functions of the abscissa s and time t, are displayed. The forces must be null at the free end.

By integrating the previous equations, they return the definitions of the positional fields $x(s,t)$ and $y(s,t)$, where the integration constants, $x(0,t)$ and $y(0,t)$, describe the position of the tip at $s = 0$,

$$x(s,t) = x(0,t) + \int_0^s \cos\theta(s,t)ds \tag{4.3a}$$

$$y(s,t) = y(0,t) + \int_0^s \sin\theta(s,t)ds \tag{4.3b}$$

The derivative with respect to time, the velocity, is simply,

$$\dot{x}(s,t) = \dot{x}(0,t) - \int_0^s \dot{\theta}(s,t)\sin\theta(s,t)ds \tag{4.4a}$$

$$\dot{y}(s,t) = \dot{y}(0,t) + \int_0^s \dot{\theta}(s,t)\cos\theta(s,t)ds \tag{4.4b}$$

The rheonomic constraint is applied at $s = 0$ of the rod and is expressed by an explicit function of time $g(t)$ with,

$$\theta(0,t) = g(t) \tag{4.5}$$

The functional $L(t)$, in order to take into account the constraints and still assume the form of a free variational problem, must be defined as,

$$\begin{aligned} L(t) = \mathcal{T}(t) - \mathcal{V}(t) + \int_0^l N_x(s,t)\left[x'(s,t) - \cos\theta(s,t)\right] ds + \\ + \int_0^l N_y(s,t)\left[y'(s,t) - \sin\theta(s,t)\right] ds + \\ + M(0,t)\left[\theta(0,t) - g(t)\right] \end{aligned} \tag{4.6}$$

where $N_x(s,t)$ and $N_y(s,t)$ are the λ-parameters, that mechanically represent the vertical and horizontal components of the axial internal forces. These forces, as we have already seen in Section 2.3.3, arise in order to maintain a constraint, in this specific case: the inextensibility. The quantity $M(s,t)|_{s=0}$ plays the same role, since it represents the concentrated momentum that reacts to the rheonomic constraint, at $s = 0$, where the rotation is imposed. The kinetic energy can be expressed in the following way,

$$\mathcal{T} = \frac{1}{2}\int_0^l \gamma\left[\dot{x}(s,t)^2 + \dot{y}(s,t)^2\right] ds \tag{4.7}$$

where γ is the linearly distributed density of the rod. Furthermore, the potential energy can be identify as the elastic energy of the deformed rod, while shear forces are neglected, due to the rods slenderness. Hence, the curvature $\chi = \theta'$ is proportional to the bending moment[7] as follows,

[7] This is, actually, the Bernoulli assumption for slender beams as reported in [15] and used in [6]

$$\begin{aligned} \mathcal{V} \equiv \mathcal{E} &= \frac{1}{2}\int_0^l M(s,t)\theta'(s,t) ds \\ &= \frac{1}{2}\int_0^l B\theta'(s,t)\theta'(s,t) ds \\ &= \frac{1}{2}\int_0^l B\theta'(s,t)^2 ds \end{aligned} \tag{4.8}$$

With the principle of least action, one can find the positional and rotational fields that make the functional $L(t)$ stationary with,

$$\delta\mathcal{A}(t) = \delta\int_{t_0}^{t_1} L(t)dt = \delta\int_{t_0}^{t_1}\left\{\int_0^l \mathcal{L}\,ds + \right. \\ \left. + M_0\left[\theta_0 - g(t)\right]\right\}dt \quad (4.9)$$

where $M_0 = M(s,t)|_{s=0}$ and $\theta_0 = \theta(s,t)|_{s=0}$, while $\mathcal{L}$ is the Lagrangian density, defined as,

$$\mathcal{L} = \frac{1}{2}\left[\gamma\left(\dot{x}^2+\dot{y}^2\right) - B(\theta')^2\right] + N_x\left(x' - \cos\theta\right) + \\ + N_y\left(y' - \sin\theta\right) \quad (4.10)$$

which is an explicit function of $\mathcal{L} = \mathcal{L}\left(\theta, \dot{x}, \dot{y}, x', y', \theta', N_x, N_y\right)$. By applying the definition of Equation (3.38), the first variation of the Lagrangian density reads,

$$\int_{t_0}^{t_1}\int_0^l \delta\mathcal{L}\;ds\;dt = \int_{t_0}^{t_1}\int_0^l \Big(\mathcal{L}_\theta\delta\theta + \mathcal{L}_{\dot{x}}\delta\dot{x} + \mathcal{L}_{\dot{y}}\delta\dot{y} + \mathcal{L}_{x'}\delta x' + \\ + \mathcal{L}_{y'}\delta y' + \mathcal{L}_{\theta'}\delta\theta' + \mathcal{L}_{N_x}\delta N_x + \mathcal{L}_{N_y}\delta N_y\Big)\;ds\;dt \quad (4.11)$$

where $\mathcal{L}_q = \frac{\partial\mathcal{L}}{\partial q}$ as shown in Section 2.4. In order to release the derivatives of $\delta\dot{x}$, $\delta\dot{y}$, $\delta x'$, $\delta y'$ and $\delta\theta'$ we apply integration by parts

to those terms of $\mathcal{L}$ which display the aforementioned variations,

$$\int_{t_0}^{t_1} (\mathcal{L}_{\dot{x}}\delta\dot{x})\, dt = \cancelto{0}{\mathcal{L}_{\dot{x}}\delta x\Big|_{t_0}^{t_1}} - \int_{t_0}^{t_1} \left(\frac{\partial \mathcal{L}_{\dot{x}}}{\partial t}\delta x\right) dt$$

$$\int_{t_0}^{t_1} (\mathcal{L}_{\dot{y}}\delta\dot{y})\, dt = \cancelto{0}{\mathcal{L}_{\dot{y}}\delta y\Big|_{t_0}^{t_1}} - \int_{t_0}^{t_1} \left(\frac{\partial \mathcal{L}_{\dot{y}}}{\partial t}\delta y\right) dt$$

$$\int_0^l (\mathcal{L}_{x'}\delta x')\, ds = \mathcal{L}_{x'}\delta x\Big|_0^l - \int_0^l \left(\frac{\partial \mathcal{L}_{x'}}{\partial s}\delta x\right) ds$$

$$\int_0^l (\mathcal{L}_{y'}\delta y')\, ds = \mathcal{L}_{\dot{y}}\delta y\Big|_0^l - \int_0^l \left(\frac{\partial \mathcal{L}_{y'}}{\partial s}\delta y\right) ds$$

$$\int_0^l (\mathcal{L}_{\theta'}\delta\theta')\, ds = \mathcal{L}_{\dot{\theta}}\delta\theta\Big|_0^l - \int_0^l \left(\frac{\partial \mathcal{L}_{\theta'}}{\partial s}\delta\theta\right) ds$$

Note that the terms evaluated at the borders of the temporal domain must vanish, as pointed out in Section 2.2.3. Equation (4.11) combined with the previous calculations takes up the form,

$$\begin{aligned}\int_{t_0}^{t_1}\int_0^s \delta\mathcal{L}\, ds\, dt = \int_{t_0}^{t_1} \Bigg\{ &\mathcal{L}_{x'}\delta x\Big|_0^l + \mathcal{L}_{y'}\delta y\Big|_0^l + \mathcal{L}_{\theta'}\delta\theta\Big|_0^l + \\ - \int_0^s \Bigg[&\left(\frac{\partial \mathcal{L}_{\dot{x}}}{\partial t} + \frac{\partial \mathcal{L}_{x'}}{\partial s}\right)\delta x + \left(\frac{\partial \mathcal{L}_{\dot{y}}}{\partial t} + \frac{\partial \mathcal{L}_{y'}}{\partial s}\right)\delta y + \\ &+ \left(\frac{\partial \mathcal{L}_{\theta'}}{\partial s} - \mathcal{L}_{\theta}\right)\delta\theta - \mathcal{L}_{N_x}\delta N_x - \mathcal{L}_{N_y}\delta N_y \Bigg] ds \Bigg\} dt \end{aligned} \tag{4.12}$$

Finally, the variation of the action must vanish, which allows us to write Equation (4.9) as,

$$\delta\mathcal{A} = \int_{t_0}^{t_1} \left\{ L_{M_0}\delta M_0 + L_{\theta_0}\delta\theta_0 + \int_0^s \delta\mathcal{L}\, ds \right\} dt = 0 \tag{4.13}$$

Due to the fact that t_0 and t_1 as well as the variations (which by definition are virtual) are chosen arbitrarily, the following expressions must hold true, in order to let $\delta\mathcal{A}$ vanish,

$$\forall\delta x \implies \frac{\partial\mathcal{L}_{x'}}{\partial s} + \frac{\partial\mathcal{L}_{\dot{x}}}{\partial t} = 0 \tag{4.14a}$$

$$\forall\delta y \implies \frac{\partial\mathcal{L}_{y'}}{\partial s} + \frac{\partial\mathcal{L}_{\dot{y}}}{\partial t} = 0 \tag{4.14b}$$

$$\forall\delta\theta \implies \frac{\partial\mathcal{L}_{\theta'}}{\partial s} - \mathcal{L}_{\theta} = 0 \tag{4.14c}$$

$$\forall\delta x_0 \implies \mathcal{L}_{x'}|_{s=0} = 0 \tag{4.14d}$$

$$\forall\delta x_l \implies \mathcal{L}_{x'}|_{s=l} = 0 \tag{4.14e}$$

$$\forall\delta y_0 \implies \mathcal{L}_{y'}|_{s=0} = 0 \tag{4.14f}$$

$$\forall\delta y_l \implies \mathcal{L}_{y'}|_{s=l} = 0 \tag{4.14g}$$

$$\forall\delta\theta_0 \implies \mathcal{L}_{\theta'}|_{s=0} + L_{\theta_0} = 0 \tag{4.14h}$$

$$\forall\delta\theta_l \implies \mathcal{L}_{\theta'}|_{s=l} = 0 \tag{4.14i}$$

$$\forall\delta N_x \implies \mathcal{L}_{N_x} = 0 \tag{4.14j}$$

$$\forall\delta N_y \implies \mathcal{L}_{N_y} = 0 \tag{4.14k}$$

$$\forall\delta M_0 \implies L_{M_0} = 0 \tag{4.14l}$$

Here, Equations (4.14a-c) represent the equations of motions of the system in object; Equations (4.14d-i) are the boundary conditions applied to the spatial boundaries $s = 0, l$; the final three conditions to be satisfy are the constraints, where (4.14j) and (4.14k) represent the inextensibility, while (4.14l) is the imposed rotation at $s = 0$.

Let us, now, evaluate Equation (4.14) starting from the definitions (4.9) and (4.10) with,

$$\int_0^l \mathcal{L}_\theta \delta\theta ds = \int_0^l \left(N_x \sin\theta - N_y \cos\theta\right) \delta\theta ds$$
$$\int_0^l \frac{\partial \mathcal{L}_{\theta'}}{\partial s} \delta\theta ds = -\frac{1}{2}\int_0^l \frac{\partial}{\partial s}\left(2B\theta'\right) \delta\theta ds = -\int_0^l B\theta'' \delta\theta ds$$
$$\int_0^l \frac{\partial \mathcal{L}_{x'}}{\partial s} \delta x ds = \int_0^l \frac{\partial N_x}{\partial s} \delta x ds = \int_0^l N_x' \delta x ds$$
$$\int_0^l \frac{\partial \mathcal{L}_{\dot{x}}}{\partial t} \delta x ds = \frac{1}{2}\int_0^l \frac{\partial}{\partial s}\left(2\gamma\dot{x}\right) \delta x ds = \int_0^l \gamma\ddot{x}\delta x ds$$
$$\int_0^l \frac{\partial \mathcal{L}_{y'}}{\partial s} \delta y ds = \int_0^l \frac{\partial N_y}{\partial s} \delta y ds = \int_0^l N_y' \delta y ds$$
$$\int_0^l \frac{\partial \mathcal{L}_{\dot{y}}}{\partial t} \delta y ds = \frac{1}{2}\int_0^l \frac{\partial}{\partial s}\left(2\gamma\dot{y}\right) \delta y ds = \int_0^l \gamma\ddot{y}\delta y ds$$

Moreover, due to the concentrated momentum working on the imposed rotational constraint the following two equations hold,

$$L_{\theta_0}\delta\theta_0 = M_0\delta\theta_0$$
$$L_{M_0}\delta M_0 = \left(\theta_0 - g(t)\right)\delta M_0$$

Eventually, the equations of motion (4.14a-c) assume this form,

$$\gamma\ddot{x}(s,t) + {N_x}'(s,t) = 0 \tag{4.15a}$$
$$\gamma\ddot{y}(s,t) + {N_y}'(s,t) = 0 \tag{4.15b}$$
$$B\theta''(s,t) + N_x(s,t)\sin\theta(s,t) - N_y(s,t)\cos\theta(s,t) = 0 \tag{4.15c}$$

Furthermore, the boundary conditions result to be (4.14d-i),

$$N_x(0,t) = 0 \tag{4.16a}$$
$$N_x(l,t) = 0 \tag{4.16b}$$
$$N_y(0,t) = 0 \tag{4.16c}$$
$$N_y(l,t) = 0 \tag{4.16d}$$
$$M(0,t) = -B\frac{\partial\theta(s,t)}{\partial t}\bigg|_{s=0} \tag{4.16e}$$
$$M(l,t) = 0 \tag{4.16f}$$

We would like to point out that the previous conditions respect the physics of the problem. More precisely, the boundary conditions highlight where the internal forces must vanish, because of the free end at $s = l$, while at the opposing end, at $s = 0$, where the rotational constraint is applied, a concentrated moment must arise, in order to maintain the kinematic equilibrium. Finally, in a very natural way, also the constraint equations (4.14j-l) are recovered from the formulation,

$$x'(s,t) = \cos\theta(s,t) \tag{4.17a}$$
$$y'(s,t) = \sin\theta(s,t) \tag{4.17b}$$
$$\theta(0,t) = g(t) \tag{4.17c}$$

Non-conservative dissipative forces At this point, we need to add the interaction with the environment, which is introduced as a distributed load. This load, acting along all the body, has three characteristics: i) it is dissipative and viscous, that means it is proportional to the velocities at each point and opposing their directions; ii) it is following, which entails that it is dependent of the local orientation of the system; and iii) it is anisotropic, meaning that it behaves differently in the tangential direction with respect to the normal direction. Therefore, We can split the load p in a

vectorial sum of two vectors,

$$\mathbf{p} = \mathbf{p}_t + \mathbf{p}_n \tag{4.18}$$

where $\mathbf{p}_t$ is acting in the tangential and $\mathbf{p}_n$ in the normal direction. The expressions of the two vectors are,

$$\mathbf{p}_t = -\xi_t \left(\dot{\mathbf{r}} \cdot \mathbf{t}\right) \mathbf{t} \tag{4.19}$$

$$\mathbf{p}_n = -\xi_n \left(\dot{\mathbf{r}} \cdot \mathbf{n}\right) \mathbf{n} \tag{4.20}$$

where, $\xi_n > \xi_t$ are the parameters of proportionality of the velocities. The inequality is justified by geometric factors related to, for example, the angle at which the surface of the body moves against the environment. $\mathbf{t}$ and $\mathbf{n}$ are the unit vector of the local reference frame,

$$\mathbf{t} = \{\cos\theta, \sin\theta\} \tag{4.21}$$

$$\mathbf{n} = \{-\sin\theta, \cos\theta\} \tag{4.22}$$

By substituting (4.19) through (4.22) in Equation (4.18) we obtain the following form for the load $\mathbf{p}$,

$$\begin{aligned} \mathbf{p} &= \begin{bmatrix} -\dot{x}\left(\xi_t \cos^2\theta + \xi_n \sin^2\theta\right) - \dot{y}\left(\xi_t - \xi_n\right)\sin\theta\cos\theta \\ -\dot{x}\left(\xi_t - \xi_n\right)\sin\theta\cos\theta - \dot{y}\left(\xi_t \sin^2\theta + \xi_n \cos^2\theta\right) \end{bmatrix} \\ &= \begin{bmatrix} -\xi_t \cos^2\theta + \xi_n \sin^2\theta & -\left(\xi_t - \xi_n\right)\sin\theta\cos\theta \\ -\left(\xi_t - \xi_n\right)\sin\theta\cos\theta & -\xi_t \sin^2\theta + \xi_n \cos^2\theta \end{bmatrix} \begin{bmatrix} \dot{x} \\ \dot{y} \end{bmatrix} \end{aligned} \tag{4.23}$$

As treated in Section 2.1.5 we can recognise the structure of Equation (2.30), here reported as,

$$p_i = \sum_{j=1}^{2} c_{ij} \dot{r}_j \tag{4.24}$$

where the c_{ij} are the dissipative coefficients, while $\dot{r}_1$, $\dot{r}_2$, in this case, result to be $\dot{x}$, $\dot{y}$, respectively. Therefore, Rayleigh's dissipative function can be written as,

$$\mathcal{R} = \sum_{i,j=1}^{2} c_{ij}\dot{r}_i\dot{r}_j \tag{4.25}$$

which enters the right-hand-side of the equation of motion (see e.g. Section 2.4 Equation (2.112)) in the following way,

$$\frac{\partial \mathcal{L}_{\phi_i'}}{\partial s} + \frac{\partial \mathcal{L}_{\dot{\phi}_i}}{\partial t} - \mathcal{L}_{\phi_i} = \frac{\partial \mathcal{R}_{\dot{\phi}_i}}{\partial t} \tag{4.26}$$

Alternatively we can proceed with the more general method by writing down the infinitesimal virtual work of the forces that must be added to the formulation of the Lagrangian function, Equation (4.6), with,

$$\begin{aligned} \delta w_p &= \int_0^l \sum_{i=1}^{3} \mathbf{p} \cdot \frac{\partial \mathbf{r}}{\partial \phi_i}\, \delta\phi_i \, ds \\ &= \int_0^l \left(p_x \delta x + p_y \delta y\right) ds \end{aligned} \tag{4.27}$$

Note that δw_p is a function of the variations of the two positional fields, δx and δy. Then, (4.14a-b) are the only two equations that are affected by the previous considerations and become,

$$\frac{\partial \mathcal{L}_{x'}}{\partial s} + \frac{\partial \mathcal{L}_{\dot{x}}}{\partial t} = p_x \tag{4.28a}$$

$$\frac{\partial \mathcal{L}_{y'}}{\partial s} + \frac{\partial \mathcal{L}_{\dot{y}}}{\partial t} = p_y \tag{4.28b}$$

Moreover, between the two formulations subsist the relation,

$$p_x = \frac{\partial \mathcal{R}_{\dot{x}}}{\partial t}$$

$$p_y = \frac{\partial \mathcal{R}_{\dot{y}}}{\partial t}$$

Finally, we can rewrite the Equations (4.15) by taking into account the dissipative force, Equation (4.23), with,

$$\gamma \ddot{x}(s,t) + N_x{}'(s,t) = -\dot{x}(s,t)\big(\xi_t \cos^2\theta(s,t) + \\ + \xi_n \sin^2\theta(s,t)\big) - \dot{y}(s,t)\,(\xi_t - \xi_n)\sin\theta(s,t)\cos\theta(s,t) \tag{4.29a}$$

$$\gamma \ddot{y}(s,t) + N_y{}'(s,t) = -\dot{x}(s,t)\,(\xi_t - \xi_n)\sin\theta(s,t)\cos\theta(s,t) \\ - \dot{y}(s,t)\,\big(\xi_t \sin^2\theta(s,t) + \xi_n \cos^2\theta(s,t)\big) \tag{4.29b}$$

$$B\theta''(s,t) + N_x(s,t)\sin\theta(s,t) - N_y(s,t)\cos\theta(s,t) = 0 \tag{4.29c}$$

This system needs to be solved under the consideration of the boundary conditions from Equations (4.16) and Equations (4.17). Also some suitable initial conditions are required, which fundamentally determine the configuration of the rod at the beginning of time, and may be set to,

$$\theta(s,0) = 0 \tag{4.30a}$$

$$x(s,0) = x_0(0) + \int_0^s \cos\theta(s,0)ds = x_0 + s = s \tag{4.30b}$$

$$y(s,0) = y_0(0) + \int_0^s \sin\theta(s,0)ds = y_0 + s = y_0 = 0 \tag{4.30c}$$

where x_0 and y_0 are the position of the point $s = 0$ of the body. For simplicity, we make them coincide with the origin of the reference frame: $\{x_0(0), y_0(0)\} = \{0, 0\}$. In order to obtain a well-posed problem, we must impose the initial velocity values of the fields,

with,

$$\dot{\theta}(s,0) = 0 \tag{4.31a}$$

$$\dot{x}(s,0) = 0 \tag{4.31b}$$

$$\dot{y}(s,0) = 0 \tag{4.31c}$$

These initial conditions in the fields and their time derivatives describe, essentially, the straight and motionless initial configuration of the rod.

As final remark we should point out that the fields $x(s,t)$ and $y(s,t)$ are functions of field $\theta(s,t)$, through an integral, Equation (4.3), that means our system is composed of two second order (in time) integro-partial differential equations of the unknown fields x, y, N_x, N_y, θ and one second order (in space) partial differential equation of the unknown θ, N_x, N_y.

4.1.2 Nondimensional form

We, now, propose a nondimensionalisation of the equations found so far. In order to accomplish this task, we chose the following nondimensional relations,

$$\tilde{s} = \frac{s}{l}; \quad \tilde{x} = \frac{x}{l}; \quad \tilde{y} = \frac{y}{l}; \tag{4.32}$$

$$\tilde{t} = \frac{t}{\tau}; \quad \tau = l\sqrt{\frac{\gamma}{\beta}}; \quad \beta = \frac{B}{l^2}; \quad B = EI; \tag{4.33}$$

$$\tilde{N}_x = \frac{N_x}{\beta}; \quad \tilde{N}_y = \frac{N_y}{\beta}; \quad \tilde{M} = \frac{M}{\alpha}; \quad \alpha = \beta l = \frac{B}{l}; \tag{4.34}$$

$$\tilde{\xi} = \frac{\xi_t}{\xi_n} \leq 1; \tag{4.35}$$

$$\chi = \frac{l^2}{\sqrt{\gamma\beta}}\xi_n; \tag{4.36}$$

Therefore, the nondimensional positional fields that describe the horizontal and vertical position of any point belonging to the rod

become,

$$\tilde{x}\left(\tilde{s},\tilde{t}\right) = \tilde{x}(0,\tilde{t}) + \int_0^{\tilde{s}} \cos\left[\theta\left(\tilde{s},\tilde{t}\right)\right] d\tilde{s} \tag{4.37a}$$

$$\tilde{y}\left(\tilde{s},\tilde{t}\right) = \tilde{y}(0,\tilde{t}) + \int_0^{\tilde{s}} \sin\left[\theta\left(\tilde{s},\tilde{t}\right)\right] d\tilde{s} \tag{4.37b}$$

Note that the rotational field does not need any nondimensionalisation. The equations of motion (4.29) become,

$$\begin{aligned}\frac{\partial^2\tilde{x}}{\partial\tilde{t}^2} + \frac{\partial\tilde{N}_x}{\partial\tilde{s}} = -\chi\Bigg[&\frac{\partial\tilde{x}}{\partial\tilde{t}}\left(\tilde{\xi}\cos^2\theta + \sin^2\theta\right) + \\ &+ \frac{\partial\tilde{y}}{\partial\tilde{t}}\left(\tilde{\xi}-1\right)\sin\theta\cos\theta\Bigg]\end{aligned} \tag{4.38a}$$

$$\begin{aligned}\frac{\partial^2\tilde{y}}{\partial\tilde{t}^2} + \frac{\partial\tilde{N}_y}{\partial\tilde{s}} = -\chi\Bigg[&\frac{\partial\tilde{x}}{\partial\tilde{t}}\left(\tilde{\xi}-1\right)\sin\theta\cos\theta + \\ &+ \frac{\partial\tilde{y}}{\partial\tilde{t}}\left(\tilde{\xi}\sin^2\theta + \cos^2\theta\right)\Bigg]\end{aligned} \tag{4.38b}$$

$$\frac{\partial^2\theta}{\partial\tilde{s}^2} + \tilde{N}_x\sin\theta - \tilde{N}_y\cos\theta = 0 \tag{4.38c}$$

The boundary conditions proposed in Equations (4.16) take the following nondimensional form,

$$\tilde{N}_x(0,\tilde{t}) = 0 \tag{4.39a}$$

$$\tilde{N}_x(1,\tilde{t}) = 0 \tag{4.39b}$$

$$\tilde{N}_y(0,\tilde{t}) = 0 \tag{4.39c}$$

$$\tilde{N}_y(1,\tilde{t}) = 0 \tag{4.39d}$$

$$\tilde{M}(0,\tilde{t}) = -\frac{\partial\theta\left(\tilde{s},\tilde{t}\right)}{\partial\tilde{s}}\bigg|_{\tilde{s}=0} \tag{4.39e}$$

$$\tilde{M}(1,\tilde{t}) = 0 \tag{4.39f}$$

Eventually, the equations of constraint (4.17) assume the expressions,

$$\frac{\partial \tilde{x}(\tilde{s},\tilde{t})}{\partial \tilde{s}} = \cos\theta(\tilde{s},\tilde{t}) \tag{4.40a}$$

$$\frac{\partial \tilde{y}(\tilde{s},\tilde{t})}{\partial \tilde{s}} = \sin\theta(\tilde{s},\tilde{t}) \tag{4.40b}$$

$$\theta\left(0,\tilde{t}\right) = \tilde{g}\left(\tilde{t}\right) \tag{4.40c}$$

The initial conditions (4.30) on the nondimensional fields must be prescribed as,

$$\theta(\tilde{s},0) = 0 \tag{4.41a}$$

$$\tilde{x}(\tilde{s},0) = \tilde{s} \tag{4.41b}$$

$$\tilde{y}(\tilde{s},0) = 0 \tag{4.41c}$$

and their velocities (4.31) evaluated at $t = 0$ become,

$$\left.\frac{\partial \theta(\tilde{s},\tilde{t})}{\partial \tilde{t}}\right|_{t=0} = 0 \tag{4.42a}$$

$$\left.\frac{\partial \tilde{x}(\tilde{s},\tilde{t})}{\partial \tilde{t}}\right|_{t=0} = 0 \tag{4.42b}$$

$$\left.\frac{\partial \tilde{y}(\tilde{s},\tilde{t})}{\partial \tilde{t}}\right|_{t=0} = 0 \tag{4.42c}$$

Despite, the system results being compact and clear it is extremely difficult to be solved (numerically) due to the integral coupling between the positional fields and the rotational one, as expressed in Equations (4.37).

4.2 A second approach: two fields

In order to reduce the fields and pass from a system of integro-partial differential equations (IPDE) to a partial differential equations system, we follow the procedure of the previous section but

this time we substitute θ with its definition,

$$\theta(s,t) = \arctan\left(\frac{y'(s,t)}{x'(s,t)}\right) \tag{4.43}$$

The previous relation can be easily obtained from Equation (4.2): the inextensibility condition. The latter can be reformulated as follows,

$$\Big(x'(s,t)\Big)^2 + \Big(y'(s,t)\Big)^2 - 1 = 0 \tag{4.44}$$

Moreover, it is indispensable to introduce the spatial derivative of θ, named curvature and represented with χ. The curvature is a function of the first and second spatial derivatives of the positional fields,

$$\chi = \frac{\partial\theta}{\partial s} = \frac{y''x' - x''y'}{(x')^2 + (y')^2} \tag{4.45}$$

As in the previous section, the rheonomic rotational constraint is applied at $s = 0$, and reads,

$$\theta(0,t) = \arctan\left(\frac{y'(s,t)\big|_{s=0}}{x'(s,t)\big|_{s=0}}\right) = \arctan\left(\frac{y'_0(s,t)}{x'_0(s,t)}\right) \tag{4.46}$$

An important quantity is the kinetic energy that formally remains unaltered with respect to Section 4.2 and reads,

$$\mathcal{T} = \frac{1}{2}\int_0^l \gamma\left[\dot{x}(s,t)^2 + \dot{y}(s,t)^2\right] ds \tag{4.47}$$

The second important quantity, we must calculate in order to obtain the Lagrangian function is the potential energy that for the problem at hand coincides with the strain energy of the slender elastic body. The definition (4.8) combined with Equation (4.45)

returns,

$$\begin{aligned}\mathcal{V} \equiv \mathcal{E} &= \frac{1}{2}\int_0^l B\chi(s,t)^2 ds \\ &= \frac{1}{2}\int_0^l B\left(\frac{y''x' - x''y'}{x'^2 + y'^2}\right)^2 ds\end{aligned} \tag{4.48}$$

Hence, the Lagrangian function, combined with the constraints through the unknown Lagrangian multipliers λ and Λ, reads,

$$\begin{aligned}L = \mathcal{T} - \mathcal{V} + \int_0^l \lambda(s,t)\left[x'(s,t)^2 + y'(s,t)^2 - 1\right] ds \\ + \Lambda(0,t)\left[\arctan\left(\frac{y_0'(s,t)}{x_0'(s,t)}\right) - g(t)\right]\end{aligned} \tag{4.49}$$

L can be reorganised by introducing a density, defined per unit of length, plus another quantity $\bar{L}$ which takes into account the imposed rotation and its reaction Λ,

$$\begin{aligned}L &= \Lambda(0,t)\left[\arctan\left(\frac{y_0'(s,t)}{x_0'(s,t)}\right) - g(t)\right] + \int_0^l \left\{\frac{\gamma}{2}\left(\dot{x}^2 + \dot{y}^2\right) - \right. \\ &\qquad \left. - \frac{B}{2}\left(\frac{y''x' - x''y'}{x'^2 + y'^2}\right)^2 + \lambda\left(x'^2 + y'^2 - 1\right)\right\} ds \\ &= \bar{L}(\Lambda, x_0', y_0') + \int_0^l \mathcal{L}(\dot{x}, \dot{y}, x', y', x'', y'', \lambda; s, t)\, ds\end{aligned} \tag{4.50}$$

We are, now, ready to perform the variation of the functional $\mathcal{A}$,

$$\begin{aligned}\delta\mathcal{A} &= \int_{t_0}^{t_1} \delta L(\dot{x}, \dot{y}, x', y', x'', y'', \lambda, \Lambda; s, t) dt \\ &= \int_{t_0}^{t_1}\left[\int_0^l \left(\mathcal{L}_{\dot{x}}\delta\dot{x} + \mathcal{L}_{\dot{y}}\delta\dot{y} + \mathcal{L}_{x'}\delta x' + \mathcal{L}_{y'}\delta y' + \right.\right. \\ &\qquad \left.\left. + \mathcal{L}_{x''}\delta x'' + \mathcal{L}_{y''}\delta y'' + \mathcal{L}_{\lambda}\delta\lambda\right) ds + \right. \\ &\qquad \left. + \bar{L}_{\Lambda}\delta\Lambda + \bar{L}_{x_0'}\delta x_0' + \bar{L}_{y_0'}\delta y_0'\right] dt\end{aligned} \tag{4.51}$$

By manipulating those terms characterised by variations of field derivatives and by applying the rule of integration by parts, we obtain,

$$\int_{t_0}^{t_1} \left(\mathcal{L}_{\dot{x}}\delta\dot{x}\right) dt = \cancelto{0}{\mathcal{L}_{\dot{x}}\delta x\Big|_{t_0}^{t_1}} - \int_{t_0}^{t_1} \left(\frac{\partial \mathcal{L}_{\dot{x}}}{\partial t}\delta x\right) dt$$

$$\int_0^l \left(\mathcal{L}_{x'}\delta x'\right) ds = \mathcal{L}_{x'}\delta x\Big|_0^l - \int_0^l \left(\frac{\partial \mathcal{L}_{x'}}{\partial s}\delta x\right) ds$$

$$\int_0^l \left(\mathcal{L}_{x''}\delta x''\right) ds = \mathcal{L}_{x''}\delta x'\Big|_0^l - \frac{\mathcal{L}_{x''}}{\partial s}\delta x\Big|_0^l + \int_0^l \left(\frac{\partial^2 \mathcal{L}_{x''}}{\partial s^2}\delta x\right) ds$$

$$\int_{t_0}^{t_1} \left(\mathcal{L}_{\dot{y}}\delta\dot{y}\right) dt = \cancelto{0}{\mathcal{L}_{\dot{y}}\delta y\Big|_{t_0}^{t_1}} - \int_{t_0}^{t_1} \left(\frac{\partial \mathcal{L}_{\dot{y}}}{\partial t}\delta y\right) dt$$

$$\int_0^l \left(\mathcal{L}_{y'}\delta y'\right) ds = \mathcal{L}_{y'}\delta y\Big|_0^l - \int_0^l \left(\frac{\partial \mathcal{L}_{y'}}{\partial s}\delta y\right) ds$$

$$\int_0^l \left(\mathcal{L}_{y''}\delta y''\right) ds = \mathcal{L}_{y''}\delta y'\Big|_0^l - \frac{\mathcal{L}_{y''}}{\partial s}\delta y\Big|_0^l + \int_0^l \left(\frac{\partial^2 \mathcal{L}_{y''}}{\partial s^2}\delta y\right) ds$$

We can rewrite the variation of the action, which, finally, after equating it with 0, yields,

$$\begin{aligned}
&\int_{t_0}^{t_1} \Bigg\{ \left(\mathcal{L}_{x'} - \frac{\partial \mathcal{L}_{x''}}{\partial s}\right)\delta x\Big|_0^l + \mathcal{L}_{x''}\delta x'\Big|_l + \left(\bar{L}_{x'} - \mathcal{L}_{x''}\right)\delta x'\Big|_0 + \\
&+ \left(\mathcal{L}_{y'} - \frac{\partial \mathcal{L}_{y''}}{\partial s}\right)\delta y\Big|_0^l + \mathcal{L}_{y''}\delta y'\Big|_l + \left(\bar{L}_{y'} - \mathcal{L}_{y''}\right)\delta y'\Big|_0 + \\
&+ \bar{L}_\Lambda \delta\Lambda + \int_0^l \Bigg[\left(\frac{\partial^2 \mathcal{L}_{x''}}{\partial s^2} - \frac{\partial \mathcal{L}_{x'}}{\partial s} - \frac{\partial \mathcal{L}_{\dot{x}}}{\partial t}\right)\delta x + \\
&+ \left(\frac{\partial^2 \mathcal{L}_{y''}}{\partial s^2} - \frac{\partial \mathcal{L}_{y'}}{\partial s} - \frac{\partial \mathcal{L}_{\dot{y}}}{\partial t}\right)\delta y + \mathcal{L}_\lambda \delta\lambda \Bigg] ds \Bigg\} dt = 0 \quad (4.52)
\end{aligned}$$

In order to verify Equation (4.52), defined for arbitrary time limits, the following conditions must be satisfied for all virtual variations,

$$\forall \delta x \implies \frac{\partial^2 \mathcal{L}_{x''}}{\partial s^2} - \frac{\partial \mathcal{L}_{x'}}{\partial s} - \frac{\partial \mathcal{L}_{\dot{x}}}{\partial t} = 0 \tag{4.53a}$$

$$\forall \delta y \implies \frac{\partial^2 \mathcal{L}_{y''}}{\partial s^2} - \frac{\partial \mathcal{L}_{y'}}{\partial s} - \frac{\partial \mathcal{L}_{\dot{y}}}{\partial t} = 0 \tag{4.53b}$$

$$\forall \delta x_0 \implies \mathcal{L}_{x'} - \frac{\partial \mathcal{L}_{x''}}{\partial s} = 0 \tag{4.53c}$$

$$\forall \delta x_l \implies \mathcal{L}_{x'} - \frac{\partial \mathcal{L}_{x''}}{\partial s} = 0 \tag{4.53d}$$

$$\forall \delta y_0 \implies \mathcal{L}_{y'} - \frac{\partial \mathcal{L}_{y''}}{\partial s} = 0 \tag{4.53e}$$

$$\forall \delta y_l \implies \mathcal{L}_{y'} - \frac{\partial \mathcal{L}_{y''}}{\partial s} = 0 \tag{4.53f}$$

$$\forall \delta x'_0 \implies \bar{L}_{x'_0} - \mathcal{L}_{x''} = 0 \tag{4.53g}$$

$$\forall \delta x'_l \implies \mathcal{L}_{x''} = 0 \tag{4.53h}$$

$$\forall \delta y'_0 \implies \bar{L}_{y'_0} - \mathcal{L}_{y''} = 0 \tag{4.53i}$$

$$\forall \delta y'_l \implies \mathcal{L}_{y''} = 0 \tag{4.53j}$$

$$\forall \delta \lambda \implies \mathcal{L}_{\lambda} = 0 \tag{4.53k}$$

$$\forall \delta \Lambda \implies \mathcal{L}_{\Lambda} = 0 \tag{4.53l}$$

The first two Equations (4.53a-b) are the Lagrange equations of motion. From (4.53c) to (4.53j) emerge the spatial boundary conditions, while Equations (4.53k-l) retrieve the applied constraints of Equation (4.44) and Equation (4.46), respectively.

Dissipative distributed force The distributed load, due to the presence of the viscous environment has the same structure as in Section 4.2, here reported with,

$$\mathbf{p} = \underbrace{\left(-\xi_t \left(\dot{\mathbf{r}} \cdot \mathbf{t}\right) \mathbf{t}\right)}_{\mathbf{p}_t} + \underbrace{\left(-\xi_n \left(\dot{\mathbf{r}} \cdot \mathbf{n}\right) \mathbf{n}\right)}_{\mathbf{p}_n} \tag{4.54}$$

In this specific case, we must define the unit vector as a function of $x'(s,t)$ and $y'(s,t)$,

$$\mathbf{t} = \{x', y'\} \tag{4.55}$$
$$\mathbf{n} = \{-y', x'\} \tag{4.56}$$

Therefore, the load $\mathbf{p}$ takes the form,

$$\begin{aligned}\mathbf{p} &= \begin{bmatrix} -\dot{x}\left(\xi_t (x')^2 + \xi_n (y')^2\right) - \dot{y}\left(\xi_t - \xi_n\right) y' x' \\ -\dot{x}\left(\xi_t - \xi_n\right) y' x' - \dot{y}\left(\xi_t (y')^2 + \xi_n (y')^2\right) \end{bmatrix} \\ &= \begin{bmatrix} p_x \\ p_y \end{bmatrix}\end{aligned} \tag{4.57}$$

and affects the equations of motion (4.53a-b) in the following way,

$$\frac{\partial^2 \mathcal{L}_{x''}}{\partial s^2} - \frac{\partial \mathcal{L}_{x'}}{\partial s} - \frac{\partial \mathcal{L}_{\dot{x}}}{\partial t} = -p_x \tag{4.58a}$$
$$\frac{\partial^2 \mathcal{L}_{y''}}{\partial s^2} - \frac{\partial \mathcal{L}_{y'}}{\partial s} - \frac{\partial \mathcal{L}_{\dot{y}}}{\partial t} = -p_y \tag{4.58b}$$

As final observation we want to highlight that the derived system is, now, composed of two (fourth order in space and second order in time) partial differential equations with the unknown quantities $x(s,t), y(s,t), \lambda(s,t)$ and $\Lambda(t)$.

4.3 FEniCS implementation: a trial code

The idea of this section is to provide a formulation of the problem that can be implemented in a FEniCS code.

FEniCS is an open-source software project aimed at solving partial differential equations by taking advantage of the finite element methods and is based on the high-level programming languages Python and C++ [2]. Basically, the program requires a variational form of the problem (weak form), and takes care of

the discretisation into elements, once the user provided the suitable function space [57]. The weak form of the problem is slightly different from the previous two sections. In fact, we provide a function based on the principle of virtual work combined with Lagrange multipliers and, of course, the take care of the inertial part by applying the d'Alambert principle.

The positional fields are expressed as functions of the horizontal $u_x(s,t)$ and vertical $u_y(s,t)$ displacements,

$$x(s,t) = s + u_x(s,t) \tag{4.59}$$
$$y(s,t) = u_y(s,t) \tag{4.60}$$

The spatial derivatives of the two fields are,

$$x'(s,t) = 1 + u'_x(s,t) \tag{4.61}$$
$$y'(s,t) = u'_y(s,t) \tag{4.62}$$

Furthermore, the first time derivative, named velocity $\mathbf{v}(s,t)$ becomes,

$$\dot{x}(s,t) = \dot{u}_x(s,t) \tag{4.63}$$
$$\dot{y}(s,t) = \dot{u}_y(s,t) \tag{4.64}$$

whereas the second time derivative named acceleration $\mathbf{a}(s,t)$ reads,

$$\ddot{x}(s,t) = \ddot{u}_x(s,t) \tag{4.65}$$
$$\ddot{y}(s,t) = \ddot{u}_y(s,t) \tag{4.66}$$

Another field that can be derived from Equations (4.59) is the rotational field,

$$\theta(s,t) = \arctan\left(\frac{y'(s,t)}{x'(s,t)}\right) = \arctan\left(\frac{u'_y(s,t)}{1+u'_x(s,t)}\right) \tag{4.67}$$

and its first spatial derivative: the curvature $\chi(s,t)$ reads,

$$\chi(s,t) = \frac{\partial\theta(s,t)}{\partial s} = \frac{u_y''(1+u_x') - (1+u_x'')u_y'}{(1+u_x')^2 + (u_y')^2} \tag{4.68}$$

which is a nonlinear function of the first and second derivatives of the displacement fields u_x and u_y.

The virtual work principle in dynamics can be expressed as the equality between the virtual internal work and the virtual work done by the inertial and dissipative forces plus the virtual work done by the constraints imposed on the body,

$$\underbrace{\int_\Omega B\chi\delta\chi\, d\omega}_{\text{internal work}} = \overbrace{\int_\Omega \gamma\ddot{\mathbf{r}}\cdot\delta\ddot{\mathbf{r}}\, d\omega - \int_\Omega \mathbf{p}\cdot\delta\mathbf{r}\, d\omega +}^{\text{work inertial and dissipative forces}} \underbrace{+\int_\Omega \delta\left(\lambda c_i\right)\, d\omega + \int_{\partial\tilde{\Omega}} \delta\left(\Lambda C_{ii}\right)\, d\partial\tilde{\omega}}_{\text{work constraints}} \tag{4.69}$$

where $\mathbf{r}$ is the position vector, $\ddot{\mathbf{r}} = \mathbf{a} = \{\ddot{x}(s,t), \ddot{y}(s,t)\}$ the acceleration and $\mathbf{p}$ the distributed dissipative load from Equation (4.57). Let us take a deeper look at the constraints, where $c_i(s,t)$ is the inexstensibility condition applying to the entire domain,

$$\begin{aligned} c_i(s,t) &= \Big(1+u_x'(s,t)\Big)^2 + \Big(u_y'(s,t)\Big)^2 - 1 \\ &= c_i(u_x', u_y'; s, t) \end{aligned} \tag{4.70}$$

while, $C_{ii}(t)$ is, actually, the imposed rotation at the rod's end, where $s = 0$. In fact, the integral is defined along a subset at the boundary of the domain $\delta\tilde{\Omega} = \delta\Omega \setminus \{l\} \implies \delta\tilde{\Omega} = \{0\}$ and is defined as,

$$\begin{aligned} C_{ii}(t) &= \arctan\left(\frac{u_y'(s,t)}{1+u_x'(s,t)}\right)\Bigg|_{s=0} - g(t) \\ &= C_{ii}(u_x', u_y'; 0, t) \end{aligned} \tag{4.71}$$

The variation of the curvature $\chi(u'_x, u'_y, u''_x, u''_y)$ is equal to,

$$\delta\chi = \frac{\partial\chi}{\partial u'_x}\delta u'_x + \frac{\partial\chi}{\partial u'_y}\delta u'_y + \frac{\partial\chi}{\partial u''_x}\delta u''_x + \frac{\partial\chi}{\partial u''_y}\delta u''_y \tag{4.72}$$

Due to the high non-linearity of the problem, we chose an explicit Newmark-β, or *GN*-β [91], time integration scheme, in order to avoid non-linear iterations within one time step. On the one hand, this simplifies the FEniCS code, while on the other hand, the instability of the solver needs to be taken into consideration when selecting the time step. The maximal time step size for an explicit solver is tightly connected to the highest eigenfrequency of the model under study, which to this point, is unknown. Therefore, as a conservative approach, we chose a very small time step size of $\Delta t = 10^{-5}$ s. Once the time step size is chosen, the method can be solved directly for the acceleration $\mathbf{a}_{n+1}$ at the next time step of the simulation and yields the displacement and velocity with,

$$\mathbf{u}_{n+1} = \mathbf{u}_n + \Delta t\mathbf{v}_n + \frac{1}{2}\Delta t^2\mathbf{a}_n \tag{4.73}$$

$$\mathbf{v}_{n+1} = \mathbf{v}_n + (1-\beta)\Delta t\mathbf{a}_n + \beta\Delta t\mathbf{a}_{n+1} \tag{4.74}$$

where $\#_n$ are known quantities at the current time step n, while the vector $\mathbf{a}_{n+1}$ contains the unknown accelerations at the $n+1$-th time step, and $\mathbf{u}_{n+1}$ and $\mathbf{v}_{n+1}$ are the displacements and velocities that need to be updated, respectively.

Therefore, the program requires the functional $\mathcal{F}$, Equation (4.69), in its time discretised form. The above formulas Equations (4.73) and 4.74 must be substituted in the functional, in order to obtain it in function of the following quantities,

$$\mathcal{F} = \mathcal{F}\Big(\underbrace{\mathbf{a}_{n+1}, \lambda, \Lambda}_{\text{unknowns}}; \overbrace{\mathbf{u}_n, \mathbf{v}_n, \mathbf{a}_n}^{\text{knowns}}\Big) \tag{4.75}$$

```
from ufl import *
from dolfin import *
from fenics import *

# Time-stepping parameters
T = 1.0                  # final Time
num_steps = 10**5             # number of time steps
dt = Constant(T / num_steps)  # time step size

# GN-beta method parameter
beta=0.5

#  Material constants
b = 1.0           # base
l = 100.0         # length
E = 1000.0          # Young's modulus
rho = 1.0         # density
I = Constant((b**4)/12)   # inertia
B = Constant(E*I)     # bending stiffness

# Constraint constants
A = 1.0       # amplitude
om = 1.0/(10.0*pi)  # angular frequency

# Viscous constants
xit = 1.0
xin = 5.0

# Mesh and function space
mesh = UnitIntervalMesh(10)       # s \in [0,1]
P1 = FiniteElement('P', interval , 2)   # This is a C^0
     space
el4 = MixedElement([P1, P1, P1, P1])  # Mixed
    formulation for the 4 unknown fields
U = FunctionSpace(mesh, el4)
el2 = MixedElement([P1, P1])
V = FunctionSpace(mesh, el2)

# Define Trial&Test functions
alL_ = TestFunction(U)
u_ = TestFunction(V)
```

```
40
41 # Split trial&test functions to access the components
42 ax_, ay_, lambd_, LAMBD_ = split(alL_)
43 ux_, uy_ = split(u_)
44
45 # Define function for displacement, velocities,
       accelerations and Lagrangian multipliers
46 u = Function(V)
47 v = Function(V)
48 alL = Function(U)
49 u_n = Function(V)
50 v_n = Function(V)
51 alL_n = Function(U)
52
53 # Split functions to access the components
54 ux, uy = split(u)
55 vx, vy = split(v)
56 ax, ay, lambd, LAMBD = split(alL)
57 ux_n, uy_n = split(u_n)
58 vx_n, vy_n = split(v_n)
59 ax_n, ay_n, lambd_n, LAMBD_n = split(alL_n)
60
61 # Define boundary
62 def left(x, on_boundary):
63   return near(x[0], 0) and on_boundary
64
65 ############## time discretisation ####################
66 # Newmark formulas for updating displacement and
       velocity
67 # Displacement
68 def ux_upd(ux_n, vx_n, ax_n):
69   return ux_n + dt*vx_n + dt**2*(ax_n)/2
70
71 def uy_upd(uy_n, vy_n, ay_n):
72   return uy_n + dt*vy_n + dt**2*(ay_n)/2
73
74 # Velocity
75 def vx_upd(vx_n, ax_n, ax):
76   return vx_n + dt*(1 - beta)*ax_n +beta*dt*ax
77
78 def vy_upd(vy_n, ay_n, ay):
```

```
  return vy_n + dt*(1 - beta)*ay_n +beta*dt*ay
############ time discretization ###################

# Define rotation,curvature, constraints
def theta(ux, uy):
  return atan(div(uy)/(1+div(ux)))

def chi(ux, uy):
  return div(theta(ux, uy))

def c(ux, uy):
  return (1+div(ux))**2 + (div(uy))**2 - 1

g = Expression("A*sin(om*t)", A = A, om = om, t=0,
    degree=2)    # g(t) to be update at each time step
def C(ux, uy, g):
  return theta(ux, uy) - g

# Define the nonconservative forces
def px(ux, uy, vx, vy):
  div(uy)*xin*(-div(uy)*vx + vy*(div(ux) + 1)) - xit*(
    div(ux) + 1)*(div(uy)*vy + vx*(div(ux) + 1))

def py(ux, uy, vx, vy):
  -div(uy)*xit*(div(uy)*vy + vx*(div(ux) + 1)) - xin*(
    div(ux) + 1)*(-div(uy)*vx + vy*(div(ux) + 1))

# Variation through the derivative function
def dchi(ux, uy):
  return derivative(chi(ux, uy), u, u_)

def dg(ux, uy):
  return derivative(c(ux, uy), u, u_)

def dh(ux, uy, g):
  return derivative(C(ux, uy, g), u, u_)

F = + rho*(ax*ax_ + ay*ay_)*dx \
  - (B*chi(ux_upd(ux_n,vx_n,ax_n), uy_upd(uy_n,vy_n,
    ay_n))*dchi(ux_upd(ux_n,vx_n,ax_n), uy_upd(uy_n,
    vy_n,ay_n)))*dx \
```

```
  + c(ux_upd(ux_n,vx_n,ax_n), uy_upd(uy_n,vy_n,ay_n))*
    lambd_*dx + lambd*dg(ux_upd(ux_n,vx_n,ax_n), uy_upd
    (uy_n,vy_n,ay_n))*dx \
  + C( ux_upd(ux_n,vx_n,ax_n), uy_upd(uy_n,vy_n,ay_n),g
    )*LAMBD_*ds + LAMBD*dh(ux_upd(ux_n,vx_n,ax_n),
    uy_upd(uy_n,vy_n,ay_n), g)*ds \
  - (px(ux_upd(ux_n, vx_n, ax_n), uy_upd(uy_n,vy_n,ay_n
    ), vx_upd(vx_n,ax_n,ax), vy_upd(vy_n,ay_n,ay))*ux_)
    *dx - (py(ux_upd(ux_n,vx_n,ax_n), uy_upd(uy_n,vy_n,
    ay_n), vx_upd(vx_n,ax_n,ax), vy_upd(vy_n,ay_n,ay))*
    uy_)*dx

# Solver
t = 0
for n in range(num_steps):

  # Update current time
  t += dt

  # Update the rotational constrain
  g.t = t

  # Solve variational problem for time step
  solve(F == 0, alL)

  # Update previous solution
  u_n.assign(u)       # Displacements
  v_n.assign(v)       # Velocities
  alL_n.assign(alL)   # Accelerations and Lagrangian
    multipliers
```

Listing 4.1: Possible code to be implemented in FEniCS

Open problems The numerical solution of the equations due to the high order of derivatives in the non-linear problem proved to be particular difficult. In fact, a proper numerical solution of the problem has not been established thus far. More precisely, the solution of the equations with Mathematica was not yet successful, since Mathematica did not allow the high order of non-linear differential equations in the applied solvers. Futhermore,

another advanced FEM software called FEniCS project was also employed to solve the problem. However, in order to ensure the convergence of any finite element simulation, the *principle of compatibility* demands that the function space, the space where the shape functions are defined, must be continuous at least one order less than the maximum derivative order contained in the functional. Note that in χ, Equation (4.68), the displacement appears with its second derivative, which requires a finite element space of $\mathcal{C}^1$. Unfortunately, FEniCS contains only the standard $\mathcal{C}^0$ finite element space, at the point of this writing, which denies us from solving the equations numerically for the time being. It is worth mentioning though that FEniCS is a rapidly expanding high level finite element package that may support higher order element spaces in the near future.

4.4 Conclusion

This chapter provides the analytical equations of motion for a continuous slender body immersed in a viscous medium represented via resistive forces. While the equations have been established and presented herein, a numerical solution of their application is yet missing. Due to the high level of non-linearities, geometrical in first place and attributed to the applied non conservative forces, even advanced FE software solutions, in particular Mathematica and FEniCS, were not useful to solve the problem. However, once a numerical solver will be established, in principle, these equations may be used to better understand the motion of slender body organisms moving through materials such as sand, soil and other fluid or semi fluid media. Furthermore, they may also be used to control and optimise the motion of bio-inspired soft robots, characterised by components that are actuated continuously along their body.

5

Neurofibres: an ad-hoc experiment for the locomotion

Decades of intense research activities brought an advanced knowledge of spinal cord injury. However, several mechanisms regarding the lesion are still unknown, which inhibits the development of an effective treatment for the pathology. Neurofibres is a Horizon 2020 FET PROACTIVE project, aiming to develop and test a device composed of bio-functionalised electro-conducting microfibres for the regeneration of the lesioned spinal cord tissue. The experiment proposed in this chapter was, originally, intended to test the dynamic behaviour of a microfibre that escaped from the implant. Escaped microfibers, indeed, represent a dangerous issue observed by the partners of the project during

the first phases of the device's testing campaign, and was therefore, requested, specifically by the reviewers of the project, to be studied in more detail.

This chapter aims to experimentally demonstrate the migration of a microfibre, de facto a slender body, surrounded by a viscous medium. Moreover, we give some prescriptions for avoiding the migration of microfibres into the spinal cord tissue.

5.1 Introduction

Spinal cord injury (SCI) is the partial or total loss of continuity of the spinal cord tissue, which leads to the temporary or permanent change of its functions. Every year in the world, from 250˙000 to 500˙000 people suffer from SCI [67]: vehicle crashes, falls, acts of violence and sports/recreation activities are the main causes [31], whereas also non-traumatic spinal cord injuries exist. After decades of research, there is still no gold standard for the treatment of this pathology [36]. While spinal cord injury is not among the top ten causes of death [78], premature death is about 2 to 5 times more frequent in people with a spinal lesion with respect to people with a healthy spinal cord [67].

The complexity of researching an efficient treatment is due to the low regenerative potential of the central nervous system [72]. Shortly after injury, natural tissue regeneration begins, but a degenerative aggressive environment slows it soon, leading to poor regrowth of axons through the diseased area and the consequent formation of impenetrable barriers of scar tissue [30, 35]. However, above and below the site of injury, intact but non-functional circuits persist. Therapies under study try to contrast this degenerative process and address tissue dynamics toward a proper regeneration. A recent study showed a re-population of the injured site by axons grown rostro-caudally and following tortuous paths [34]. This spread growth suggested the need of providing

structural support and guidance for axon regrowth and migration of new neurons to achieve the complete regeneration of the spinal cord tissue after an injury [65]. One of the many different scaffolding units studied to obtain the directional regeneration of the spinal tissue are the microfibres: the micro-size diameter of these fibres is comparable to the width of axons, thereby enabling the fibres to create a nature-like environment that acts as a guide for tissue regrowth [25, 47, 77, 84]. However, even if microfibres seem a promising solution for the treatment of SCI, results obtained are not optimal: cortico-spinal tract regeneration has not been achieved yet, suggesting that something more than mechanical and chemical stimuli is needed. Indeed, several studies report that the intra-spinal micro-stimulation (ISMS) plays an important role in the recovery of motor functions after SCI [11]. Carbon microfibres have been studied as implantable neural electrodes for ISMS, due to their combination of favourable small dimensions and high electrical conductivity ($\approx 10^5$ Sm^{-1}) [17]. A further step forward was done by modifying the surface of the carbon microfibres with conductive polymers to improve the electrical performance and by introducing bio-functionalisation, which emits specific signals that aid the regeneration of the tissue [5, 86]. Thus, these fibres could provide both a physical guidance that assists the axons regrowth and a connection that transmits electrical stimuli to the area of interest. Once implanted, the fibres must integrate with the surrounding tissue and stay fixed in the injured area to impose stimuli and allow regrowth. However, since the spinal cord is subjected to physiological and pathological movements such as: vibrations, heart beats, variable chest pressure, cellular processes associated to tissue healing and body movements [73, 89], the task of keeping fibres fixed in place can be difficult. Note that the movement of an implanted microfibre away from its target location is, among several other failure modes, one of the most dangerous scenarios possible. Indeed, random displacements could compromise the efficiency of

the treatment from the very beginning and moreover cause damage to other healthy areas of the spinal cord or even other tissues (e.g. the circulatory system). Movements of the microfibres could therefore damage the embedding tissue, postpone the healing process and weaken the therapeutic presence of the structure in the injured area. The aim of this work is the experimental and numerical evaluation of the possible dangerous displacements of implanted fibres induced by flexion of the spinal cord. Numerical simulations were implemented to better characterise the dynamics of the microfibre embedded in the spinal cord medium. Subsequently, an ad-hoc experimental set-up was designed to mimic the physiological bending strains of the spine on an implant, by embedding a microfibre in a spinal cord like-matrix. The escape speed (i.e. the eventual displacement during the imposed movement) of the fibres was recorded to estimate the possible migration.

5.2 Experimental tests

5.2.1 Samples and spinal cord-like matrix

The aim of the experiments was to investigate the dynamic behaviour and consequently the possible migration of a single microfibre, once implanted in the spinal cord, see Figure 5.2.1. The analysed samples were 10 mm long bare carbon microfibres (Goodfellow C 005722) with 7μm diameter, placed inside a rectangular silicone chamber and embedded in a gelatin matrix. Edible gelatin was used to represent the spinal cord, since a transparent matrix was needed to observe the eventual displacement of the microfibre. The aim of the experiments was to simulate the worst case scenario for the migration of the microfibre. Thus, the typical environment of the acute phase was considered, which is characterised by haemorrhage, inflammation and fluid buildup [29, 65]. Gelatin was prepared mixing water and isinglass with

a 1 : 40 ratio. Compression tests performed on this gel solution showed a compression modulus comparable to the compressibility of spinal cords [52]. To simulate the liquid environment of the injured area in the acute phase, tests were performed using the gel solution. In order to obtain the experimental setup, the solution was poured in the silicone chamber to produce the specimen representing the spine. Subsequently, the carbon fibre was placed inside the gel after the chamber was filled, with a distance of circa 5 mm from one of the short sides of the rectangle, as shown in Figure 5.2.1.

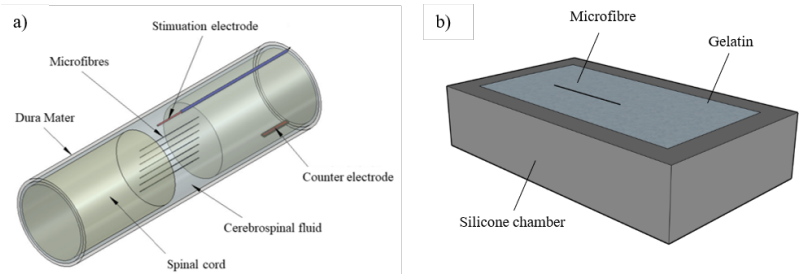

Figure 5.2.1: a) Final configuration of the device, composed by several carbon microfibres connected wireless to the stimulator. b) Scheme of the samples used to perform the measurements: a carbon microfibre embedded in a gelatin matrix, contained in a silicone chamber.

Experimental set-up and measurements An experimental set-up, Figure 5.2.2, was designed for two reasons: i) to simulate the movements transmitted from the flexion of the spine to the spinal cord tissue; and ii) to record the displacement of the fibres through an optical microscope (Olympus BX61). The dimensions of the silicone chamber were thus limited to fit the field of view of the microscope. The chamber was fixed on the short side closed to the fibre, and attached to the axle of a shaker (TIRA GmbH) on the other side. The sinusoidal movement of the axle simulated the bending of the spinal cord during physiological movements of the body. Different amplitudes and frequencies of the imposed

sinusoidal movement were tested, namely: 5 and 6 mm amplitudes, and 1 and 4 Hz frequencies. All the amplitude-frequency combinations were tested, and each combination was tested on three different samples. The strain imposed by the shaker, due to the amplitudes, was estimated between 1 and 2%, in accordance with the lower strain values found in literature [73, 89]. The assumed movements imposed by the shaker are thus suitable to simulate the small physiological movements of the spinal cord. Moreover, the frequencies were preliminarily chosen as the minimum technical value of 1 Hz and around the first natural frequency of the system $\approx$ 4 Hz, see Section 5.2.2.

By means of the microscope, one picture of the chamber and fibre system was taken every 5 minutes, for 30 minutes in total, (typical images are shown in Figure 5.2.5). Furthermore, ImageJ [80] was used to measure the displacements and rotations with respect to the initial position of the fibres. The displacement was considered positive when moving towards the axle of the shaker. Given the displacements, the velocity of the fibres was eventually calculated.

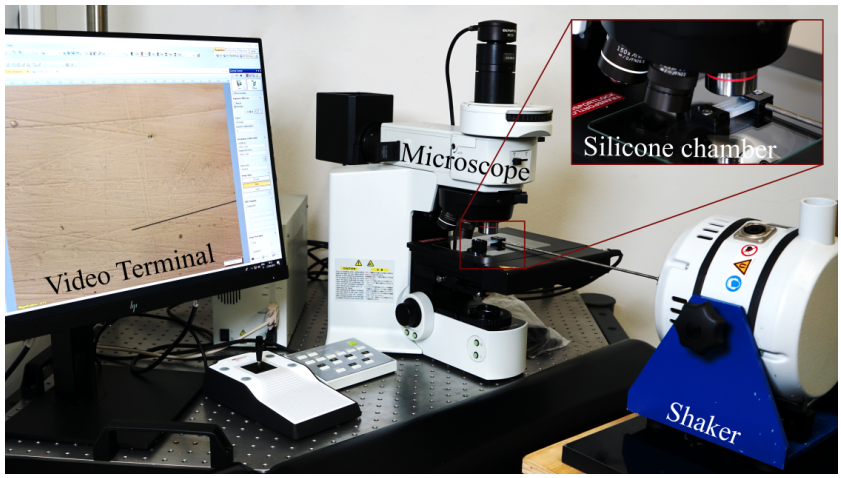

Figure 5.2.2: Set-up of the experiment.

5.2.2 Numerical dynamic characterisation

The aim of this section is to provide a preliminary dynamic characterisation of the sample presented in the previous section. The numerical simulations are mainly performed to give some interesting support to the experiment. In fact, we can take advantage of the results and calibrate the shaker in order to test the relevant frequencies of solicitation of the sample. The first step was to find the lower natural frequencies of the system (chamber, gelatin and fibre). Subsequently, we can estimate the eventual fibre displacement, with respect to the fibre axis, by performing a forced vibration analysis by applying a load along the y direction of the chamber, which coincides with the direction of the shakers axle.

As shown in Figure 5.2.3, in order to reproduce the experimental set-up presented in the section above, the system under study is clamped on one side of the chamber (indicated with a red boundary); while the other side is excited with a sinusoidal forced displacement (indicated with a green boundary). The sys-

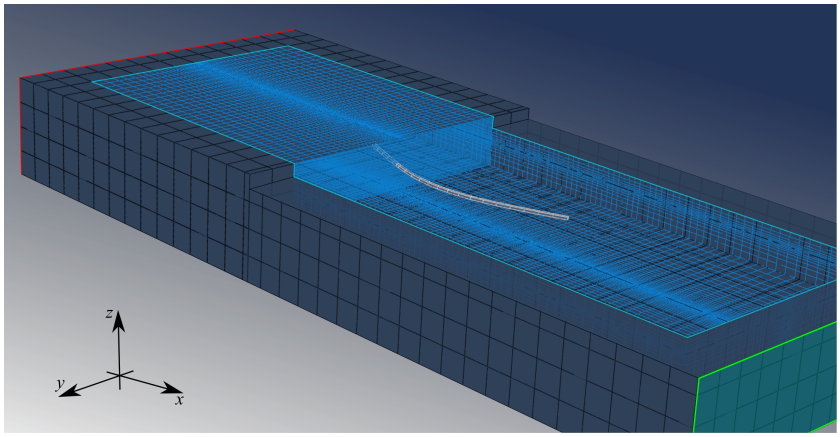

Figure 5.2.3: Set-up of the numerical simulation. White mesh is used for the fibre, light blue for the gelatin and black for the silicone chamber. The red lines delimited the clamped side, while green side represents the surface subjected to a sinusoidal excitation along the y direction. Furthermore, rotations and other displacement are not allowed.

tem analysed is composed of three parts: a silicone chamber filled with gelatin gel that embeds the carbon fibre. The silicone chamber and the carbon fibre are modelled as linear elastic materials using 7560 brick elements of type C3D20RH and 248 brick elements of type C3D20R, respectively. The gelatin is taken into account as an acoustic medium with 78592 brick elements of type AC3D20, that has the peculiarity to transmit the solicitations, exchanged between the chamber and the fibre, as pressure waves. Therefore, the bulk modulus K of the gel must be defined. The mechanical properties are listed in Table 5.2.1.

Material	Symbol	Unit	Value
Carbon microfibre [18]	E	[MPa]	$272 \cdot 10^3$
	ρ	[Kg m^{-3}]	2250
	ν	[-]	0.2
Silicone chamber [70]	E	[MPa]	$5 \cdot 10^3$
	ρ	[Kg m^{-3}]	1180
	ν	[-]	0.47
Gelatin [88]	K	[MPa]	$4 \cdot 10^3$
	ρ	[Kg m^{-3}]	1483

Table 5.2.1: Mechanical properties of the materials used in the simulations.

In order to perform the simulation it is necessary to couple the acoustic medium with the elastic components, through the contact surfaces. It is good practice to generate a mesh that is refined near the contact surfaces with the structural elements [1], whereas the size ratio between acoustic and structural elements in all other areas amounts to $1 : 4$, i.e. the structural elements are 4 times larger then the acoustic ones. Moreover, the top surface of the gelatin must not reflect any waves, thus, the acoustic impedance must be prescribed to the free surface.

Eigenfrequencies of the system The perturbation analysis is performed in order to find the first natural frequencies of the system. The perturbation method used in abaqus for extracting the

eigenfrequencies is based on the Lanczos solver [1]. The geometrical nonlinearities are not taken into account and the normalisation of the eigenvector is based on the mass. In order to perform the analysis at least three parameter are requested: (i) number of eigenvalues to be calculated, (ii) minimum frequency of interest in [Hz] and (iii) maximum frequency of interest in [Hz]. Table 5.2.2 summarises the first 4 eigenfrequencies found by spanning a range from 0 Hz to 12 Hz. The system perturbed is represented in Figure 5.2.3, with one side clamped and the other one free to slide in the y direction, while rotations and displacements in the other directions are not allowed. A

i	Frequency ω_n^i [Hz]	Chamber	Fibre	Plane
1	3.6959	✓	✓	xy
2	4.0431	✓	✓	xy
3	6.0526	✓	✓	xy
4	8.6291		✓	xz
4	8.6306		✓	xy

Table 5.2.2: Natural frequencies of the system. The check mark indicates which element is deformed at the natural frequency value ω_n^i. Last column specifies the deformation plane in which the fibre is deformed. Note that the last two lines represent the same mode shapes in perpedicular planes.

Steady state dynamic analysis This analysis evaluates the displacement in the orthogonal direction of the fibre once the system enters a steady state response to the sinusoidal solicitation on the green side of the model, see also Figure 5.2.3. The imposed force maintains a constant magnitude, while the frequency is spanning the very same range of frequencies adopted in the previous modal analysis, from 0 Hz to 12 Hz. Once the steady state at any of the imposed frequencies is reached, the displacement of the system is recorded. In particular, we are interested in the fibre deflection, which is responsible for the propulsion of the fibre, as we have seen in [76]. Therefore, Figure 5.2.4 depicts

the response of the fibre when the system is subjected to a steady state dynamic analysis, in particular, we can appreciate the normalised relative y-displacement plotted as a function of the normalised frequency. The displacement is normalised with respect to the length of the fibre l_0, while the frequency is normalised with respect to the first natural frequency ω_n^1.

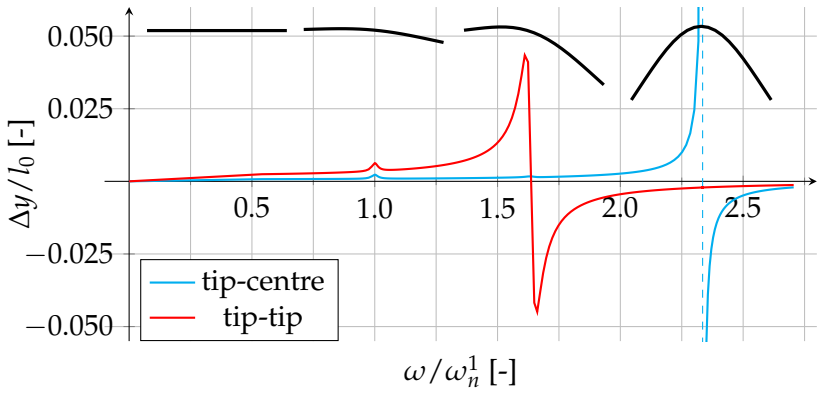

Figure 5.2.4: Steady state dynamic analysis of the system shows different peaks in correspondence to the eigenfrequencies of the system. The red line represents the relative displacement between the fibre tips, while the blue line depicts the displacement of the right tip with respect the centre of the fibre. In black we report the deformed shape of the fibre in correspondence to the peaks.

5.2.3 Results

Experimental study on the migration of the fibre embedded in a spinal cord-like matrix The images obtained from the experiment show an effective migration of the fibres for various amplitudes and frequencies tested. In 10 tests out of 12, the migration of the fibre was recorded toward the axle of the shaker (i.e. in the positive direction, see Figure 5.2.5), while in the other two cases the fibre did not manifest a displacement or showed only an insignificant motion $\Delta_{\%}\bar{x} \leq 1\%$. Table 5.2.3 summarises the results obtained: the percentage of displacement $\Delta_{\%}\bar{x} = 100 \cdot (\Delta\bar{x}/l_0)$ with respect to the length of the microfibre ($l_0 = 10$ mm) and

the average escape speed, calculated as the average of the speeds recorded every 5 minutes, Δt, during the test, as follows,

$$\begin{aligned} \bar{v}_{30} &= \frac{1}{3}\sum_{i=1}^{3}\frac{1}{6}\sum_{j=1}^{6}\bar{v}_{5j}^{i} = \frac{1}{3}\sum_{i=1}^{3}\frac{1}{6}\sum_{j=1}^{6}\frac{x_{5j}^{i} - x_{5(j-1)}^{i}}{\Delta t} \\ &= \frac{\Delta \bar{x}_{30}}{\Delta t} \end{aligned} \tag{5.1}$$

where index i identifies the sample, while j is the time interval.

By considering the tests performed with the same amplitude, the escape speeds increase by increasing the frequency. By increasing the frequency from 1 Hz to 4 Hz, the average escape speed increases 20-fold and 50-fold for 5 mm and 6 mm amplitudes, respectively. An increase of 1 mm in the stimulating amplitude doubles the escape speed when applying 4 Hz instead of 1 Hz. Moreover, considering a 4 Hz frequency, the displacement doubles if the samples are stimulated with 6 mm with respect to 5 mm (from about 65% to 140% and from circa 3% to 4%).

Amplitude [mm]	Frequency [Hz]	Displacement $\Delta_{\%}\bar{x}_{30}$ [%]	Average velocity $\bar{v}_{30}$ [mm/s]
5.0	1.0	3	0.00076
5.0	4.0	65	0.01737
6.0	1.0	4	0.00080
6.0	4.0	143	0.04167

Table 5.2.3: Preliminary results of the experimental tests

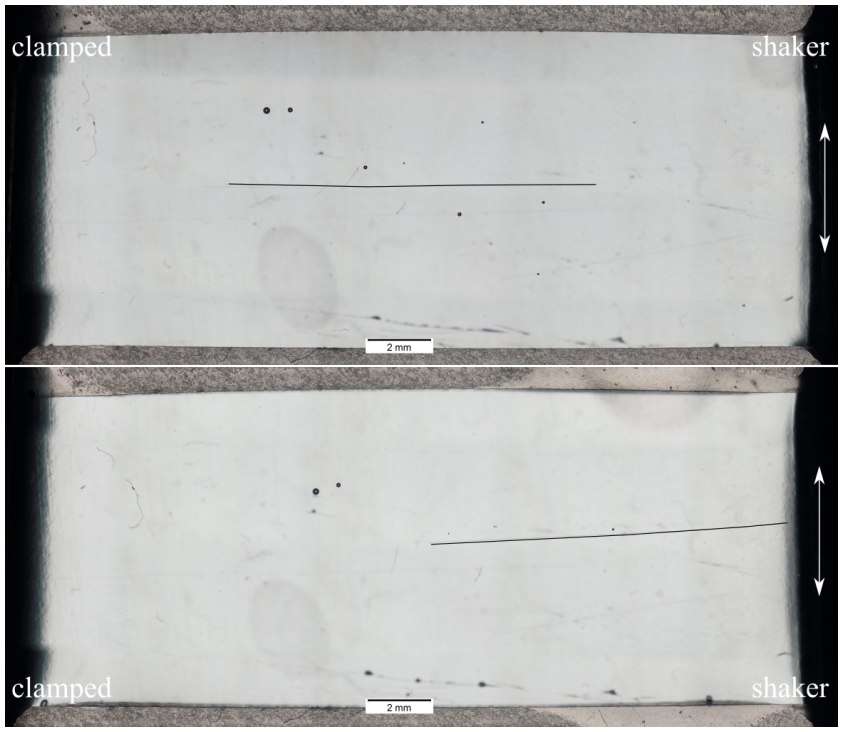

Figure 5.2.5: Two pictures taken before (above) and after (below) the experimental test.

5.3 Conclusion and considerations

Preliminary results of the experimental tests highlighted the possible danger of migrating microfibres. The experimental set-up was designed to evaluate the behaviour of the implanted microfibres during the acute phase, and thus when surrounded by a mostly liquid environment. The aim was to understand whether precautionary measures are needed, in order to avoid a harmful displacement of the fibres. The average escape speed of the microfibres was evaluated by imposing a sinusoidal movement characterised by different amplitudes and frequencies. Investigating the role of these two movement parameters, we found a substantial increase in escape speed when increasing the frequency of excitation from 1 Hz to 4 Hz. Furthermore, an increase

in amplitude from 5 mm to 6 mm also resulted in larger displacement, particularly for the high frequency experiments, i.e. 4 Hz. It is thus reasonable to hypothesise that further increases of the frequency could lead to yet higher escape speeds, due to a presumably higher deflection of the fibre, as shown in Figure 5.2.4 and augmented energy input.

In sum, the results clearly show the need for an anchorage point of the fibres or the presence of a system that limits or immobilises the spine during the first phases of patient recovery. A migration of these fibres needs to be avoided for the sake of the patients health and is therefore of vital importance.

6

Concluding Remarks

6.1 Conclusion and open issues

Locomotion played a key role in the animal evolution. In particular this work is focused on a specific kind of locomotion: undulatory locomotion. For the movement through various environments, such as sands and liquids, undulatory locomotion has emerged as an easy, successful and robust tool, particularly for limbless species. The motion is characterised by the propagation of waves along the body of an organism, which in turn produces lifting and propulsive forces. Therefore, undulatory locomotion is important not only because of its widespread presence in the animal kingdom but also as a source of inspiration for us. Bio-inspired robots find useful application in real life, such as: (i) the exploration of complex substrates where wheeled devices fail; (ii) inspection of difficult to reach places like the insides of pipelines;

(iii) rescue operations; and (iv) non-invasive surgical operations for medical purposes. In the near future, even extraterrestrial exploration will profit from undulatory locomotion, due to its robustness and versatility. Moreover, it is a fact that modern technology has opened the exploration of the micro- and nano-scale. At these scales, low Reynolds number physics become dominant, and undulatory locomotion strategies can be used for micro- and nano-robots, drug delivery systems and non invasive diagnostic. This growing interest in applications needs a solid analytical and numerical background. In this context, the work done herein provides an alternative and simple tool for the interpretation and optimisation of undulatory locomotion in soil-like materials, combining numerical simulation, analytical theories and experiments.

The undulatory locomotion consists of three ingredients: a locomotor, an environment for the locomotor to interact with, and a control strategy. In this work the locomotor is described through the mathematical framework offered by analytical mechanics, discussed in detail in Chapter 2.

In Chapter 3 an undulatory system interacting with a granular material is studied. A numerical model that involves the coupling of finite elements, representing the locomotor, with discrete elements, embodying the granular environment, is proposed. A parametric study on different solicitation scenarios investigates the impact of frequency and amplitude changes on locomotion. The right combination of parameters triggering the most effective locomotion is therefore analysed. It is interesting to note that the locomotor reaches a steady state, where it propels itself at a constant velocity through the medium. Subsequently, the dynamics of a discrete multi bar system is studied and compared with the results obtained from the numerical investigation. This analytical model has the peculiarity of taking into account the forces exchanged with the environment through the Resistive Force Theory, a theory originally developed for describing locomotion in

viscous fluids. The analytical model, even if conceptually simpler, reveals to be very accurate in describing the simulations, e.g. deformed shape and locomotion velocity. Due to its versatility, the model can be used in the prediction and energy optimisation of snake-like robots in future studies.

In Chapter 4 an extension of the discrete analytical model is presented. In particular, we show the procedure to derive the equations of motion for a continuous slender body surrounded by a viscous environment. Resistive Force Theory, once again, provides the framework for describing the interaction with the surroundings. The presented formulations, once a numerical solver will be complete, may also offer alternative tools, with respect to the computationally expensive simulations, for describing and optimising soft slender bio-inspired robots.

In both, discrete and continuous locomotor systems (described in Chapter 3 and 4), the control strategy was specifically set as the least restrictive possible, by actuating one degree of freedom in the discrete model (i.e. the head's rotation), and by imposing a punctual kinematic constraint in the continuous case. This condition, for the purpose of controlling a system, is the most difficult and unfavourable possible, due to the lack of control in the remaining body. Despite this, we were able to simulate and predict a steady state forward undulatory locomotion.

Chapter 5 experimentally demonstrates the migration of a carbon microfibre embedded in a spinal cord-like gelatin subjected to sinusoidal oscillations. This behaviour could potentially be dangerous to the patients health when regenerative devices are implanted in the spinal cord. In fact, carbon microfibres find application in the Intraspinal Micro-Stimulation (IsMS) technique for functional regeneration after a spinal cord injury. The work presented highlights and quantitatively describes the migration of microfibres through spinal chord like substances. Future studies aim to apply the models developed in chapters 3 and 4 to the issue of microfibre migration, due to the following evident

similarities: (i) the microfibre is, *de facto* a slender body, and (ii) the spinal cord, when lesioned, can be described as a viscous medium.

Bibliography

[1] *Abaqus documentation*. abaqus-docs.mit.edu. 2017.

[2] M. S. Alnæs, J. Blechta, J. Hake, A. Johansson, B. Kehlet, A. Logg, C. Richardson, J. Ring, E. Rognes, and G. N. Wells. "The FEniCS Project Version 1 . 5". In: *Archive of Numerical Software* 3.100 (2015), pp. 9–23. DOI: https://doi.org/10.11588/ans.2015.100.20553.

[3] F. Alouges, A. DeSimone, L. Giraldi, and M. Zoppello. "Can Magnetic Multilayers Propel Artificial Microswimmers Mimicking Sperm Cells?" In: *Soft Robotics* 2.3 (Sept. 2015), pp. 117–128. DOI: 10.1089/soro.2015.0007.

[4] F. Alouges, A. Desimone, and A. Lefebvre. "Optimal strokes for low reynolds number swimmers: An example". In: *Journal of Nonlinear Science* 18.3 (2008), pp. 277–302. DOI: 10.1007/s00332-007-9013-7.

[5] A. Alves-Sampaio, C. García-Rama, and J. E. Collazos-Castro. "Biofunctionalized PEDOT-coated microfibers for the treatment of spinal cord injury". In: *Biomaterials* 89 (2016), pp. 98–113. DOI: 10.1016/j.biomaterials.2016.02.037.

[6] C. Armanini, F. Dal Corso, D. Misseroni, and D. Bigoni. "Configurational forces and nonlinear structural dynamics". In: *Journal of the Mechanics and Physics of Solids* 130 (2019), pp. 82–100. DOI: 10.1016/j.jmps.2019.05.009.

[7] M. Arroyo, L. Heltai, D. Millán, and A. DeSimone. "Reverse engineering the euglenoid movement". In: *Proceedings of the National Academy of Sciences of the United States of America* 109.44 (2012), pp. 17874–17879. DOI: 10.1073/pnas.1213977109.

[8] H. Askari and K. Kamrin. "Intrusion rheology in grains and other flowable materials". In: *Nature Materials* 15.12 (2016), pp. 1274–1279. DOI: 10.1038/nmat4727.

[9] H. C. Astley, J. R. Mendelson, J. Dai, C. Gong, B. Chong, J. M. Rieser, P. E. Schiebel, S. S. Sharpe, R. L. Hatton, H. Choset, and D. I. Goldman. "Surprising simplicities and syntheses in limbless self-propulsion in sand". In: *The Journal of Experimental Biology* 223.5 (Mar. 2020), jeb103564. DOI: 10.1242/jeb.103564.

[10] Y. O. Aydin, J. M. Rieser, C. M. Hubicki, W. Savoie, and D. I. Goldman. "Physics approaches to natural locomotion: Every robot is an experiment". In: *Robotic Systems and Autonomous Platforms*. Elsevier, 2019, pp. 109–127. DOI: 10.1016/B978-0-08-102260-3.00006-8.

[11] J. A. Bamford and V. K. Mushahwar. *Intraspinal microstimulation for the recovery of function following spinal cord injury*. 1st ed. Vol. 194. Elsevier B.V., 2011, pp. 227–239. DOI: 10.1016/B978-0-444-53815-4.00004-2.

[12] W. Baumgartner, F. Fidler, A. Weth, M. Habbecke, P. Jakob, C. Butenweg, and W. Böhme. "Investigating the locomotion of the sandfish in desert sand using NMR-Imaging". In: *PLoS ONE* 3.10 (2008). DOI: 10.1371/journal.pone.0003309.

[13] H. C. Berg. "Motile Behavior of Bacteria". In: *Physics Today* 53.1 (Jan. 2000), pp. 24–29. DOI: 10.1063/1.882934.

[14] S. Berri, J. H. Boyle, M. Tassieri, I. A. Hope, and N. Cohen. "Forward locomotion of the nematode C. elegans is achieved through modulation of a single gait". In: *HFSP Journal* 3.3 (June 2009), pp. 186–193. DOI: 10.2976/1.3082260.

[15] D. Bigoni. *Nonlinear Solid Mechanics*. Vol. 53. 9. Cambridge: Cambridge University Press, 2012, pp. 1689–1699. DOI: 10.1017/CBO9781139178938.

[16] C. M. Breder. "The locomotion of fishes". In: *Zoologica : scientific contributions of the New York Zoological Society.* 4.5 (1926), pp. 159–297.

[17] D. Budai. "Carbon fiber-based microelectrodes and microbiosensors". In: *Intelligent and Biosensors* (2010), pp. 269–288. DOI: http://dx.doi.org/10.5772/57353.

[18] *Carbon Fiber C 005722 - Goodfellow Catalog*. goodfellowusa.com.

[19] T. Chambrion, L. Giraldi, and A. Munnier. "Optimal strokes for driftless swimmers: A general geometric approach". In: *ESAIM - Control, Optimisation and Calculus of Variations* 25 (2019). DOI: 10.1051/cocv/2017012.

[20] N. Cohen and J. H. Boyle. "Swimming at low Reynolds number: a beginners guide to undulatory locomotion". In: *Contemporary Physics* 51.2 (Mar. 2010), pp. 103–123. DOI: 10.1080/00107510903268381.

[21] S. J. Cook et al. "Whole-animal connectomes of both Caenorhabditis elegans sexes". In: *Nature* 571.7763 (2019), pp. 63–71. DOI: 10.1038/s41586-019-1352-7.

[22] R. G. Cox. "The motion of long slender bodies in a viscous fluid Part 1. General theory". In: *Journal of Fluid Mechanics* 44.04 (Dec. 1970), p. 791. DOI: 10.1017/S002211207000215X.

[23] J. l. R. D'Alembert. *Traité de dynamique*. First Edit. Paris: Chez Fuchs, 1758.

[24] T. Dear, S. D. Kelly, M. Travers, and H. Choset. "Locomotion of a multilink nonholonomic snake robot". In: *ASME 2017 Dynamic Systems and Control Conference, DSCC 2017* 2 (2017), pp. 1–10. DOI: 10.1115/DSCC2017-5349.

[25] T. L. Downing, A. Wang, Z. Q. Yan, Y. Nout, A. L. Lee, M. S. Beattie, J. C. Bresnahan, D. L. Farmer, and S. Li. "Drug-eluting microfibrous patches for the local delivery of rolipram in spinal cord repair". In: *Journal of Controlled Release* 161.3 (2012), pp. 910–917. DOI: 10.1016/j.jconrel.2012.05.034.

[26] R. Dreyfus, J. Baudry, M. L. Roper, M. Fermigier, H. A. Stone, and J. Bibette. "Microscopic artificial swimmers". In: *Nature* 437.7060 (2005), pp. 862–865. DOI: 10.1038/nature04090.

[27] R. Dubuc et al. "Initiation of locomotion in lampreys". In: *Brain Research Reviews* 57.1 (2008), pp. 172–182. DOI: 10.1016/j.brainresrev.2007.07.016.

[28] C. Duprat and H. Stone. *Fluid-Structure Interactions in Low-Reynolds-Number Flows*. Soft Matter Series. Cambridge: Royal Society of Chemistry, 2015. DOI: 10.1039/9781782628491.

[29] N. S. Elliott, A. D. Lucey, D. A. Lockerby, and A. R. Brodbelt. "Fluid–structure interactions in a cylindrical layered wave guide with application in the spinal column to syringomyelia". In: *Journal of Fluids and Structures* 70.November 2016 (2017), pp. 464–499. DOI: 10.1016/j.jfluidstructs.2016.11.007.

[30] A. Ertürk et al. "Three-dimensional imaging of the unsectioned adult spinal cord to assess axon regeneration and glial responses after injury". In: *Nature Medicine* 18.1 (2012), pp. 166–172. DOI: https://doi.org/10.1038/nm.2600.

[31] "Facts and Figures at a Glance". In: *The Journal of Spinal Cord Medicine* 30.4 (Jan. 2018), pp. 304–305. DOI: 10.1080/10790268.2007.11753944.

[32] A. Fasano and S. Marmi. *Analytical Mechanics*. OXFORD University Press, 2002, p. 773.

[33] J. Feng and S. K. Cho. "Mini and micro propulsion for medical swimmers". In: *Micromachines* 5.1 (2014), pp. 97–113. DOI: 10.3390/mi5010097.

[34] K. K. Fenrich, P. Weber, M. Hocine, M. Zalc, G. Rougon, and F. Debarbieux. "Long-term in vivo imaging of normal and pathological mouse spinal cord with subcellular resolution using implanted glass windows". In: *The Journal of Physiology* 16.590 (2012), pp. 3665–3675. DOI: 10.1113/jphysiol.2012.230532.

[35] M. T. Fitch and J. Silver. "CNS injury, glial scars, and inflammation: Inhibitory extracellular matrices and regeneration failure". In: *Experimental Neurology* 209.2 (2008), pp. 294–301. DOI: 10.1016/j.expneurol.2007.05.014.

[36] M. Gazdic, V. Volarevic, C. Harrell, C. Fellabaum, N. Jovicic, N. Arsenijevic, and M. Stojkovic. "Stem Cells Therapy for Spinal Cord Injury". In: *International Journal of Molecular Sciences* 19.4 (2018), p. 1039. DOI: 10.3390/ijms19041039.

[37] H. Goldstein, C. P. Poole, and J. L. Safko. *Classical Mechanics*. Third. Pearson, 2002, p. 664.

[38] N. Gravish, P. B. Umbanhowar, and D. I. Goldman. "Force and flow transition in plowed granular media". In: *Physical Review Letters* 105.12 (2010), pp. 1–4. DOI: 10.1103/PhysRevLett.105.128301.

[39] J. Gray and H. W. Lissmann. "The Locomotion of Nematodes". In: *J. Exp. Biol* 41 (1964), pp. 3–4.

[40] J. Gray and G. J. Hancock. "The Propulsion of Sea-Urchin Spermatozoa". In: *J. Exp. Biol.* 32.4 (1955), pp. 802–814.

[41] J. Gray. "The movement of fish with special reference to the eel". In: *Journal of Experimental Biology* 10.3 (1933), pp. 88–104.

[42] D. T. Greenwood. *Classical Dynamics*. Dover Publication, Inc., 1977.

[43] Z. V. Guo and L. Mahadevan. "Limbless undulatory propulsion on land". In: *Proceedings of the National Academy of Sciences of the United States of America* 105.9 (2008), pp. 3179–3184. DOI: 10.1073/pnas.0705442105.

[44] J. J. Head, J. I. Bloch, A. K. Hastings, J. R. Bourque, E. A. Cadena, F. A. Herrera, P. D. Polly, and C. A. Jaramillo. "Giant boid snake from the Palaeocene neotropics reveals hotter past equatorial temperatures". In: *Nature* 457.7230 (2009), pp. 715–717. DOI: 10.1038/nature07671.

[45] J. K. Hopkins, B. W. Spranklin, and S. K. Gupta. "A survey of snake-inspired robot designs". In: *Bioinspiration and Biomimetics* 4.2 (2009). DOI: 10.1088/1748-3182/4/2/021001.

[46] D. L. Hu, J. Nirody, T. Scott, and M. J. Shelley. "The mechanics of slithering locomotion". In: *Proceedings of the National Academy of Sciences of the United States of America* 106.25 (2009), pp. 10081–10085. DOI: 10.1073/pnas.0812533106.

[47] A. Hurtado, J. M. Cregg, H. B. Wang, D. F. Wendell, M. Oudega, R. J. Gilbert, and J. W. McDonald. "Robust CNS regeneration after complete spinal cord transection using aligned poly-l-lactic acid microfibers". In: *Biomaterials* 32.26 (2011), pp. 6068–6079. DOI: 10.1016/j.biomaterials.2011.05.006.

[48] N. Ibrahim et al. “Tail-propelled aquatic locomotion in a theropod dinosaur”. In: *Nature* 581.May (2020), pp. 1–4. DOI: 10.1038/s41586-020-2190-3.

[49] A. J. Ijspeert. “Central pattern generators for locomotion control in animals and robots: A review”. In: *Neural Networks* 21.4 (2008), pp. 642–653. DOI: 10.1016/j.neunet.2008.03.014.

[50] A. J. Ijspeert, A. Crespi, D. Ryczko, and J. M. Cabelguen. “From swimming to walking with a salamander robot driven by a spinal cord model”. In: *Science* 315.5817 (2007), pp. 1416–1420. DOI: 10.1126/science.1138353.

[51] R. Johnson and C. Brokaw. “Flagellar hydrodynamics. A comparison between resistive-force theory and slender-body theory”. In: *Biophysical Journal* 25.1 (Jan. 1979), pp. 113–127. DOI: 10.1016/S0006-3495(79)85281-9.

[52] A. Karimi, A. Shojaei, and P. Tehrani. “Mechanical properties of the human spinal cord under the compressive loading”. In: *Journal of Chemical Neuroanatomy* (2017). DOI: 10.1016/j.jchemneu.2017.07.004.

[53] P. Katsamba and E. Lauga. “Propulsion by stiff elastic filaments in viscous fluids”. In: *Physical Review E* 99.5 (2019). DOI: 10.1103/PhysRevE.99.053107.

[54] V. Kuznetsov, B. Lugovtsov, and Y. Sher. “On the Motive Mechanism of Snakes and Fish”. In: *Archive for Rational Mechanics and Analysis* 25.5 (1967), pp. 367–387. DOI: doi.org/10.1007/BF00291937.

[55] J.-L. Lagrange. *Mécanique analytique*. First Edit. Paris: Chez la Veuve Desaint, 1788, p. 522.

[56] C. Lanczos. *The Variational Principles of Mechanics*. New York: Dover Publication, Inc, 1949.

[57] H. P. Langtangen and A. Logg. *Solving PDEs in Python: The FEniCS Tutorial*. Vol. I. 2017, p. 153. DOI: 10.1073/pnas.202491499.

[58] E. Lauga. “Life around the scallop theorem”. In: *Soft Matter* 7.7 (2011), pp. 3060–3065. DOI: 10.1039/c0sm00953a.

[59] E. Lauga and T. R. Powers. "The hydrodynamics of swimming microorganisms". In: *Reports on Progress in Physics* 72.9 (2009). DOI: 10.1088/0034-4885/72/9/096601.

[60] M. J. Lighthill. "Large-amplitude elongated-body theory of fish locomotion". In: *Proceedings of the Royal Society of London. Series B. Biological Sciences* 179.1055 (Nov. 1971), pp. 125–138. DOI: 10.1098/rspb.1971.0085.

[61] R. D. Maladen, Y. Ding, C. Li, and D. I. Goldman. "Undulatory swimming in sand: Subsurface locomotion of the sandfish lizard". In: *Science* 325.5938 (2009), pp. 314–318. DOI: 10.1126/science.1172490.

[62] R. D. Maladen, Y. Ding, P. B. Umbanhowar, A. Kamor, and D. I. Goldman. "Mechanical models of sandfish locomotion reveal principles of high performance subsurface sand-swimming". In: *Journal of the Royal Society Interface* 8.62 (2011), pp. 1332–1345. DOI: 10.1098/rsif.2010.0678.

[63] A. Munnier and T. Chambrion. "Generalized Scallop Theorem for Linear Swimmers". In: (Aug. 2010).

[64] R. R. Murphy, S. Tadokoro, D. Nardi, A. Jacoff, P. Fiorini, H. Choset, and A. M. Erkmen. "Search and Rescue Robotics". In: *Springer Handbook of Robotics*. Berlin, Heidelberg: Springer Berlin Heidelberg, 2008, pp. 1151–1173. DOI: 10.1007/978-3-540-30301-5{_}51.

[65] M. D. Norenberg, J. Smith, and A. Marcillo. "The Pathology of Human Spinal Cord Injury: Defining the Problems". In: *Journal of Neurotrauma* 21.4 (2004), pp. 429–440. DOI: 10.1089/089771504323004575.

[66] G. Noselli, A. Beran, M. Arroyo, and A. DeSimone. "Swimming Euglena respond to confinement with a behavioural change enabling effective crawling". In: *Nature Physics* 15.5 (2019), pp. 496–502. DOI: 10.1038/s41567-019-0425-8.

[67] W. H. Organization and I. S. C. Society. *International Perspectives on Spinal Cord Injury*. Tech. rep. World Health Organization, and International Spinal Cord Society, 2013. DOI: 10.1007/978-1-4899-1028-8{_}18.

[68] T. Ota, A. Degani, D. Schwartzman, B. Zubiate, J. McGarvey, H. Choset, and M. A. Zenati. "A Highly Articulated Robotic Surgical System for Minimally Invasive Surgery". In: *Annals of Thoracic Surgery* 87.4 (2009), pp. 1253–1256. DOI: 10.1016/j.athoracsur.2008.10.026.

[69] S. Park, H. Hwang, S. W. Nam, F. Martinez, R. H. Austin, and W. S. Ryu. "Enhanced Caenorhabditis elegans locomotion in a structured microfluidic environment". In: *PLoS ONE* 3.6 (2008), pp. 1–5. DOI: 10.1371/journal.pone.0002550.

[70] *Properties: Silicone Rubber*. azom.com.

[71] E. M. Purcell. "Life at low Reynolds number". In: *American Journal of Physics* 45.1 (1977), pp. 3–11. DOI: 10.1119/1.10903.

[72] T. A. Rando. "Stem cells, ageing and the quest for immortality". In: *Nature* 441.7097 (2006), pp. 1080–1086. DOI: 10.1038/nature0495.

[73] J. D. Reid. "Effects of flexion-extension movements of the head and spine upon the spinal cord and nerve roots". In: *Journal of neurology, neurosurgery, and psychiatry* 23 (1960), pp. 214–221. DOI: 10.1136/jnnp.23.3.214.

[74] O. Reynolds. "An experimental investigation of the circumstances which determine whether the motion of water shall be direct or sinuous, and of the law of resistance in parallel channels". In: *Philosophical Transactions of the Royal Society of London* 174 (Dec. 1883), pp. 935–982. DOI: 10.1098/rstl.1883.0029.

[75] A. Rodella, I. Corridori, D. Misseroni, B. Mazzolai, A. Motta, and N. M. Pugno. "An experimental and numerical study of the migration of a carbon microfibre used for intraspinal microstimulation". In: *Under internal revision* (2020).

[76] A. Rodella, B. Mazzolai, and N. M. Pugno. "Undulatory locomotion in granular media of an elastic slender body: a comparison between Finite-Discrete element simulations and Resistive Force Theory". In: *Under internal revision* (2020).

[77] J. A. Roman, I. Reucroft, R. A. Martin, A. Hurtado, and H. Q. Mao. "Local Release of Paclitaxel from Aligned, Electrospun Microfibers Promotes Axonal Extension". In: *Advanced Healthcare Materials* 5.20 (2016), pp. 2628–2635.

[78] G. A. Roth et al. "Global, regional, and national age-sex-specific mortality for 282 causes of death in 195 countries and territories, 1980–2017: a systematic analysis for the Global Burden of Disease Study 2017". In: *The Lancet* 392.10159 (2018), pp. 1736–1788. DOI: 10.1016/S0140-6736(18)32203-7.

[79] P. E. Schiebel, J. M. Rieser, A. M. Hubbard, L. Chen, D. Z. Rocklin, and D. I. Goldman. "Mechanical diffraction reveals the role of passive dynamics in a slithering snake". In: *Proceedings of the National Academy of Sciences* 116.11 (Mar. 2019), pp. 4798–4803. DOI: 10.1073/pnas.1808675116.

[80] C. A. Schneider, W. S. Rasband, and K. W. Eliceiri. "NIH Image to ImageJ: 25 years of image analysis". In: *Nature Methods* 9.7 (2012), pp. 671–675. DOI: 10.1038/nmeth.2089.

[81] M. Sfakiotakis, A. Chatzidaki, T. Evdaimon, A. Kazakidi, and D. P. Tsakiris. "Effects of compliance in pedundulatory locomotion over granular substrates". In: *24th Mediterranean Conference on Control and Automation, MED 2016* (2016), pp. 532–538. DOI: 10.1109/MED.2016.7536061.

[82] M. Sfakiotakis and D. P. Tsakiris. "Biomimetic centering for undulatory robots". In: *International Journal of Robotics Research* 26.11-12 (2007), pp. 1267–1282. DOI: 10.1177/0278364907083394.

[83] G. G. Stokes. "On the Effect of the Internal Friction of Fluids on the Motion of Pendulums". In: *Mathematical and Physical Papers*. Vol. 13. 189. Cambridge: Cambridge University Press, 1927, pp. 1–10. DOI: 10.1017/CBO9780511702266.002.

[84] K. Sugai, S. Nishimura, M. Kato-Negishi, H. Onoe, S. Iwanaga, Y. Toyama, M. Matsumoto, S. Takeuchi, H. Okano, and M. Nakamura. "Neural stem/progenitor cell-laden microfibers promote transplant survival in a mouse transected spinal cord injury model". In: *Journal of Neuroscience Research* 93.12 (2015), pp. 1826–1838. DOI: 10.1002/jnr.23636.

[85] G. Taylor. "Analysis of the Swimming of Long and Narrow Animals". In: *Proceedings of the Royal Society A: Mathematical, Physical and Engineering Sciences* 214.1117 (1952), pp. 158–183. DOI: 10.1098/rspa.1952.0159.

[86] H. Vara and J. E. Collazos-Castro. "Enhanced spinal cord microstimulation using conducting polymer-coated carbon microfibers". In: *Acta Biomaterialia* 90 (2019), pp. 71–86. DOI: 10.1016/j.actbio.2019.03.037.

[87] G. Vizsnyiczai, G. Frangipane, S. Bianchi, F. Saglimbeni, D. Dell'Arciprete, and R. Di Leonardo. "A transition to stable one-dimensional swimming enhances E. coli motility through narrow channels". In: *Nature Communications* 11.1 (2020), p. 2340. DOI: 10.1038/s41467-020-15711-0.

[88] J. Winter and D. Shifler. "The material properties of gelatin gels". In: *USA Ballistics Research Laboratory* Contractor.127 (1975), p. 157.

[89] Q. Yuan, L. Dougherty, and S. S. Margulies. *In vivo human cervical spinal cord deformation and displacement in flexion*. 1998. DOI: 10.1097/00007632-199808010-00012.

[90] T. Zhang and D. I. Goldman. "The effectiveness of resistive force theory in granular locomotion". In: *Physics of Fluids* 26.10 (2014). DOI: 10.1063/1.4898629.

[91] O. C. Zienkiewicz and R. Taylor. *The Finite Element Method for Solid and Structural Mechanics*. Elsevier, 2005. DOI: 9781493302895.

Acknowledgements

This work was made possible by the support that I have received from many people throughout my education and professional career.
I would like to thank my supervisors: Prof. Nicola Maria Pugno and Dr. Barbara Mazzolai. They helped me to continue my education and gave me the freedom to explore new topics.
I would like to thank Prof. Lorenzo Bardella of the University of Brescia for the guidance through my master studies that got me into the world of solid mechanics.
Last but not the least, my family and friends have my deepest gratitude for supporting me during stressful as well as joyfull times .

Declaration of Authorship

I, Andrea RODELLA, declare that this thesis titled, "Analytical and numerical modelling of undulatory locomotion for limbless organisms in granular/viscous media" and the work presented in it are my own. I confirm that:

- This work was done wholly or mainly while in candidature for a research degree at this University.
- Where any part of this thesis has previously been submitted for a degree or any other qualification at this University or any other institution, this has been clearly stated.
- Where I have consulted the published work of others, this is always clearly attributed.
- Where I have quoted from the work of others, the source is always given. With the exception of such quotations, this thesis is entirely my own work.
- I have acknowledged all main sources of help.
- Where the thesis is based on work done by myself jointly with others, I have made clear exactly what was done by others and what I have contributed myself.

Signed:

_____

Date:

_____